TABLE OF CONTENTS

Chapter	Title	Page	
	FOREWORD	i	1/A5
	ABSTRACT	ii	1/A6
	LIST OF TABLES	v	1/A9
	LIST OF FIGURES	vi	1/A10
1	HYGROTHERMAL DEGRADATION OF GRAPHITE-EPOXY COMPOSITES	1-1	1/B1
	1.0 INTRODUCTION	1-1	1/B1
	1.1 ASSESSMENT OF HYGROTHERMAL DEGRADATION - LITERATURE REVIEW	1-6	1/B6
	1.1.1 Definition of Environment	1-6	1/B6
	1.1.2 Effect of Moisture on Mechanical Properties	1-7	1/B7
	1.1.3 Effect of Hygrothermal Cycling on Kinetics of Moisture Sorption	1-10	1/B10
	1.1.4 Effect of Hygrothermal Cycling on Mechanical Properties	1-12	1/B12
	1.1.5 Assessment of Hygrothermal Degradation Mechanisms	1-12	1/B12
	1.2 PROGRAM DESCRIPTION	1-14	1/B14
	1.3 MATERIAL PROCESSING	1-19	1/C5
2	THE COUPLING BETWEEN APPLIED AND RESIDUAL STRESS AND MOISTURE SORPTION	2-1	1/C8
	2.1 DIMENSIONAL CHANGES CAUSED BY MOISTURE ABSORPTION	2-1	1/C8
	2.2 MOISTURE ALTERED RESIDUAL STRESSES	2-5	1/C12
	2.3 DESORPTION UNDER STRESS	2-9	1/D4
	2.4 INFLUENCE OF APPLIED STRESS DURING DESORPTION ON RESIDUAL STRESSES	2-17	1/E2
	2.5 HYGROTHERMAL CYCLING EXPERIMENTS	2-20	1/E7
3	THE INFLUENCE OF HYGROTHERMAL HISTORY ON MATRIX AND INTERFACE DOMINATED LAMINATE PROPERTIES	3-1	1/E12
	3.1 INPLANE SHEAR TESTS	3-1	1/E12
	3.2 INTERLAMINAR SHEAR TESTS	3-10	1/F7
4	MICROSCOPIC EVIDENCE FOR DAMAGE DUE TO HYGROTHERMAL CYCLING	4-1	1/G8
	4.1 MICROSCOPIC EXAMINATION AFTER 10 HYGROTHERMAL CYCLES	4-1	1/G8
	4.2 MICROSCOPIC EXAMINATION AFTER 100 HYGROTHERMAL CYCLES	4-1	1/G8

TABLE OF CONTENTS (continued)

Chapter	Title	Page	
5	ANALYSIS OF HYGROTHERMALLY INDUCED STRESS IN GRAPHITE-EPOXY LAMINATES	5-1	2/A10
	5.1 ANALYSIS DESCRIPTION	5-1	2/A10
	5.2 ANALYSIS OF MOISTURE INDUCED STRESSES	5-3	2/A12
	5.3 HYGROTHERMAL STRESS ANALYSIS	5-7	2/B2
6	DISCUSSION OF RESULTS	6-1	2/C14
	6.1 ASSESSING PERMANENT AND REVERSIBLE INTERFACIAL BOND DEGRADATION	6-1	2/C14
	6.2 ENERGY CONCEPTS FOR INITIATION AND GROWTH OF HYGRO-THERMAL DAMAGE	6-5	2/D4
	6.3 CONCLUSIONS	6-11	2/D10
	REFERENCES	7-1	2/D13
Appendices			
A	MATERIAL PROCESSING INFORMATION	A-1	2/E4
B	MECHANICAL TESTING TABULATION	B-1	2/F7

NAS1.26:3189

COMPLETED

NASA Contractor Report 3189

Hygrothermal Damage Mechanisms in Graphite-Epoxy Composites

Frank W. Crossman, R. Ernest Mauri,
and W. John Warren

CONTRACT NAS2-9563
DECEMBER 1979

NASA

156

NASA Contractor Report 3189

Hygrothermal Damage Mechanisms in Graphite-Epoxy Composites

Frank W. Crossman, R. Ernest Mauri,
and W. John Warren
Lockheed Missiles and Space Co., Inc.
Palo Alto, California

Prepared for
Ames Research Center
under Contract NAS2-9563

National Aeronautics
and Space Administration

Scientific and Technical
Information Branch

1979

A

FOREWORD

This final report documents the work performed under NASA contract NAS 2-9563 during the period 10 April 1977 to 10 May 1978. Dr. Howard Nelson of NASA/Ames Research Center served as the technical monitor. Dr. F. W. Crossman was principal investigator and program manager. He was assisted by Mr. R. E. Mauri who supervised the composite fabrication and characterization and by Mr. W. J. Warren who supervised moisture conditioning, hygrothermal cycling and mechanical testing.

The authors wish to express their gratitude for the contributions of Ms. Colleen Miller and Mrs. Vivian Avery in the preparation of this final report and previous progress reports under this contract.

ABSTRACT

This report covers experimental and analytical studies of T300/5209 and T300/5208 graphite-epoxy laminates: (1) to determine the coupling between applied stress, internal residual stress, and moisture sorption kinetics, (2) to examine the microscopic damage mechanisms due to hygrothermal cycling, (3) to evaluate the effect of absorbed moisture and hygrothermal cycling on inplane shear response, (4) to determine the permanent loss of interfacial bond strength after moisture absorption and drying, and (5) to evaluate the three-dimensional stress state in laminates under a combination of hygroscopic, thermal and mechanical loads. Specimens were conditioned to equilibrium moisture content under steady exposure to 55 or 95% RH at 70 or 93°C. Some specimens were tested subsequent to moisture conditioning and 100 cycles between -54°C and either 70°C or 93°C.

The transverse and through thickness expansion of unidirectional composites due to absorption of equilibrium moisture concentrations were determined. Desorption of moisture at 70°C was found to be insensitive to initial moisture content, applied stress and internal residual stress. Dimensional changes on $(0_4,90_4)_T$ laminates were measured during hygrothermal cycling to assess alteration of laminate residual stress. Elastic laminated plate theory was successfully used to predict the moisture altered residual stress state of T300/5208 laminates. In T300/5209 the strong dependence of residual stress on hygrothermal history was indicative of viscoelastic behavior.

The inplane shear response was determined as a function of moisture content, temperature, and hygrothermal cycling history. Permanent alteration in room temperature interlaminar shear strength after hygrothermal cycling was also assessed. Cycling was found to have no measurable effect on inplane shear and interlaminar shear response and caused no significant microstructural damage after 100 cycles.

Finite element analysis showed that the most severe stresses near laminate free edges were introduced during moisture desorption and combined mechanical loading. Arguments based on fracture mechanics concepts indicate that edge cracking due to hygrothermal loading alone will be more pronounced in thick laminates and suppressed in the thin 8-ply laminates examined in this study.

TABLE OF CONTENTS

Chapter	Title	Page
	FOREWORD	i
	ABSTRACT	ii
	LIST OF TABLES	v
	LIST OF FIGURES	vi
1	HYGROTHERMAL DEGRADATION OF GRAPHITE-EPOXY COMPOSITES	1-1
	1.0 INTRODUCTION	1-1
	1.1 ASSESSMENT OF HYGROTHERMAL DEGRADATION - LITERATURE REVIEW	1-6
	1.1.1 Definition of Environment	1-6
	1.1.2 Effect of Moisture on Mechanical Properties	1-7
	1.1.3 Effect of Hygrothermal Cycling on Kinetics of Moisture Sorption	1-10
	1.1.4 Effect of Hygrothermal Cycling on Mechanical Properties	1-12
	1.1.5 Assessment of Hygrothermal Degradation Mechanisms	1-12
	1.2 PROGRAM DESCRIPTION	1-14
	1.3 MATERIAL PROCESSING	1-19
2	THE COUPLING BETWEEN APPLIED AND RESIDUAL STRESS AND MOISTURE SORPTION	2-1
	2.1 DIMENSIONAL CHANGES CAUSED BY MOISTURE ABSORPTION	2-1
	2.2 MOISTURE ALTERED RESIDUAL STRESSES	2-5
	2.3 DESORPTION UNDER STRESS	2-9
	2.4 INFLUENCE OF APPLIED STRESS DURING DESORPTION ON RESIDUAL STRESSES	2-17
	2.5 HYGROTHERMAL CYCLING EXPERIMENTS	2-20
3	THE INFLUENCE OF HYGROTHERMAL HISTORY ON MATRIX AND INTERFACE DOMINATED LAMINATE PROPERTIES	3-1
	3.1 INPLANE SHEAR TESTS	3-1
	3.2 INTERLAMINAR SHEAR TESTS	3-10
4	MICROSCOPIC EVIDENCE FOR DAMAGE DUE TO HYGROTHERMAL CYCLING	4-1
	4.1 MICROSCOPIC EXAMINATION AFTER 10 HYGROTHERMAL CYCLES	4-1
	4.2 MICROSCOPIC EXAMINATION AFTER 100 HYGROTHERMAL CYCLES	4-1

TABLE OF CONTENTS (continued)

Chapter	Title	Page
5	ANALYSIS OF HYGROTHERMALLY INDUCED STRESS IN GRAPHITE-EPOXY LAMINATES	5-1
	5.1 ANALYSIS DESCRIPTION	5-2
	5.2 ANALYSIS OF MOISTURE INDUCED STRESSES	5-3
	5.3 HYGROTHERMAL STRESS ANALYSIS	5-7
6	DISCUSSION OF RESULTS	6-1
	6.1 ASSESSING PERMANENT AND REVERSIBLE INTERFACIAL BOND DEGRADATION	6-1
	6.2 ENERGY CONCEPTS FOR INITIATION AND GROWTH OF HYGROTHERMAL DAMAGE	6-5
	6.3 CONCLUSIONS	6-11
	REFERENCES	7-1
Appendices		
A	MATERIAL PROCESSING INFORMATION	A-1
B	MECHANICAL TESTING TABULATION	B-1

LIST OF TABLES

Table No.	Title	Page
1	Average Moisture Content of Saturated* Component Specimens	2-2
2	Results of Four-Point Flexure Tests (ℓ' = L/3)	3-15
A1	Laminate Processing Procedure	A-9
A2	Volume Fraction Analysis of Laminate Panels	A-10
B1	Hygrothermoelastic Constants at 25°C	B-2
B2	Four-Point Flexure Testing	B-3
B3	$(\pm 45_2)_s$ T300/5208 and T300/5209 Tensile Test Results	B-4
B4	$(0_{16})_T$ T300/5208 and T300/5209 Interlaminar Shear Strength Results	B-12

LIST OF FIGURES

Figure Number	Title	Page
1	Dimensional Changes in Transverse ($\Delta v/v$) and Through Thickness ($\Delta z/z$) Directions in Unidirectional Composites vs. Equilibrium Moisture Content	2-4
2	Measured and Predicted Curvature of Nonsymmetric $(0_4,90_4)_T$ T300/5208 Laminates vs. Equilibrium Moisture Content and Exposure Temperature	2-6
3	Measured and Predicted Curvature of Nonsymmetric $(0_4,90_4)_T$ T300/5209 Laminates vs. Equilibrium Moisture Content and Exposure Temperature	2-7
4	Appearance of Clad T300/5208 and T300/5209 (Spec. 3-10 Only) After Exposure to 55% RH and 95% RH (Spec. 21-8 Only) at 93°C. Note Edge Delamination of 3-10 and Buckling of 21-10 and 21-8	2-10
5	Diagram of Fixture Employed to Stress Laminates During Desorption at 70°C. Note that the Radius of Curvature is Constant Over the Center Section	2-13
6	T300/5208 Desorption Under Stress Experiments. Values of Desorption Coefficient at 70°C are Shown. Specimens Flexed to 25% of Ultimate Curvature Based on Table B2	2-14
7	T300/5209 Desorption Under Stress Experiments. Values of Desorption Coefficient at 70°C are Shown. Specimens Flexed to 25% of Ultimate Curvature Based on Table B2	2-15
8	Appearance of $(0/90)_{2s}$ Clad T300/5209 Laminates Equilibrated at 93°C/55% RH and Then Desorped Under Flexure at 70°C	2-16
9	25°C Curvature of T300/5208 $(0_4,90_4)_T$ Laminates Exposed to Different Hygrothermal and Mechanical Histories	2-18
10	25°C Curvature of T300/5209 $(0_4,90_4)_T$ Laminates Exposed to Different Hygrothermal and Mechanical Histories	2-19
11	Effect of Hygrothermal Cycling on Equilibrium Moisture Content	2-22
12	25°C Curvature of T300/5208 $(0_4,90_4)_T$ Laminates as a Function of Hygrothermal History	2-23

LIST OF FIGURES (continued)

Figure Number	Title	Page
13	25°C Curvature of T300/5209 $(0_4,90_4)_T$ Laminates as a Function of Hygrothermal History	2-24
14	Appearance of $(+45_2)_S$ Laminates After Tensile Testing (a) 22-15 is T300/5208 Equilibrated at 70°C/95% RH and Tested at 25°C (b) 7-14 is T300/5209, Equilibrated at 70°C/95% RH and Tested at 25°C (c) 8-29 is T300/5209, Dry, Tested at 70°C. Note Necking (d) 10-72 is T300/5209, Dry, Cycled 100 Times to 93°C and Tested at 93°C	3-2
15	The Influence of 100 Hygrothermal Cycles on the In Plane Shear Strength of T300/5208 at 25°C	3-4
16	The Influence of 100 Hygrothermal Cycles on the In Plane Shear Strength of T300/5209 at 25°C	3-5
17	The Influence of 100 Hygrothermal Cycles on the Shear Behavior of T300/5208 at 93°C	3-6
18	Representative Shear Stress-Strain Response at 25°C as a Function of Equilibrium Exposure to Moisture . . .	3-7
19	Representative Shear Stress-Strain Response at 70°C as a Function of Equilibrium Exposure to Moisture	3-8
20	Representative Shear Stress-Strain Response at 93°C as a Function of Equilibrium Exposure to Moisture	3-9
21	Shear Modulus of T300/5208 vs. Temperature. Range Bands Include Data for All Cycled and Uncycled Specimens	3-11
22	Shear Modulus of T300/5209 vs. Temperature. Ranges Include All Cycled and Uncycled Specimen Data	3-12
23	In Plane Shear Strength of T300/5209 vs. Temperature. Ranges Include All Cycled and Uncycled Specimen Data .	3-13
24	In Plane Shear Strength of T300/5208 vs. Temperature. Ranges Include All Cycled and Uncycled Specimen Data .	3-14

LIST OF FIGURES (continued)

Figure Number	Title	Page
25	Analysis of Expected Failure Modes in Unidirectional Composites as a Function of Span to Depth L/h Ratio and Flexure Test Configuration (See Fig. 26)	3-17
26	(a) Flexural Test Geometry for Short Beam Shear (SBS) and Four-Point Bend (FPB) Tests (b) Typical Shear Failures in the Four-Point Bending (S = L/3) Fixture. See Table B4 for Specimen Hygrothermal History	3-18
27	Interlaminar Shear Strength of T300/5208 vs. Equilibrium Moisture Absorbed Prior to Cycling, Drying and Testing .	3-20
28	Interlaminar Shear Strength of T300/5209 vs. Equilibrium Moisture Absorbed Prior to Cycling, Drying and Testing .	3-21
29	Schematic of Surfaces Examined by Metallography and Metallographic Procedure	4-2
30	(a) Plate D2826, 100X, $(0_8)_T$ T300/5209, Spec 1-4, Dry, -54°C to 93°C/100 Cycles (b) Plate D2828, 1000X, Spec. 1-4	4-4
31	(a) Plate D2829, 100X, $(+45/-45/0/90)_S$ T300/5209, Spec 12-4, Dry, -54°C to 93°C/100 Cycles (b) Plate D2831, 1000X, Spec. 12-4	4-5
32	(a) Plate D2834, 100X, $(45/-45/0/90)_S$ T300/5209, Spec 12-8, Exposed 70°C/95% RH, -54°C to 93°C/100 Cycles (b) Plate D2832, 500X, T300/5209, Spec. 12-6, Exposed 70°C/95% RH, -54°C to 70°C/100 Cycles	4-6
33	(a) Plate D2837, 100X, T300/5209, Spec. 13-2, Exposed 70°C/95% RH, -54°C to 70°C/100 Cycles (b) Plate D2838, 500X, Spec. 13-2	4-8
34	(a) Plate 2836, 500X, $(90/0/+45)_S$, Spec 15-8, Exposed 70°C/95% RH, -54°C to 70°C/100 Cycles (b) Plate D2840, 500X, T300/5209, Spec. 15-4, Exposed 70°C/95% RH, -54°C to 93°C/100 Cycles	4-9
35	(a) Plate D2807, 100X, $(+45/0/90)_S$ T300/5208, Spec 27-4, Dry, -54°C to 93°C/100 Cycles (b) Plate D2815, 100X, T300/5208, Spec. 27-12, Exposed 70°C/55% RH, -54°C to 93°C/100 Cycles	4-10

LIST OF FIGURES (continued)

Figure Number	Title	Page
36	(a) Plate D2810, 100X, T300/5208, Spec. 27-8, Exposed 70°C/95% RH, -54°C to 93°C/100 Cycles (b) Plate D2811, 100X, Spec. 27-8, Section at 90° to (a)	4-11
37	(a) Plate D2817, 100X, $(90/0/45/-45)_s$ T300/5208, Spec 30-2, Dry, -54°C to 60°C/100 Cycles (b) Plate D2823, 100X, T300/5208, Spec. 30-8, Exposed to 70°C/95% RH, -54°C to 93°C/100 Cycles	4-13
38	(a) Plate D2843, 80X, $(90/0/\pm45)_s$ T300/5208, Spec 28-4, Exposed to 70°C/95% RH, -54°C to 93°C/100 Cycles (b) Plate D2844, 500X, Spec. 28-4	4-14
39	(a) Geometry of Symmetric 8-Ply Laminate (b) Finite Element Grid	5-2
40	(a) Average Weight Gain (Loss) during Absorption (Desorption) Relative to the Equilibrium Moisture Content M_s (b) Moisture Concentration C/C_s after Absorption Time t_4 ($M/M_s \approx 4\%$) (c) Moisture Concentration C/C_s after Absorption Time t_{45} ($M/M_s \approx 45\%$)	5-4
41	(a) σ_z Through Thickness Distribution near Free Edge of Unidirectional 8-Ply Laminate during Desorption from Equilibrium Moisture Content M_s (b) σ_z Distribution Along Midplane of Unidirectional 8-Ply Laminate during Desorption	5-8
42	σ_z Through Thickness Distributions in $(90, 0, 45, -45)_s$ Laminate due to Temperature, Moisture, and Tensile Strain	5-10
43	σ_z Through Thickness Distributions in $(45, -45, 0, 90)_s$ Laminate due to Temperature, Moisture, and Tensile Strain	5-11
44	σ_z Through Thickness Distributions in $(\pm45, 0, 90)_s$ and $(90, 0, \pm45)_s$ Laminate at Temperatures Indicated Following a Desorption Time t_{-4} from Equilibrium Level M_s	5-12
45	σ_z Through Thickness Distributions in $(90_2, 0_2)_s$ Laminate Due to Temperature and Moisture	5-14

LIST OF FIGURES (continued)

Figure Number	Title	Page
46	σ_z Through Thickness Distributions in $(90_2, 0_2)_s$ Laminate after Desorption Time t_{-4} Following Saturation at Moisture Content M_s	5-15
47	σ_z Through Thickness Distributions in $(0_2, 90_2)_s$ Laminate due to Temperature and Moisture	5-16
48	The Time Dependence of σ_z (z = 0) during Desorption in 8-Ply Unidirectional Laminate at Three Positions near the Free Edge (y = b). Moisture Content during Desorption Also Plotted	5-17
49	σ_z Through Thickness Distributions in $(\pm 45, 0, 90)_s$ and $(90, 0, \pm 45)_s$ Laminates after a Desorption Time t_{-4} Following Saturation to M_s and under an Applied Tensile Strain of 5000 μin/in	5-20
A1	Differential Scanning Calorimetry of Narmco T300/5208 and T300/5209 Prepreg	A-2
A2	Dynamic Dielectric Analysis of T300/5208 Prepreg	A-3
A3	Dynamic Dielectric Analysis of T300/5209 Prepreg	A-4
A4	(a) T300/5208, Panel 17, As Fabricated (b) T300/5208, Panel 21, As Fabricated	A-5
A5	(a) T300/5208, Panel 27, As Fabricated (b) T300/5208, Panel 28, As Fabricated	A-6
A6	(a) T300/5209, Panel 2, As Fabricated (b) T300/5209, Panel 6, As Fabricated	A-7
A7	(a) T300/5209, Panel 12, As Fabricated (b) T300/5209, Panel 13, As Fabricated	A-8

CHAPTER 1

HYGROTHERMAL DEGRADATION OF GRAPHITE-EPOXY COMPOSITES

1.0 INTRODUCTION

Since the study of Hertz et al. [1] in 1972, it has been known that the thermomechanical properties of graphite-epoxy laminates can be degraded by the absorption of moisture from humid environments. The nature of degradation in a particular property can be attributed to the effect of absorbed water on the fiber, the matrix, and the fiber-matrix interface or combinations of these three. Because of a number of studies which have determined little effect of water on fiber-dominated composite properties [2-4], it is generally accepted that graphite fibers, unlike glass fibers [5], are not degraded by exposure to moisture. On the other hand, there is much evidence that the matrix or interface sensitive composite response, particularly under transverse normal, inplane shear, and interlaminar shear loading, is strongly altered by the hygrothermal history and test conditions [4-7]. Repeated exposure to temperature cycles such as those caused by aerodynamic heating of supersonic aircraft or space shuttle or even by radiative solar heating of commercial aircraft on the runway has been found to alter the moisture sorption kinetics of graphite-epoxy composites. There is concern that the thermo-mechanical properties may also be degraded by hygrothermal cycling [7,8].

Epoxy resins are particularly susceptible to significant moisture absorption because of their hydrophilic polar character. The epoxy polymer absorbs moisture by volumetric diffusion. The absorbed water exists in the form of hydrogen-bonded molecules or clusters of molecules within the polymer [10]. Moisture in either form acts to swell the molecular structure, increasing its "free volume" [11]. The manifestations of moisture in the polymer include plasticization, enhanced creep and stress relaxation, and reduction in ultimate strength and stiffness properties. The magnitude of these changes depends on the

amount of moisture absorbed, the moisture concentration profile and the ambient temperature. The degree of moisture absorption is in turn dependent on the composite geometry, ambient relative humidity and temperature, and the length of the exposure.

The volumetric diffusion coefficient, D, associated with moisture absorption at 20°C is several orders of magnitude smaller than the thermal diffusivity of the epoxy [12]. The time required to bring the polymer of thickness ℓ to 99.9% of equilibrium under a steady temperature and humidity is given approximately by the equation [13]

$$t_{eq} \sim 0.67\ \ell^2/D\ .$$

For a polymer of 0.25 cm thickness and a diffusion coefficient at 20°C of 5×10^{-10} cm^2/sec, the time to reach equilibrium is $8.75 \times 10^{+7}$ sec or nearly three years. Moisture diffusivity is, however, very sensitive to temperature and increases by several orders of magnitude in the 20°C to 150°C temperature range [14]. The process of moisture absorption can thus be accelerated in order to determine in a reasonably short period of weeks or months the effect of moisture on composite polymer properties.

Accelerated moisture conditioning at high temperatures and humidities can result in the sorption of unrealistically high concentrations of water in the polymer compared to what would be absorbed under the ambient environment [15]. Under extreme conditions where the glass transition temperature of the graphite-epoxy composite is exceeded during steady exposure to temperature and humidity, the composites have developed delaminations which are totally absent in specimens exposed to lower temperature and humidity [14].

The effect of moisture on the fiber-matrix interface can be at least threefold. Moisture may act to break chemical bonds (as observed in glass-epoxy composites [5]) between the fiber and matrix and result in a permanently altered interface strength even after desorbing the composite to the dry state.

Adsorption of moisture at the interface may also alter its surface free energy. By considering the effect of surface energy on the Griffith fracture equation, Kaeble et al. [16] postulate a reduction in the interfacial strength of graphite-epoxy composites containing absorbed water which can sometimes be reversed if the water is removed. Finally, the swelling of the matrix due to absorbed moisture counteracts the contraction of the matrix caused by cooling the composite from its cure temperature. At some combination of temperature and moisture the average residual stress normal to the fiber-matrix interface changes from that of compression due to the thermal contraction of the matrix around the fiber to an average state of tension [7]. The state of tension may enhance chemical bond breaking or simply lower the effective applied stress at which the interface reaches its failure stress. In viscoelastic media, such as graphite-epoxy composites, the residual stresses in the matrix, fiber, and at fiber-matrix interface can be altered by the hygrothermal history. A thirty percent increase in residual stress has been measured after hygrothermal cycling and returning the material to its initial dry state [14].

Matrix plasticization at high temperatures may also account for permanent interface damage by a mechanism proposed by Browning [36]. Browning studied a neat resin typical of the basic composition of the 175°C (350°F) curing epoxies (such as 5208, 3501 and 934). He found microcracking in the resin became apparent only when thermal cycling to a temperature greater than the wet glass transition temperature of the resin. Surface intrusions and extrusions typical of metals under fatigue loading were observed which eventually cracked after cycles at high temperatures and/or high moisture contents. Permanent dimensional changes after drying were attributed to the microcracking. Much of the microcracking was attributed to moisture enhanced creep rupture process occurring during exposure to the elevated temperature portion of the cycle. One might expect an enhancement of fiber-matrix bond rupture by the same argument.

A more insidious bond degradation can occur even at exposure temperatures below the wet glass transition temperature of the epoxy matrix. In some

material systems the partially cured polymer sizing placed on the fiber bundles before prepregging may be more susceptible to moisture enhanced degradation than the matrix epoxy. Augl and Berger [29] attributed the proportionately greater loss of shear strength of moisture exposed T300/5208, compared to HTS/5208, to the epoxy sizing on the T300 fibers. In this case, the shear strength returned to its initial value after drying. Permanent losses in the dry 175°C flexural strength of T300/934 composites after 24-hour water boil were noted by Marks et al. [28]. However when T300 fibers were sized with a more moisture-reistant polyimide having a high wet glass transition temperature, the T300/934 composite suffered negligible permanent loss in 20°C and 175°C flexural strength after 24-hour water boil and drying.

At the laminate level, additional degradation mechanisms are influenced by hygrothermal history. Nonuniform distribution of moisture has been calculated to cause steep gradients of stress near laminate surfaces [18] or at the free edges [19] which could contribute to microcracking of individual plies or delamination of plies as observed in studies by Browning and Hartness [2] and by Hedrick and Whiteside [20].

Browning [36] describes a mechanism for crack formation and growth which is related to the gradient in moisture concentration. These gradients in moisture content lead to stress gradients due to the swelling or expansion which accompanies the volumetric sorption of water into the resin matrix. Browning points out that stress relaxation can occur during thermal cycling which can result in the development of a tension-compressive stress cycle, concomitant with hygrothermal fatigue.

Another damage mechanism has been identified which does not require exposures to extreme thermal spike conditions, typical of supersonic aircraft, to initiate damage. Analysis has been made of the internal hygrothermal residual stresses in crossplied $(0/90)_s$ laminates which develop during absorption and desorption of moisture. The hygro-thermal-elastic analysis

is based on a finite element model of the laminate structure coupled to a finite element diffusion analysis of the moisture distribution which develops under non-equilibrium and equilibrium conditions [19]. Results have shown that the highest hygrothermal tensile stresses develop near the laminate edges and surfaces after short desorption times when the gradients of moisture are most severe. As a consequence of the desorption caused-near surface-tensile stresses, one might expect a greater propensity for cracking if surface desorption takes place at low temperatures where the matrix is brittle. Cracking of neat resin specimens and graphite-epoxy laminates, indeed, has been noted by both Hedrick and Whiteside [20] and Browning and Harkness [2] after drying at room temperature. However, Hedrick and Whiteside note that the microcracking is observed only in specimens thicker than 0.25 cm.

It is evident from this brief discussion that the matrix, interface, and laminate degradation mechanisms are intimately coupled in graphite-epoxy composites. The study described in this report was undertaken to elucidate the nature of this coupling and, from a deeper understanding of this process, to develop an accelerated moisture conditioning and test methodology appropriate for realistically assessing the effect of moisture on the alteration of composite thermomechanical properties. The remainder of this chapter contains a literature review of methods to assess moisture related degradation and a discussion of previous studies of hygrothermal cycling in graphite epoxy composites. An outline of the experimental and analytical program is then presented and followed by a description of the materials chosen for this study and the fabrication procedures employed. Chapter 2 describes a set of experiments designed to investigate the coupling between applied stress, internal residual stress and the kinetics of moisture sorption. Chapter 3 examines the alteration of inplane and interlaminar shear properties by hygrothermal cycling. Chapter 4 describes the microscopic examination of composite laminates subjected to hygrothermal cycling while Chapter 5 contains an elastic analysis of the stress state near laminate free edges as influenced by the gradient of moisture present during sorption. Chapter 6 discusses the implications of the results to the development of a comprehensive test methodology and makes recommendations for additional research in this area.

1.1 ASSESSMENT OF HYGROTHERMAL DEGRADATION - LITERATURE REVIEW

1.1.1 Definition of the Environment and Level of Moisture Absorption

One of the first steps taken to realistically assess the effect of moisture on composite properties was the application of volumetric diffusion theory to determine the concentration of absorbed moisture as a function of position. Shen and Springer [13] determined that under steady temperature and humidity exposure, the T300/934 composites obeyed the simplest form of the mass diffusion equations in which the mass flux J is given by

$$J = - D \nabla c$$

where ∇c is the concentration gradient and D, the diffusion coefficient, is independent of concentration. While this assumption of concentration independence greatly simplifies the mathematical modeling of diffusion in one, two, or three dimensions, Shirrell [21] has noted several additional mechanisms which can contribute to moisture transport in composites and may account for several anomalies in moisture sorption discovered by that investigator. Other studies [14] have shown that the desorption coefficient in GY70/339, T300/5209 and T300/934 systems is independent of initial equilibrium moisture content although the scatter in calculated diffusion coefficients on identically exposed specimens was typically $\pm$ 20 percent.

In the absence of well-defined diffusion models which unambiguously predict the anomalies which have been observed, the concentration independent diffusion equations have been employed in many recent studies to assess the level of moisture absorption during exposure to in-service environments. Unnam and Tenney [22] and Whiteside [23] used data available from the National Weather Bureau to define the effective relative humidity and temperature at the surface of a composite aircraft structure exposed to a runway environment. Daily, weekly, monthly and yearly weather cycles and local heating due to solar radiation were considered in the diffusion models. Typical 12-16 ply composites reached in three years of service a typical

absorbed moisture content of 1.0 - 1.2 percent water in average continental U.S. conditions, although consideration of tropical and desert climates led to a calculated range of 0.6 - 1.4 percent average water content.

Springer [24] applied idealized hygrothermal cycling boundary conditions to his diffusion model to show that daily temperature humidity cycling causes large changes in moisture concentration near the composite surface. The interior or core of the composite remains at a relatively stable moisture content. The boundary layer zone which sees large fluctuations in moisture concentration is found to be approximately 0.012 cm (or roughly one ply in thickness). Whiteside [23] verified this boundary layer size under conditions typical of tropical climates.

These calculations have important implications for the investigation of hygrothermal damage mechanisms. The thermomechanical response of composite specimens containing average moisture contents up to the maximum expected value encountered in service must be determined. In addition, it may be necessary to examine certain properties of composites which may be sensitive to a steep boundary layer gradient of moisture which develops during hygrothermal cycling. The next three sections review the literature with emphasis on those composite properties which have been found to be most sensitive to moisture sorption and hygrothermal cycling.

1.1.2 The Effects of Moisture on Mechanical Properties

Studies of the influence of absorbed moisture on ultimate tensile strength, and tensile and compressive moduli have recently been reviewed by Springer [3,4]. Longitudinal unidirectional and quasi-isotropic laminate properties were found insensitive to moisture and temperature. Transverse unidirectional composite properties were susceptible to significant reductions compared to ambient dry conditions. The loss in room temperature transverse tensile strength was as large as 50 percent in T300/5208 composites although the loss of tensile modulus was on the order of 10 percent. At elevated temperatures both transverse tensile strength and modulus was reduced

with increasing moisture content. Verette [26] showed similar results in tests of AS/3501-5 composites. Interestingly, while the reduction of transverse compressive strength, transverse tensile modulus, and transverse compressive modulus was less than 20 percent at room temperature, the transverse tensile strength was reduced by nearly 40 percent after absorbing 1.9 percent water. Verette also demonstrated the sensitivity of longitudinal compressive strength and in-plane shear strength (rail shear) to absorbed moisture.

The flexure test has been employed most often to assess the effect of moisture on composite properties. At small span-to-thickness ratios the specimen will often fail in shear near the midplane rather than by tensile or compressive failure near the outer surfaces. The existence of these three possible failure modes, coupled with local bearing failures under the loading pins, often makes it difficult to interpret the trend of moisture effect on the composite. Hertz [1] was one of the first to observe a change of failure mode from tensile to compression in flexure tests of dry and wet unidirectional composites conducted at 175°C.

A literature survey [27] shows that the observed changes in room temperature flexural strength due to absorbed moisture have been found to be either positive or negative depending on the particular graphite-epoxy system being studied. In the absence of any significant degradation in fiber dominated longitudinal tensile strength, the mixed results appear to be caused by the competition between an increased matrix ductility (allowing a more effective load transfer to the fibers and thus higher strength) and a decrease in interfacial bond strength (which promotes debonding and less effective load transfer to the fibers) [28].

Alteration of flexural failure modes due to moisture absorption makes a direct comparison of strength values meaningless in some cases. Furthermore the flexural test is also sensitive to moisture gradients. The flexural strength is dominated by the failure of the highest stressed outer plies which, depending on the hygrothermal history, may contain more or less than the average moisture concentration. Conclusive analysis of hygro-

thermal degradation mechanisms by flexural testing does not appear to be a viable experimental procedure.

Short beam shear tests are also commonly employed to evaluate moisture effects [27]. However, a loss in shear strength can be the result of a combination of matrix plasticization or loss of interfacial bond strength. Augl's study [29] of T300/5208 and HMS/5208 short beam shear properties as a function of temperature and moisture content shows distinctly different behavior for the two systems. The more rapid loss of short beam shear strength with increasing temperature and moisture in T300/5208 is attributed by Augl to the degradation of the epoxy sizing at the T300 fiber-matrix interface.

Short beam shear testing was originally developed for fiberglass composites where the test served to determine the interlaminar (or interfacial) shear strength of the composite; and in evaluating early graphite-epoxy composites, it served the same purpose. However, with the development of surface-treated graphite fibers, the interfacial shear strength of the resulting composite rose to such high values that matrix shear deformation or compressive failure under the loading pins became commonly observed failure modes [27]. Interpretation of moisture-induced degradation of short beam shear strength is clouded by the nearly uniform absence of failure mode description in these studies.

Beaumont [30] and Kaelble [9,16,31] have examined the effect of moisture exposure on the fracture energy under impact (Charpy test) and under slowly applied loads (V-notch three-point bend test). The two tests give similar fracture energy values [30]. However, the direction of change of fracture energy with moisture exposure depends upon the particular composite material chosen for study. Beaumont showed that, for a particular fiber-matrix system, the fracture energy peaks at intermediate levels of interlaminar (or interfacial) strength. By a micromechanical model, Kaelble [31] showed that the peak in the energy curve occurs at a critical shear strength of $\tau^* = \sigma_f \sqrt{2G}/[4\sqrt{E_f}\, f(V_f)]$, where σ_f is the fiber strength, E_f the fiber modulus, G the

matrix shear modulus, and $f(V_f)$ a geometric constant inversely related to fiber volume fraction. If the dry interlaminar shear strength exceeds τ^*, then moisture, by lowering the shear strength, will drive the fracture energy higher. If the dry interlaminar shear strength is already below τ^*, then moisture can only depress the fracture energy. Trends in the moisture altered fracture energy of epoxy composites reinforced by HTS, AS, Morganite I and Morganite IS fibers [27] agreed with the micromechanics model just given.

The work of fracture contains large contributions from both matrix shear and fiber pullout, both of which are influenced by the level of matrix plasticization and matrix swelling as well as by the degradation of interfacial shear strength by moisture. As was found with the flexure and short beam shear tests, measurement of fracture energy in bending does not provide a means to separate hygrothermal effects on the several failure modes which contribute to the overall composite response.

1.1.3 Effect of Hygrothermal Cycling on the Kinetics of Moisture Sorption

The first evidence that hygrothermal cycling itself could cause composite degradation was described by McKague [8] in experiments on T300/5208 which simulated the thermal spike caused by aerodynamic heating during a supersonic dive in a jet aircraft. McKague found that both the rate and level of moisture absorption were increased during and subsequent to hygrothermal cycling between -54°C and 175°C. Since that initial study, several other investigations have been conducted to assess the level of degradation in sorption kinetics as a function of temperature extreme, temperature cycling rate, level of absorbed moisture, and material selection. Bohlman and Derby [32] conditioned T300/934 laminates to one percent average moisture content and then exposed them to thirty thermal "space shuttle" spikes between 20°C and 175°C. No alteration of moisture sorption kinetics was found. The investigators observed that the rates of thermal spiking were much less than those used in McKague's study. They noted that the supersonic spike heatup rate was 50°C/min and the cooldown rate was 500°C/min. In the space shuttle

spike, the heatup rate was 6°C/min and cool down rate was 4°C/min. Although they attributed the difference in behavior to the existence of large thermal gradients through the composite thickness in the supersonic spike, the conductivity of graphite-epoxy is sufficiently high [12] to bring a 0.10 cm thick composite to equilibrium in only one second and through thickness temperature gradients of only a few degrees are possible.

Verette [26] found that room temperature moisture absorption in AS/3501-5 was increased by thermal spiking between 20°C and 120°C at heatup/cooldown rates of 50°C/min and 17°C/min respectively. Augl [29] found that the 30°C diffusion coefficient of T300/5208 progressively increased from 1.2×10^{-10} cm^2/sec to 2.54×10^{-10} cm^2/sec after exposure to 10, 40, and 80 cycles between 20°C and 150°C at a heating/cooling rate of approximately 60°C/min. The moisture content prior to spiking was 0.6 percent. A number of studies have investigated the effect of initial moisture content on thermal spike damage. Powell and Zigrang [33] examined T300/934 laminates humidified (95% RH at 60°C) to 0.6, 0.8, and 1.0% average moisture content and then exposed to 100 space shuttle thermal spikes. The specimens were subsequently dried and re-exposed to humidity (95% at 60°C). Although the initial rate of weight pickup was identical to the unspiked specimens, the equilibrium water content was greater in the spiked specimens. The largest increase was observed for the specimen humidified to 1.0 percent water prior to spiking. DeIasi and Whiteside [10] observed that thermal cycling enhanced the rate and level of moisture absorbed at 77°C in AS/3501-5 composites, when moisture contents were greater than 0.8 percent. Specimens conditioned at relative humidities less than 50% did not show any change due to thermal cycling. Studies by Mauri et al. [14] showed that increases by a factor of two in diffusion coefficient were common in T300/5209 and GY70/339 composites absorbed, desorbed and reabsorbed at 51 and 71°C and 95% relative humidity. Similar sorption tests conducted at lower relative humidity (71 and 57%) and lower temperature (20°C/95% humidity) showed little or no change in diffusion coefficient.

1.1.4 The Effect of Hygrothermal Cycling on Mechanical Properties

Although the alteration of moisture sorption characteristics by hygrothermal cycling is well documented, very little work has been done to examine the effect of cycling on the thermomechanical properties of composites. Bergman and Dill [34] examined the 0° and 90° compressive properties and rail shear properties of $(0, \pm 45, 0)_s$ T300/934 laminates after 36 to 106 space shuttle thermal spikes. The strength in all three tests decreased with increasing temperature and moisture content but was independent of the number of thermal spikes. Augl found no degradation of the dry 20°C short beam shear and flexural strengths in T300/5208 composites moisture conditioned at 75°C/80% relative humidity and thermally cycled from 20°C to 150°C for up to 40 times. In fact, both flexural and short beam shear strength were found to increase after cycling and drying prior to testing. Browning and Hartness [2] examined the flexural strength of HTS/2546 composites at 175°C after exposure to 15 cycles consisting of 22.5 hours at 50°C/95% humidity, one hour at -54°C and 30 minutes at 120°C. A 54-percent reduction in flexural strength compared to dry specimens was found, while a 16-hour water boil reduced strength by only 27%. However, it is not clear whether the thermal cycling caused a reduction in strength beyond that which would have been observed due to the absorption of water at steady conditions of 50°C/95% humidity.

1.1.5 Assessment of Hygrothermal Degradation Mechanisms in Graphite-Epoxy Composites

A strong case has been made in this survey of the literature that the degradation of graphite-epoxy composite properties due to hygrothermal exposure is related to a combination of matrix degradation and reduction of the fiber-matrix interfacial bond strength. Although we seek to assess independently the hygrothermal degradation of matrix and interface and its relative contribution to composite thermomechanical degradation, all of the mechanical tests on composites necessarily involve the coupled response of fiber, matrix, and interface. However, it is possible to determine, by means of

several experimental and analytical techniques, hygrothermal regimes where certain degradation mechanisms or coupled mechanisms predominate. When these regimes have been assessed, additional tests may then be chosen to determine the individual contribution of matrix and interface degradation due to hygrothermal exposure.

The first step that can be taken is to separate the degradation mechanisms into those which are reversible or irreversible. One might argue that the reversibility of a mechanism has little practical value for composite aircraft design since the material will rarely be returned to its original dry state; however Augl [29] points out that knowledge of reversibility enables one to predict composite strength degradation due to that mechanism as a function of the environmental variables (for example, as Unnam and Tenney [22] predict the level of moisture in composites). If we place chemical degradation of the epoxy matrix by processes such as photo-oxidation, hydrolytic polymer chain cleavage, and high-energy radiation outside the scope of this program, the major degradation mechanisms described in Section 1.0 can be classified as follows:

Component	Degradation Mechanism	Type
Matrix	Plasticization	Reversible
"	Moisture Swelling	Reversible
"	Stress Relaxation, Creep	Partially Reversible
"	Cracking, Stress Rupture	Irreversible
Interface	Moisture-Altered Surface Energy	Reversible
"	Altered Residual Stress at Interface	Reversible* (*Partially reversible if matrix stress relaxes)
"	Debonding	Irreversible
Laminate	Ply Cracking	Irreversible
"	Delamination	Irreversible

In the program which is described in this report, experiments were designed to answer some of the questions which arose in attempting to assess

the separate contributions of the mechanisms listed to thermomechanical degradation of composites. These questions were:

1. Is moisture absorption sensitive to the lamination sequence?
2. What is the level of moisture-induced swelling?
3. Is the alteration of residual stress by moisture absorption reversible or history-dependent?
4. Does applied stress alter the kinetics of moisture desorption?
5. Does the application of applied stress during desorption alter the residual stress state?
6. What is the degree of matrix plasticization as measured by composite inplane shear properties as a function of moisture content, temperature and hygrothermal cycling history?
7. What is the degree of permanent interfacial damage, as measured by composite interlaminar shear strength, after hygrothermal cycling?
8. What is the level of microscopic damage caused by hygrothermal cycling?
9. What is the calculated level of stress caused by moisture gradients near laminate surfaces and free edges which can contribute to ply cracking and delamination?

1.2 PROGRAM DESCRIPTION

Two materials were chosen for this study: T300/5209 (a 125°C curing system) and T300/5208 (cured at 180°C and post-cured to 205°C). The T300/5209 system was originally chosen for use in the NASA/Langley-sponsored program for flight service evaluation of an advanced composite vertical tail fin on the Lockheed L1011 [35], primarily because the lower cure temperature significantly reduced the cost of tooling and fabrication compared to the 180°C curing systems. However detailed thermal analysis showed that local areas of the tail fin painted with dark blue pigment and exposed to direct solar radiation and reflected radiation from the horizontal stabilizer would reach a maximum temperature of 90°C rather than the previously cal-

culated value of 70°C. The pronounced drop in T300/5209 compressive properties at this high temperature and moisture content of one percent indicated that the material would be marginal in meeting the structural requirements, and a change to the higher temperature curing T300/5208 system was agreed upon. To examine the effect of hygrothermal cycling experienced by typical commercial aircraft, the temperature ranges chosen were -54°C to 70°C and -54°C to 93°C, corresponding to the extremes calculated for the vertical fin.

The program is broken into four major tasks described separately in each of the next four chapters:

1. The coupling between moisture sorption and laminate stress.
2. The effect of moisture on inplane and interlaminar shear behavior.
3. Microscopic examination of hygrothermally cycled laminates.
4. Analysis of moisture altered laminate stresses.

An outline of the program plan follows:

TASK 1 - This task examined moisture induced swelling effects on alteration of internal residual stresses, dimensional changes and sorption kinetics.

1A. The transverse and through thickness swelling of unidirectional composites of both materials were determined for exposures to 55 and 95 percent relative humidity at 70°C. Triplicate specimens were employed.

Total: 12 specimens

1B. Residual stress changes due to hygrothermal cycling were determined by warping measurements of $(0_4, 90_4)_T$ laminates of both materials in the following states:

(a) As dried.

(b) After moisture equilibrium is reached under 55% RH/70°C
95% RH/70°C

(c) After cycling 100 times between -54°C to 70°C
-54°C to 93°C

(d) After complete desorption.

Total: 24 specimens

1C. Alteration of sorption kinetics and internal residual stresses in the absence and presence of mechanically applied stressed were studied for the following experimental variables:

1C.1 Materials 2

T300/5208

T300/5209

1C.2 Layup 5

$(0_4, 90_4)_T$†

$(0_8)_T$*

$(90_8)_T$*

$(0, 90)_{2s}$*

$(90, 0)_{2s}$*

† T denotes the total laminate construction is shown
* clad on one side with 75 μm (3 mil) Al foil

1C.3 Initial Moisture Content 2

Equilibrium @ 55% RH/93°C†

Equilibrium @ 95% RH/93°C

† Aluminum clad laminates exposed to humidity would require approximately 3 months to reach saturation at 70°C, because the absorption is from one side only (i.e., the saturation time is four times that for samples absorbing from both sides). In order to speed up the absorption process for these specimens, an exposure temperature of 93°C was used.

1C.4 Applied Stress During Desorption at 70°C 3

None

Bending (Tensile on Side 1)**

Bending (Tensile on Side 2)**

**To 25% of curvature to cause flexural failure in the dry state at 20°C

Total: 60 specimens

TASK 2. Inplane and Interlaminar Shear Properties

2A. Matrix Dominated Shear Behavior - $(\pm 45)_{2s}$ tensile tests (duplicate specimens) were conducted to determine hygrothermally altered inplane shear response. The experimental variables included:

2A.1	Materials	2
	T300/5208	
	T300/5209	
2A.2	Moisture Content	4
	Dry	
	Equilibrium at 55% RH/70°C	
	Equilibrium at 95% RH/70°C	
	Dried after equilibrium to 95% RH/70°C	
2A.3	Hygrothermal Cycling	3
	None	
	100 cycles from -54°C to 70°C	
	100 cycles from -54°C to 93°C	
2A.4	Test Temperature	3
	20°C	
	70°C	
	93°C	
	Total:	144 specimens

2B. Evaluation of Permanent Interfacial Damage - Unidirectional specimens of both material systems were tested in flexure after hygrothermal cycling and drying to determine whether cycling alters the interfacial strength of the composite. Interlaminar shear strength (triplicate specimens) was measured as a function of

2B.1	Initial Moisture Content	3
	Dry	
	Equilibrium at 55% RH/70°C	
	Equilibrium at 95% RH/70°C	

2B.2 Thermal Cycling 3

None

100 cycles from -54°C to 70°C

100 cycles from -54°C to 93°C

Total: 54 specimens

TASK 3. Microstructural Examination - the purpose of this task was to assess microstructural damage in unidirectional and quasi-isotropic laminates as a function of temperature cycling range, number of cycles and level of absorbed moisture.

3A. Materials 2

T300/5208

T300/5209

3B. Layup 3

UD

$(\pm 45, 0, 90)_s$

$(90, 0, \pm 45)_s$

3C. Initial Moisture Content 3

Dry

Equilibrium @ 55% RH/70°C

Equilibrium @ 95% RH/70°C

3D. Thermal Cycle Range 2

-54°C to 70°C

-54°C to 93°C

3E. Number of Cycles 2

10

100

Total: 72 specimens

The influence of voids on damage accumulation were studied by exposing $(\pm 45, 0, 90)_s$ "voidy" panels of both material systems to 95 percent relative humidity, then cycling according to 3D and 3E before microscopic examination.

Total: 8 specimens

TASK 4. Stress Analysis

4A. Plane Stress Analysis - The plane stress analysis code ADV*LAM was coupled to a one-dimensional diffusion solution for the moisture concentration gradient through the laminate thickness. Curvature changes in $(0_4, 90_4)_T$ laminates and Al clad laminates were calculated on the assumption of elastic behavior and compared to experimental measurements to determine the moisture-altered residual stress state.

4B. Generalized Plane Strain Analysis - An elastic generalized plane strain finite element analysis program FREE*EDGE was coupled to a two-dimensional finite element analysis of moisture diffusion to calculate the alteration of inplane and through thickness stress components in unidirectional, cross-plied and quasi-isotropic laminates as a function of hygrothermal and mechanical loading.

1.3 MATERIAL PROCESSING

T300/5208 and T300/5209 prepreg in the form of 30.5 cm (12 in) wide unidirectional tape was ordered and received from NARMCO. The prepreg was supplied in a single roll of 3.6 kg (8 lb) for each material. Samples from each roll were taken to assess the DDA (dynamic dielectric analysis) and DSC (differential scanning calorimetry) response during the manufacturer's recommended cure cycle given in Table 1 of Appendix A. Figure 1 of Appendix A plots the temperature and heat as a function of time. The recommended cure temperatures (127°C for 5209 and 177°C for 5208) fall at the initial portion of the cure exotherm as expected.

Dynamic Dielectric Analysis was made of samples taken from the two prepreg rolls of T300/5208 and T300/5209 used in fabricating the panels for this program. Leveling off of the dissipation curve shown in Figures 2 and 3 of Appendix A is indicative of completion of curing. The temperature-time profile used for each material was chosen to match the profile used during the cure of the laminates. DDA measurements show that the cure cycle chosen provides for full curing of both prepreg rolls.

Twenty-eight 30 cm by 30 cm panels of T300/5208 and T300/5209 laminates of the type listed below were fabricated according to the processes given in Table 1A. In order to obtain some $(\pm 45, 0, 90)_s$ laminates with a higher void content, the applied pressure (Item 3 in table) was reduced to 138 KN/m^2 (20 psi) for T300/5208 and 345 MN/m^2 (50 psi) for T300/5209. Several panels were successfully fabricated with a 0.008 cm aluminum foil cladding on one side.

Layup	Number
$(0_8)_T$	1
$(0_{16})_T$	1
$(\pm 45)_{2s}$	5
$(\pm 45, 0, 90)_s$	1
$(90, 0, \pm 45)_s$	1
$(0_4, 90_4)_T$	3
$(0_8)_T$ [one side Al clad]	1
$(0, 90)_{2s}$ [one side Al clad]	1
$(\pm 45, 0, 90)_s$ [2-4% voids]	1

Table 2 of Appendix A shows the volume fraction and void fraction determined by acid digestion measurements and based on assumed specific gravity of 1.746 for T300, 1.247 for 5209, and 1.265 for 5208. The negative void fractions obtained on most panels have been commonly observed on nearly fully dense composites and can be accounted for in the equation for void fraction V_v by an inaccurate value for resin or fiber density.

$$V_v = 100 - \rho_c \left[\frac{\bar{w}_R}{\rho_R} + \frac{\bar{w}_F}{\rho_F} \right]$$

where $\bar{w}$ is weight fraction, ρ is density and R,F,C subscripts refer to the resin, fiber and composite, respectively. Fiber density measurements in T300 fibers have ranged from 1.72 to 1.80 gm/cc. A fiber specific gravity variation of 1.76 $\pm$ 0.04 results in a void fraction range (and fiber volume fraction range) of $\pm$ 1.4% in a nominally void free laminate.

The results in Table A2 show that all T300/5209 panels lie in the fiber volume range of 65 $\pm$ 2%. T300/5208 panels contain fiber volume of 67-69% which lie at the high end of the acceptable range (60-68%) of fiber contents specified for NASA-sponsored L1011 ACVF program. The low viscosity of 5208 and the enhanced bleed-out at the edges of the small 30 cm x 30 cm panels fabricated for this program made it difficult to reduce the fiber volume fraction. T300/5208 panels fabricated under reduced pressure to purposely develop voids contained approximately 58% fiber and void contents of 0.7% to 1.6%. On the other hand T300/5209 "voidy" laminates (#13, 14) are indistinguishable from all other laminates in their fiber and void content.

Metallography of selected panels of each material representative of unidirectional, crossplied, clad, and quasi-isotropic layups are shown in Figures A4-A7. The T300/5208 panels are shown to be essentially void free. The "voidy" 5208 panel shows less compaction, lower fiber volume fraction and large large voids of 1-2 x 10^{-3} cm diameter interspersed primarily between plies. T300/5209 panels generally contained even smaller voids. The estimated void content in this material is less than 1%, even in the "voidy" laminates.

CHAPTER 2

THE COUPLING BETWEEN APPLIED AND RESIDUAL STRESS AND MOISTURE SORPTION

2.1 DIMENSIONAL CHANGES CAUSED BY MOISTURE ABSORPTION

After drying all specimens for 7 days at 93°C in vacuum, moisture conditioning to equilibrium moisture content at 70° and 93°C under 55 and 95 percent relative humidity was carried out in sealed desiccators containing a glycerol-water mixture of fixed proportions to provide the required relative humidity in the enclosure. The specimen chambers were placed in air circulating ovens maintained at 70 $\pm$ 2°C and 93 $\pm$ 2°C. Specimens were removed and weighed weekly until equilibrium moisture content was reached. After equilibrium was attained, specimens were stored at room temperature under the same relative humidity to which they were exposed.

Table 1 gives the average moisture content of laminates conditioned at 70°C. The observed scatter is approximately $\pm$ .05 percent. The moisture content of specimens exposed to 70°C/55% RH shows little dependence upon material or configuration. However, exposure to 95% RH at 70°C results in a considerable difference in material response. The T300/5209 specimens absorb 1.8 $\pm$ .1 percent water at this temperature and humidity, while T300/5208 samples average only 1.3 $\pm$ 0.1 percent. The $(\pm 45)_{2s}$ specimens of each material are found to absorb a slightly higher level of water as are the laminates which were fabricated to provide a higher void content. While specimens exposed to 93°C are discussed in a later section of this chapter, it is worth noting (Fig. 6, 7) that, while the equilibrium concentration of T300/5208 laminates under 55 and 95% humidity is essentially the same at 70°C and 93°C exposures, T300/5209 shows a large increase in moisture absorption when conditioned 93°C. The equilibrium moisture content under 55% RH increases from .66 percent at 70°C to 1.35 percent at 93°C in identical $(0_4, 90_4)_T$ laminates. The

Table 1

AVERAGE MOISTURE CONTENT OF SATURATED* COMPOSITE SPECIMENS

Panel ID	Material	Layup	Exposure Conditions	
			70°C/55% RH	70°C/95% RH
1	T300/5209	$[0_8]_T$	0.82	1.92
4		$[0_4, 90_4]_T$	0.66	1.82
12		$[\pm 45, 0, 90]_s$	0.78	1.78
13		$[\pm 45, 0, 90]_s$	----	1.97**
15		$[90, 0, \pm 45]_s$	0.61	1.86
7,8		$[\pm 45]_{2s}$	0.69	2.00
16	T300/5208	$[0_8]_T$	0.76	1.29
19		$[0_4, 90_4]_T$	0.74	1.32
27		$[\pm 45, 0, 90]_s$	0.81	1.35
28		$[\pm 45, 0, 90]_s$	----	1.98**
30		$[90, 0, \pm 45]_s$	0.71	1.28
22,24		$[\pm 45]_{2s}$	0.77	1.40

* Exposed for 670 hours

** "Voidy" laminates

equilibrium moisture content under 95% RH increases from 1.83 percent at 70°C to 2.90 percent at 93°C. The steep rise in equilibrium moisture content of T300/5209 with increasing temperature and humidity is typical for graphite-epoxy laminates which are moisture conditioned at a temperature which exceeds the wet glass transition temperature [15].

Dimensional changes due to absorbed moisture were determined by micrometer measurements on unidirectional 5 x 2.5 x 0.10 cm unidirectional specimens. Dimensions at three sets of fiducial marks in the longitudinal, transverse and thickness directions were taken and averaged. The change in dimensions is expressed as the difference between the value after equilibrium moisture content was obtained and the initial dry dimension, normalized by the initial value. The results are shown in Figure 1. Longitudinal changes were essentially zero and are not plotted in the figure. The inplane transverse expansion $\Delta y/y$ shows a linear dependence on moisture content between 0.6 and 2.2 percent absorbed water, but little or no swelling associated with moisture contents less than 0.4 percent. The plot contains data from an earlier study [15]. Studies by De Iasi and Whiteside [10] and Hahn [37] have shown a similar threshold concentration below which no transverse swelling is observed. One explanation of this behavior developed by Hahn is that the first water molecules which are absorbed move preferentially to microvoids (or free volume) within the polymer molecular structure where their tendency to swell the structure is considerably less. However, in unidirectional specimens one would expect the same threshold phenomenon in swelling to occur in the thickness direction as well.

The through thickness dimension change shown in the lower portion of Figure 1 appears to indicate a larger $\Delta z/z$ change than that obtained in the transverse inplane direction (the dotted line in both plots). Epoxy-rich interlaminar zones between plies may account for such diverse behavior. T300/5208 specimens exhibited greater scatter in the $\Delta z/z$ measurements. The range of measurements for each moisture content are given by the vertical bars in each plot. The estimated absolute error in the micrometer measurements is $\pm$ 2.5 x 10^{-4} cm, or an error of $\pm$ .25% for through thickness expansion measurements, compared to $\pm$ 0.01% for inplane transverse expansion.

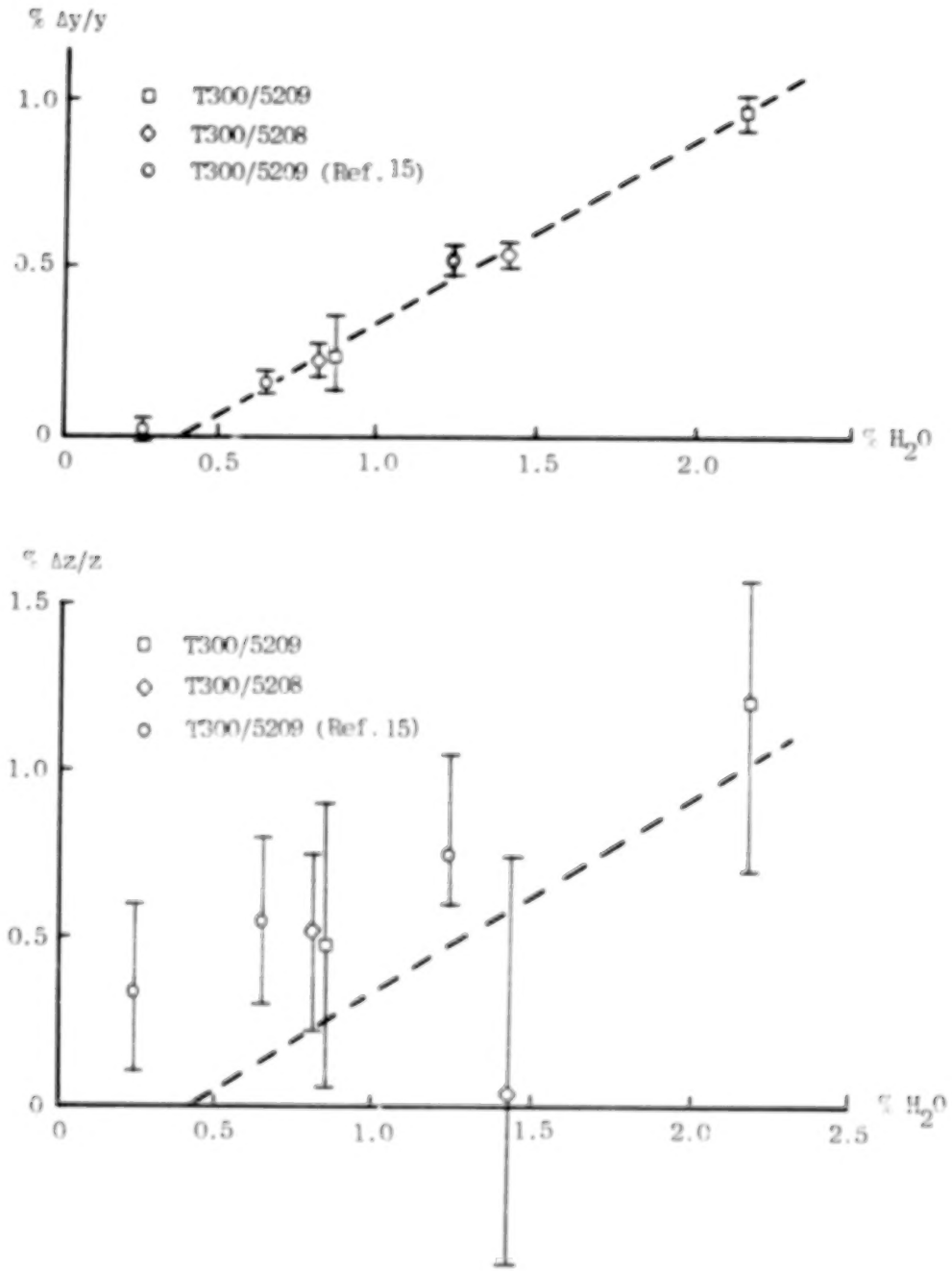

Figure 1. Dimensional Changes in Transverse (Δy/y) and Through Thickness (Δz/z) Directions in Unidirectional Composites vs. Equilibrium Moisture Content.

2.2 MOISTURE ALTERED RESIDUAL STRESSES

Figure 2 shows the curvature of T300/5208 $(0_4, 90_4)_T$ laminates before (0.0 percent water) and after sorption of equilibrium uniform moisture concentration at 70° and 93°C under 55 and 95 percent humidity. Matrix swelling due to absorbed water counteracts the matrix contraction obtained in cooling the specimen from its stress-free temperature near the cure temperature to room temperature. As a result, the curvature of these warped, nonsymmetric laminates decreases with increasing equilibrium moisture content as indicated in the figure. The curvature was determined by measuring the chord height of a 15 cm long by 2.5 cm wide specimen by means of a traveling microscope with a precision of 2.5×10^{-3} cm [14].

Longitudinal and transverse unidirectional and $(\pm 45_2)_s$ tensile coupons of T300/5208 and T300/5209 were tested to determine the elastic constants at 25°C. Handbook values for the coefficients of thermal expansion were assumed and coefficients of moisture expansion were taken from Figure 1. These properties, summarized in Table 1 of Appendix B were then used in the laminate analysis code ADV*LAM to compare the predicted elastic warping caused by the absorption of equilibrium amounts of moisture to the experimentally observed warping. DeRuntz describes the analysis procedure in an earlier paper [38].

Pipes et al [18] have discussed how swelling strains due to moisture absorption are analyzed in the same manner as expansion strains caused by a change in temperature. The analysis makes use of the concept of path independence in the analysis of elastic structural response. Hahn [39] has shown that the calculation of residual stress or strains at a given temperature requires only the elastic constants at the temperature of interest and the total swelling strains due to temperature and moisture referenced to the initial dry stress-free state at temperature T_o. In our analysis T_o was chosen by requiring the predicted warping in the dry state at 25°C to coincide with the experimentally measured value.

The predicted warping of T300/5208 $(0_4, 90_4)_T$ laminates possessing the elastic properties in Table B1 is plotted as the dashed line in Figure 2.

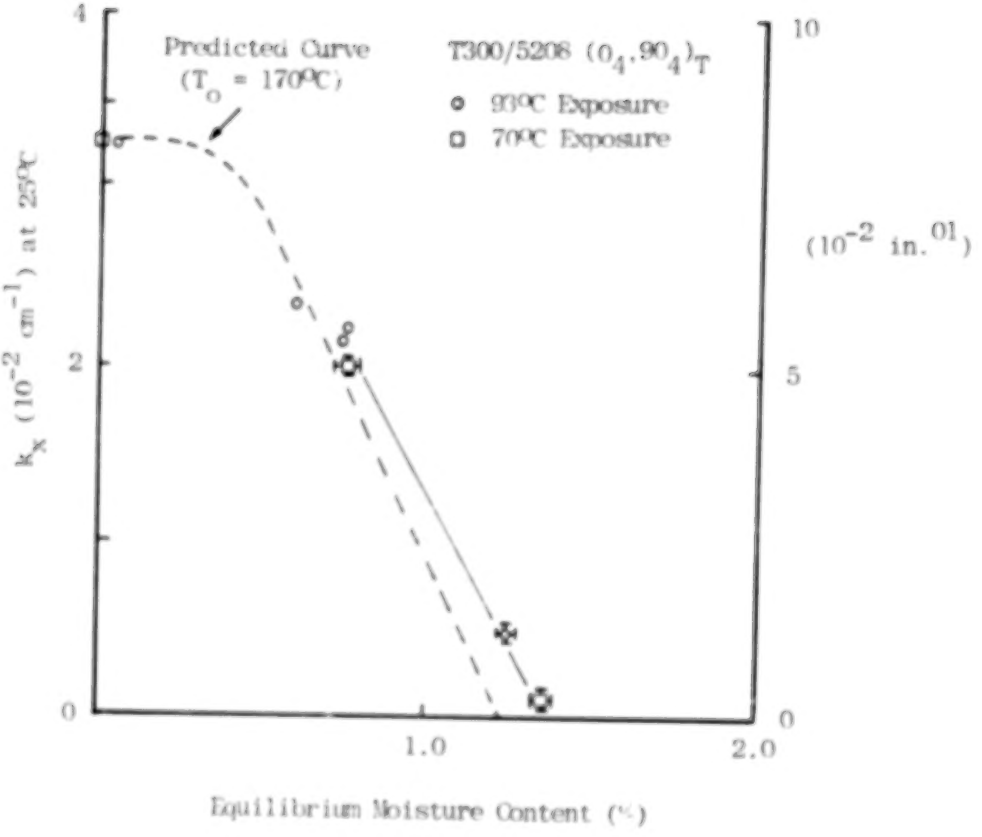

Figure 2. Measured and Predicted Curvature of Nonsymmetric $(0_4,90_4)_T$ T300/5208 Laminates vs. Equilibrium Moisture Content and Exposure Temperature.

BLANK

PAGE

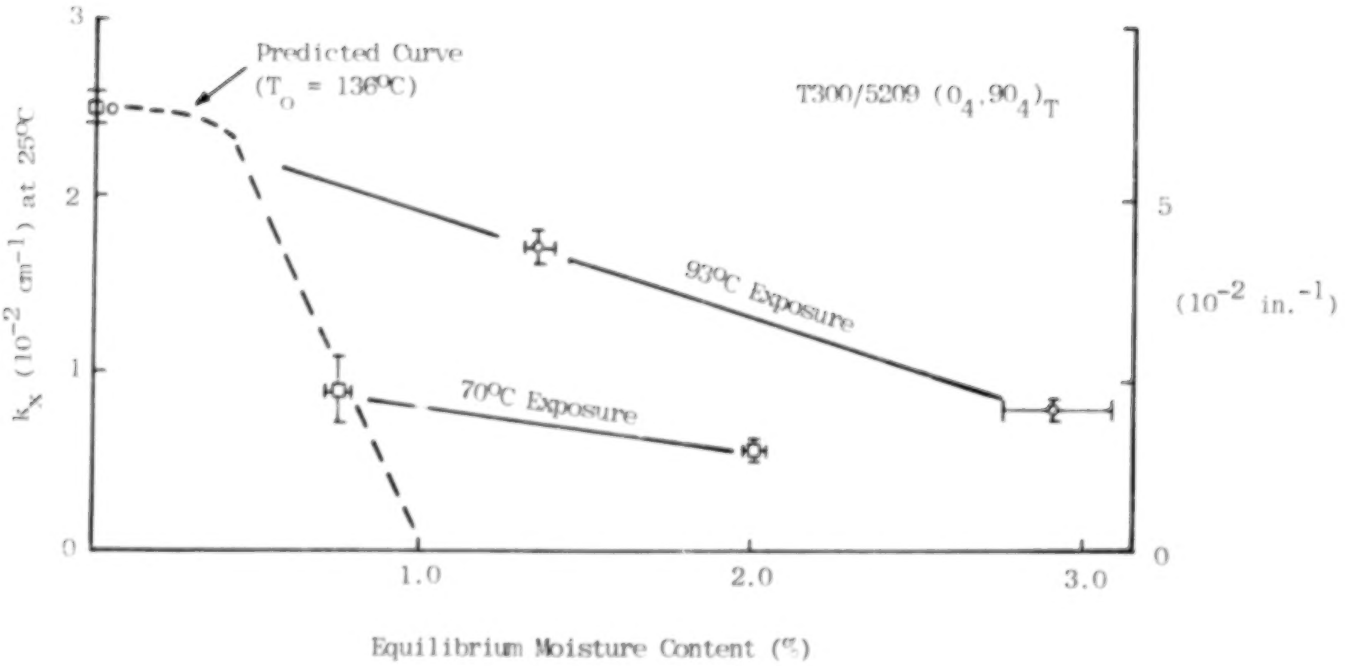

Figure 3. Measured and Predicted Curvature of Nonsymmetric $(0_4,90_4)_T$ T300/5209 Laminates vs. Equilibrium Moisture Content and Exposure Temperature.

The pronounced nonlinear relationship between curvature and moisture content is shown to be a consequence of the bilinear transverse swelling response in Figure 1. The close agreement between predicted and measured warping suggests that the assumption of elastic time independent behavior is appropriate for the analysis of T300/5208 although there is evidence for a poorer fit at moisture contents above 1 percent.

Figure 3 shows the curvature vs moisture content response observed and predicted in $(0_4, 90_4)_T$ T300/5209 specimens. The large deviation in the observed response and that predicted by linear elasticity is evident. The elastic analysis is appropriate only for moisture contents less than 0.8 percent absorbed water and exposure temperatures of 70°C or less. The history dependent curvature vs moisture content is indicative of a significant moisture altered viscoelastic response in T300/5209 at 70 and 93°C. Similar history dependent responses were found in T300/5209 $(0_4, 90_4)_T$ laminates brought to equilibrium moisture contents at 20°C and 54°C [15]. Sykes et al [40] studied the glass transition temperature and heat distortion temperature (HDT) of T300/5209 as a function of absorbed moisture. Absorption of one percent moisture lowered the HDT to 85°C from an initial value of 135°C in the dry state. Experiments in this laboratory show that the heat distortion temperature of T300/5208 drops to 45°C after absorption of two percent water [41]. It is evident from Figure 3 that viscoelastic stress relaxation acts to reduce the amount of residual stress change caused by the absorption of a particular water content and that the actual change is now highly dependent on the exposure temperature and humidity. Earlier absorption experiments on T300/5209 [15] show that under room temperature and 95% relative humidity the equilibrium moisture content is only 0.85 percent.

The use of elevated moisture exposure temperatures of 70 and 93°C causes two problems which must be dealt with in the formulation of a realistic accelerated conditioning and test program. First, the elevated exposure temperature allows the absorption of more water than will be absorbed under typical aircraft

environments near 25°C. Secondly, even if we choose to equilibrate T300/5209 to 0.85 percent by proper choice of temperature and humidity (for example, 70°C/55% RH or 93°C/20% RH), the residual stress state and moisture induced laminate dimensional changes after moisture absorption to equilibrium will not necessarily be the same as those which develop under humidity exposure at 25°C. Absorption of .85 percent water at 70°C reduces the initial warping by approximately 60 percent. Absorption of the same level of water at 93°C would reduce the initial warping by only 10 percent, based on interpolation of the 93°C data in Figure 3. The curvature results shown in Figures 2 and 3 suggest that the hygrothermal cycling experiments to be performed at 70 and 93°C on both materials systems will enable a separation between quasi-elastic degradation mechanisms in T300/5208 and viscoelastic enhanced degradation mechanisms in T300/5209.

2.3 DESORPTION UNDER STRESS

Unidirectional and crossplied laminates clad on one side with aluminum foil and additional $(0_4, 90_4)_T$ laminates were equilibrated to 55 and 95 percent humidity at 93°C in preparation for experiments designed to examine the influence of applied stress on the rate of moisture desorption. During the exposure blisters on the order of .5 to 1 cm in diameter were observed to form under the aluminum cladding, especially in those samples exposed to 95 percent humidity. As more moisture was absorbed, edge delamination of the aluminum cladding from the composite become evident in some specimens. Figure 4 shows the range in appearance of the specimens. The top two specimens show very little cladding degradation. The center specimen typifies the appearance of blisters at the edges, while the lower specimens show the center blistering and edge pealing of the cladding.

Equilibrium moisture content of the clad specimens was generally higher than the unclad $(0_4, 90_4)_T$ laminates (see Figures 6-7). The higher moisture content of the clad laminates can probably be attributed to a preferential collection of moisture in the blistered regions. The random distribution of blisters over the surface of the specimens suggests that they are caused by

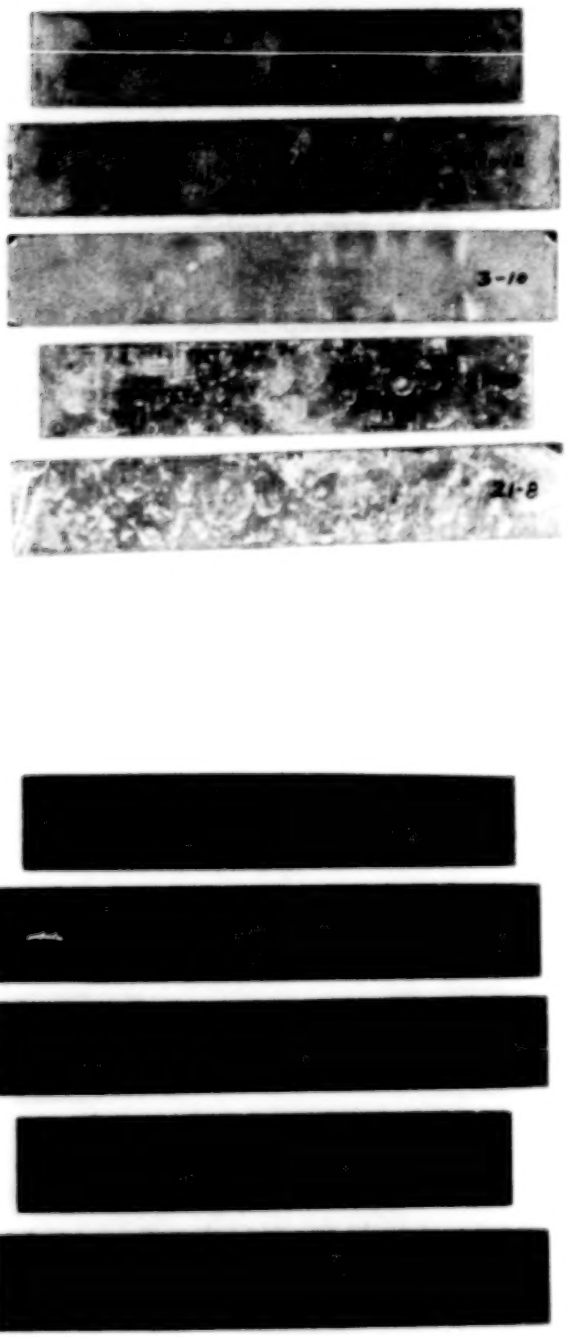

Figure 4. Appearance of clad T300/5208 and T300/5209 (Spec. 3-10 only) after exposure to 55% RH and 95% RH (Spec. 21-8 only) at 93°C. Note edge delamination of 3-10 and blistering of 21-10 and 21-8.

moisture induced swelling of the composite and a locally poor composite to aluminum bond. The aluminum foil had been sanded and cleaned prior to curing the clad prepreg. Perhaps the use of the standard FPL etch or phosphoric anodizing treatments used for adhesive bonding of aluminum joints could reduce or eliminate the tendency to blister in future experiments.

The curvatures of unidirectional and crossplied clad laminates were measured as a function of equilibrium water content after saturation at 93°C under 55 or 95 percent relative humidity. Predictions were based on the elastic constants in Table B1 and the stress free temperatures of Figures 2 and 3. In general, the dry predicted values at zero percent water were higher by a factor of 2-4 than measured curvature, while the slope of the predicted curvature vs. moisture curves followed the experimental trend for moisture contents less than 1 percent.

The large discrepancy in the predicted and experimental curvatures of the dry clad specimens was unexpected, particularly when the $(0_4, 90_4)_T$ results were so well correlated. The curvature results, higher moisture contents and blistering of the aluminum suggest that the aluminum-composite bond is poor. The implications were that desorption of clad laminates would not be strictly that due to one-sided diffusion and that a comparison between the absolute rates for the various laminate sequences may not be valid. At best one could examine the desorption rates of a given laminate configuration under positive, zero, and negative flexure to determine whether the sign of stress influences the desorption rate.

Desorption under stress experiments were conducted with flexural loading. A simplified flexural fixture was designed to allow rapid removal of specimens for weight and curvature measurement during desorption experiments. Figure 5 shows a trace of the specimen shape in the fixture which consists of an aluminum plate and stops between which the ends of the specimen are placed to obtain a specified radius of curvature. Approximately 10 cm of the specimen length (15 cm) is at a constant curvature in this fixture. Flexural tests were conducted on the dry clad materials which were employed to investigate stress effects on desorption kinetics. Flexural strengths and

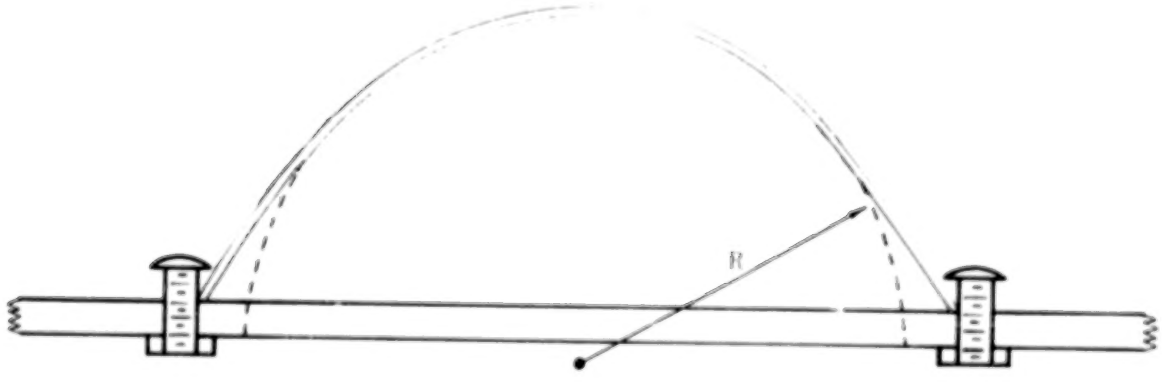

Figure 5. Diagram of Fixture Employed to Stress Laminates During Desorption at 70°C. Note that the Radius of Curvature is Constant Over the Center Section.

the appropriate radius of curvature needed to load specimens to 50 percent of ultimate strength are given in Table 2 of Appendix B.

During desorption experiments conducted at 70°C in a chamber containing Drierite dessicant, stressing was accomplished by flexing specimens to a curvature which was nominally 25 percent of the curvature which resulted in flexural failure in dry specimens tested at 25°C. The curvatures chosen for $(0_4, 90_4)_T$ laminates were 25 percent of the flexural strength of the 0_8 + Al and 90_8 + Al configurations with the clad side under compression. Audible cracking of the $(0_4, 90_4)_T$ specimens could be detected when the 90° layers were placed in tension. As a result, the applied curvature was held to a value less than 25 percent of ultimate on several of these samples, as shown in Figures 9-10.

Diffusion coefficients for the unclad T300/5208 and T300/5209 fall in a range of $4 \pm 1 \times 10^{-9}$ cm^2/sec. There is little to suggest that stress of this magnitude has any influence upon the diffusion kinetics at 70°C. Unstressed values are seen to appear below, between, or above those obtained for stressed specimens in a given series. Experiments with clad specimens provided mixed results. A majority of specimens developed bubbling and edge delamination of the aluminum cladding during absorption of water. If the cladding does not act to prevent moisture from wicking along the Al-composite interface and entering the specimen from both sides, then the effective diffusion coefficient, calculated by assuming one-sided diffusion, will be four times higher or approximately 16×10^{-9} cm^2/sec. It is clear that some of the clad specimens in Figures 6 and 7 are approaching this condition. Although the scatter in diffusion behavior is significantly greater in the clad series due to aluminum delamination, there is no consistent shift in diffusion coefficient due to tensile or compressive stress.

Evidence of viscoelastic stress relaxation or creep was found in T300/5209 $(0,90)_{2s}$ clad specimens which were placed in flexure at 70°C after equilibration to 93°C/95% RH. Figure 8 shows the permanent set taken by two specimens, one flexed to place the clad side in tension and the other flexed to put the clad side in compression. Under a constant curvature, stress

BLANK

PAGE

Laminate Type	Absorption Conditions (T°C/RH%)	(% Equil. H_2O)
UD	70/55	0.83
UD	70/95	1.42
$(0_4,90_4)_T$	93/55	0.75
"	93/95	1.35
0_8+Al	93/55	0.75
"	93/95	1.6
90_8+Al	93/55	0.78
"	93/95	2.0
$(0,90)_{2s}$ +Al	93/55	0.87
"	93/95	1.90
$(90,0)_{2s}$ +Al	93/55	0.90
"	93/95	1.95

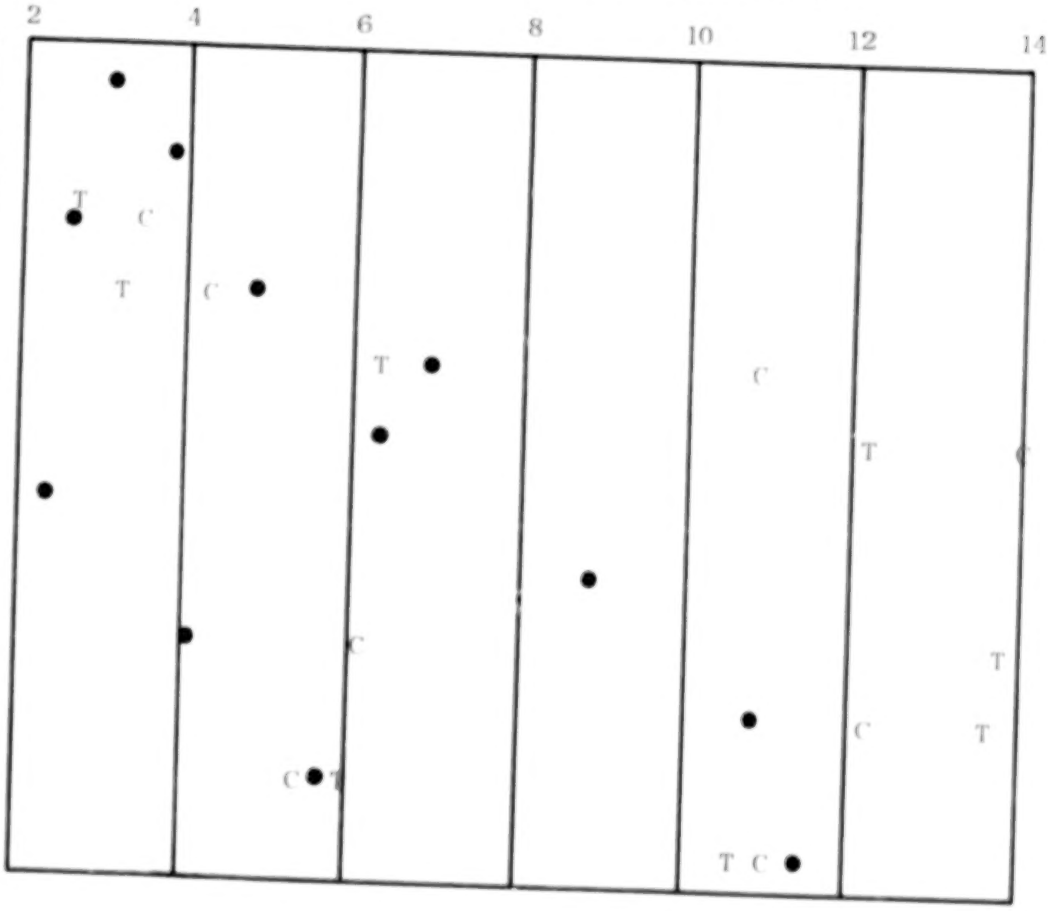

● No stress Applied

T Al clad side in tension [or 0° side in $(0_4,90_4)_T$ laminates]

C Al clad side in compression [or 0° side in $(0_4,90_4)_T$ laminates]

Figure 6. T300/5208 Desorption Under Stress Experiments. Values of Desorption Coefficient at 70°C are shown. Specimens Flexed to 25% of Ultimate Curvature Based on Table B2.

Laminate Type	Absorption Conditions (T°C/RH%)	(% Equil. H_2O)
UD	70/55	0.86
UD	70/95	2.17
$(0_4,90_4)_T$	93/55	1.35
"	93/95	2.90
0_8+Al	93/55	0.75
"	93/95	3.45
90_8+Al	93/55	1.71
"	93/95	3.70
$(0,90)_{2s}$ +Al	93/55	0.76
"	93/95	4.00
$(90,0)_{2s}$ +Al	93/55	0.80
"	93/95	3.90

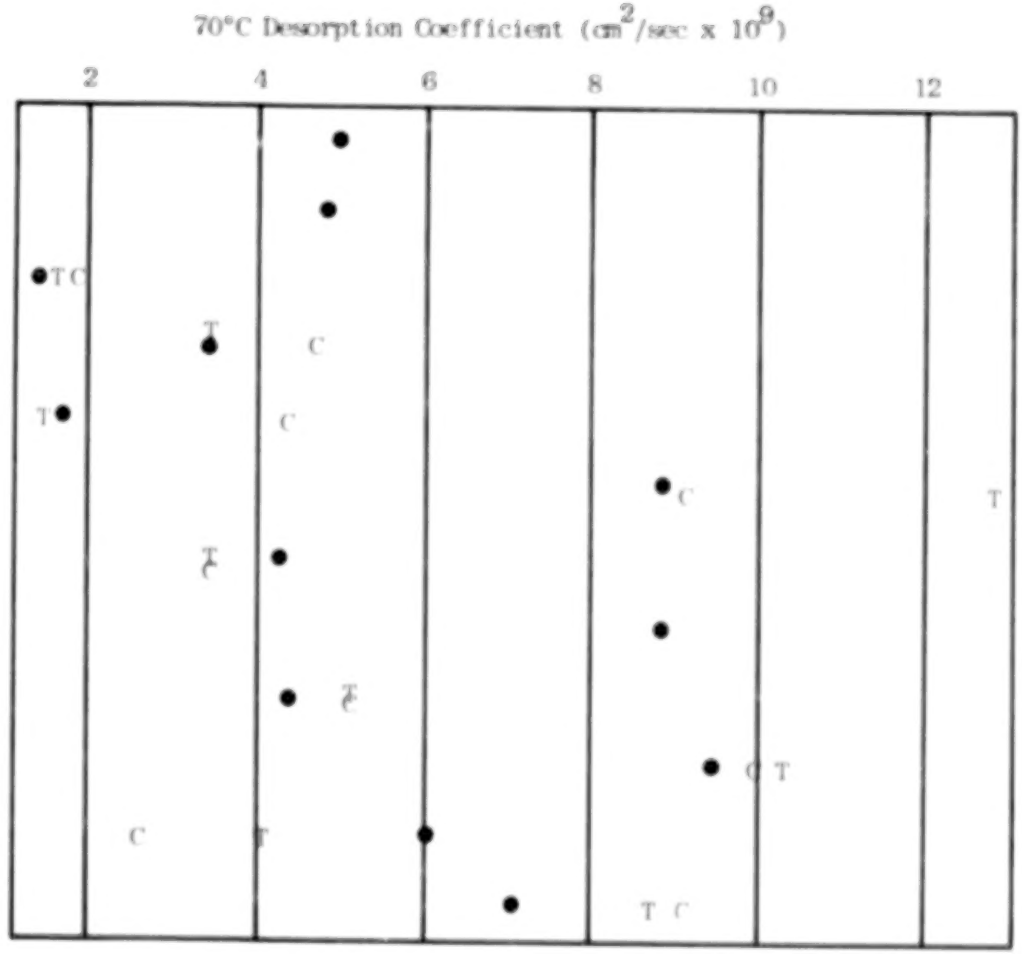

● No stress applied

T Al clad side in tension [or 0° side in $(0_4,90_4)_T$]

C Al clad side in compression [or 0° side in $(0_4,90_4)_T$]

Figure 7. T300/5209 Desorption Under Stress Experiments. Values of Desorption Coefficient at 70°C are shown. Specimens Flexed to 25% of Ultimate Curvature Based on Table B2.

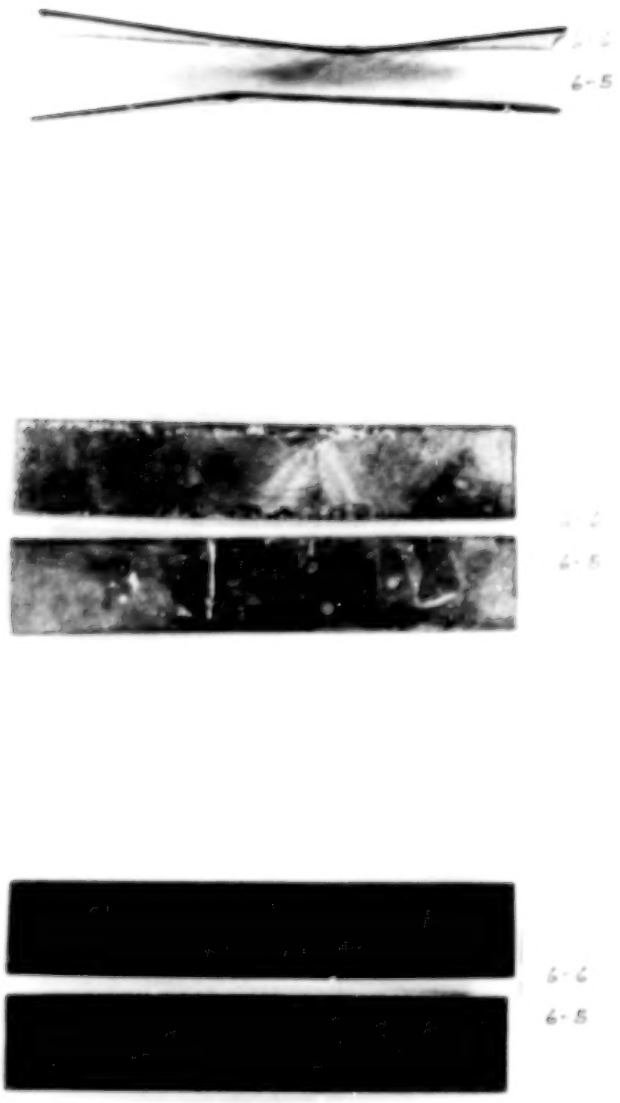

Figure 8. Appearance of $(0/90)_{2s}$ clad T300/5209 laminates equilibrated at 93°C/55% RH and then desorped under flexure at 70°C.

relaxation serves to reduce the applied stress on these specimens. Therefore, the lack of evidence for stress altered desorption kinetics in T300/5209 may be partially a consequence of the low effective applied stress due to viscoelastic relaxation.

2.4 THE INFLUENCE OF APPLIED STRESS DURING DESORPTION ON RESIDUAL STRESSES

The specimens in Figure 8 demonstrate that although the desorption kinetics are insensitive to applied flexural stress up to 25 percent of ultimate, the internal stress state or specimen dimensions can be significantly altered. Figures 9 and 10 show the original as cured, dry curvature of a series of $(0_4, 90_4)_T$ laminates and the final curvature after exposure to humidity at 93°C until equilibrium was reached and then drying at 70°C. The curvature in the specimens containing equilibrium moisture content (denoted by the symbol S) and the curvatures applied during drying at 70°C (denoted with the symbol A) are also given. Two out of three specimens in each series were flexed to place the 90° layers in either tension (low or negative curvature in the figure) or compression.

The T300/5208 laminates show about a 15-25 percent reduction in curvature in the final dry state in specimens subjected to positive or zero applied curvature. Specimens which were flexed to place the 90° layers in tension show a reduced curvature in the dry condition of 40-55 percent.

Alteration in the final curvature due to application of stress during desorption can be caused by either microcracking or by stress relaxation. If stress relaxation is the dominant mechanism, then it will tend to shift the final curvature toward the applied value. This shift should be noticed for both positive and negative applied curvatures, as is found for the T300/5209 laminates in Figure 10. Lack of shifting in T300/5208 under positive curvature suggests that the predominant mechanism for alteration of internal stresses in this material is microcracking, while in T300/5209, it is viscoelastic relaxation. Note in Figure 10 that the final curvature of T300/5209 specimens which absorbed water at 93°C and were desorbed at 70°C under no applied stress is higher than the initial dry curvature. This increase in

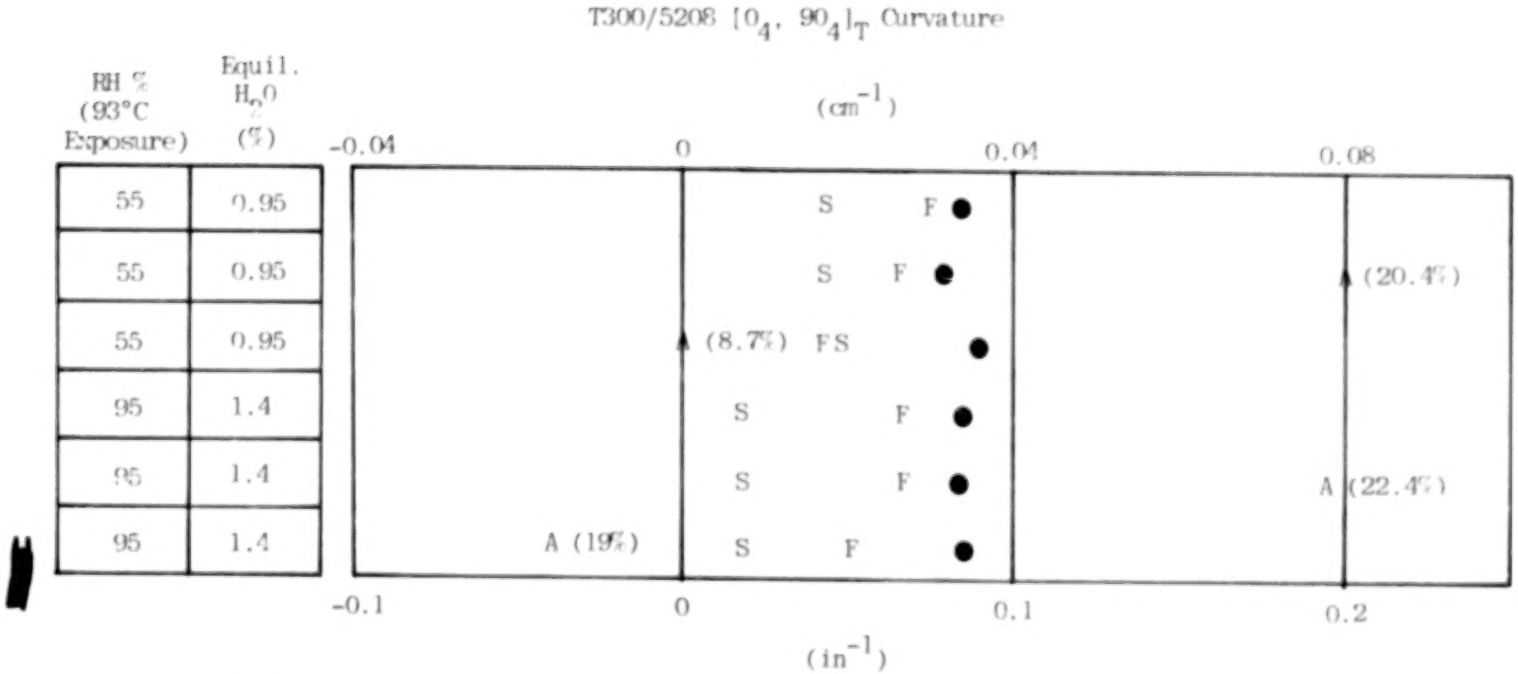

● Original dry curvature

F Final dry curvature after absorption at 93°C to equilibrium then drying at 70°C

A Applied curvature during drying (% of ultimate curvature given)

S Curvature after equilibrium moisture absorbed

Figure 9. 25°C Curvature of T300/5208 $(0_4, 90_4)_T$ Laminates Exposed to Different Hygrothermal and Mechanical Histories.

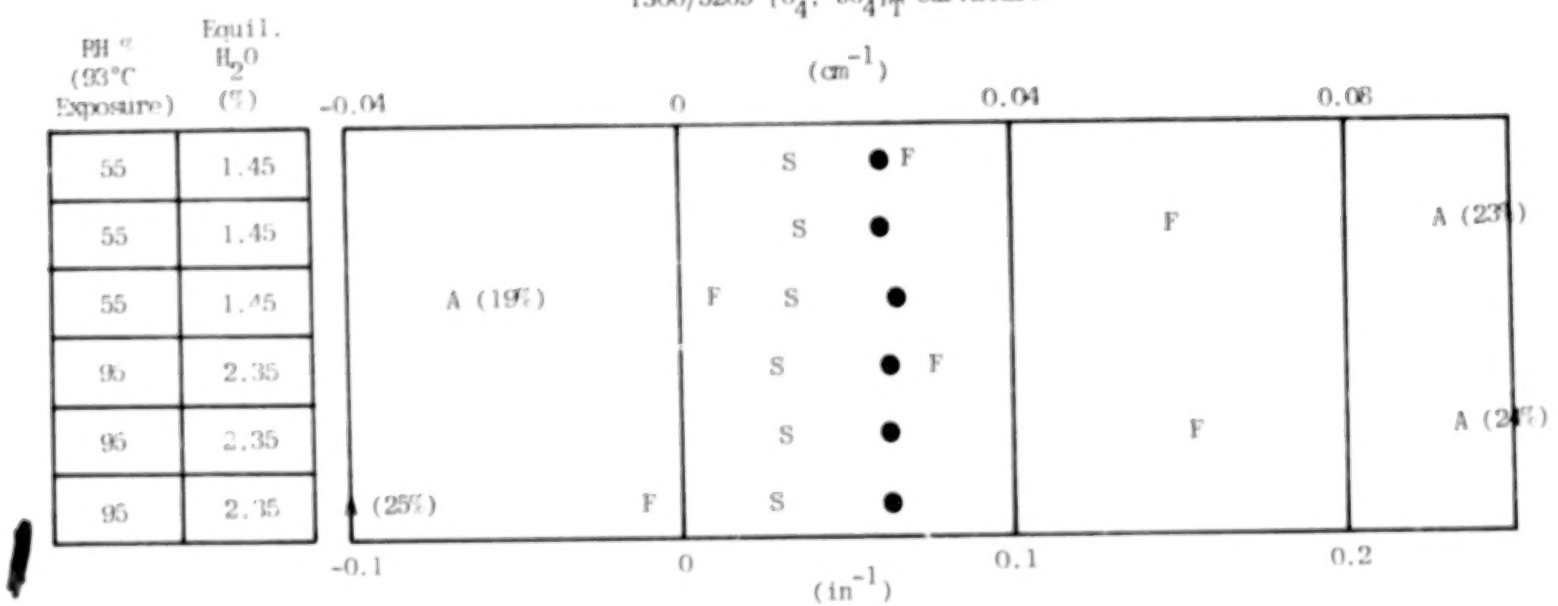

● Original dry curvature

F Final dry curvature after absorption at 93°C to equilibrium then drying at 70°C

A Applied curvature during drying (% of ultimate curvature given)

S Curvature after equilibrium moisture absorbed

Figure 10. 25°C Curvature of T300/5209 $(0_4, 90_4)_T$ Laminates Exposed to Different Hygrothermal and Mechanical Histories.

in residual stress with hygrothermal cycling has been noted in earlier studies [14] of GY70/339 and T300/5209 composites and is a consequence of moisture altered viscoelastic response [15].

2.5 HYGROTHERMAL CYCLING EXPERIMENTS

T300/5208 and T300/5209 laminate specimens destined for mechanical testing (Chapter 3), microstructural examination (Chapter 4), and residual stress analysis were subjected to 100 hygrothermal cycles between temperatures of -54°C and 70 or 93°C. Specimens were held ten to fifteen minutes at each temperature and were hard-carried between air circulating chambers maintained at the two temperature extremes. After every five cycles specimens were replaced in the humidity chambers at the temperature/humidity level to which they were initially exposed and held for two hours to reintroduce moisture to the surfaces and edges before being exposed to the next set of five cycles. A total of 15 cycles were run each day. Specimens were left overnight in the appropriate humidity chamber.

During a desorption period at 70°C, the relative loss of moisture content, ω/ω_s is given by [19]

$$\frac{\omega}{\omega_s} = \frac{4}{\sqrt{\pi}} \sqrt{\frac{Dt}{L^2}} = \frac{4}{\sqrt{\pi}} \sqrt{t^*} , \qquad \text{where } t^* = \frac{Dt}{L^2}$$

where t is the desorption time, D the diffusion coefficient and L the laminate thickness. At 70°C, the eight-ply laminates in this study have a diffusion coefficient of 4×10^{-9} cm^2/sec. During a ten minute desorption period, the non-dimensionalized time t^* is 2×10^{-4} and the expected weight loss is approximately three percent of the total moisture content. Five cycles at 70°C correspond to a total time t^* of 10^{-3} or a weight loss of 7.1 percent. The measured weight loss on unidirectional laminates after five thermal cycles between -54°C and 70°C was found to be as large as 5.1 percent. Cycling to 93°C resulted in up to a 9.0 percent loss prior to re-exposure to humidity. Thus the experimentally

measured moisture contents during cycling agree reasonably well with the predicted quantities based on diffusion theory.

Figure 11 shows the moisture content of unidirectional laminates after overnight re-exposure to humidity as a function of the number of hygrothermal cycles. No significant change in equilibrium moisture content was found. Specimens cycled 100 times were examined for evidence of surface or edge cracking. No macroscopic evidence of edge cracking, transverse microcracking or fiber-matrix debonding was found in any of the unidirectional and quasi-isotropic laminates which were examined. $(0_4, 90_4)_T$ laminates exposed to this series of 100 hygrothermal cycles were subsequently dried. Curvature measurements taken before moisture sorption, after sorption, after cycling and after redrying at 70°C are shown in Figs. 12 and 13. After thermal cycling of dry T300/5208 specimens, 19-4 and 19-2, the curvature was slightly reduced. In all other specimens of T300/5208 exposed to moisture prior to cycling, a similar reduction (less than 12 percent) in curvature was noted. No change in curvature was found immediately before and after the 100 cycles.

Thermal cycling of dry T300/5209 specimens, 4-4 and 4-2, produced no significant change in curvatures. Specimens 4-12 and 4-10 exposed to 55% humidity before cycling showed significant increases in curvature due to cycling but the final curvature was not changed from the initial dry value. By contrast specimens 4-8 and 4-10 exposed to 95% humidity prior to cycling showed little change after the 100 cycles but a large 35% increase in curvature in the final dry state. This large increase is greater than that noted in Fig. 10 for similar T300/5209 laminates moisture conditioned at 93°C and dried at 70°C. Comparing the response of T300/5208 and T300/5209, it would appear that 100 hygrothermal cycles over the -54°C to 93°C have a neglible effect on the residual stress state of the more elastic responding 5208 system. The small reduction in curvature could be attributed to some viscoelastic stress relaxation or microcracking. When there are significant changes noted in the 5209 residual stresses or curvature, it appears to be associated with the history dependent viscoelastic character of the system in this temperature range, since all changes noted show an increase in curvature. Microcracking damage would have a tendency to reduce curvature by partially decoupling the interaction of the 0 and 90 degree plies.

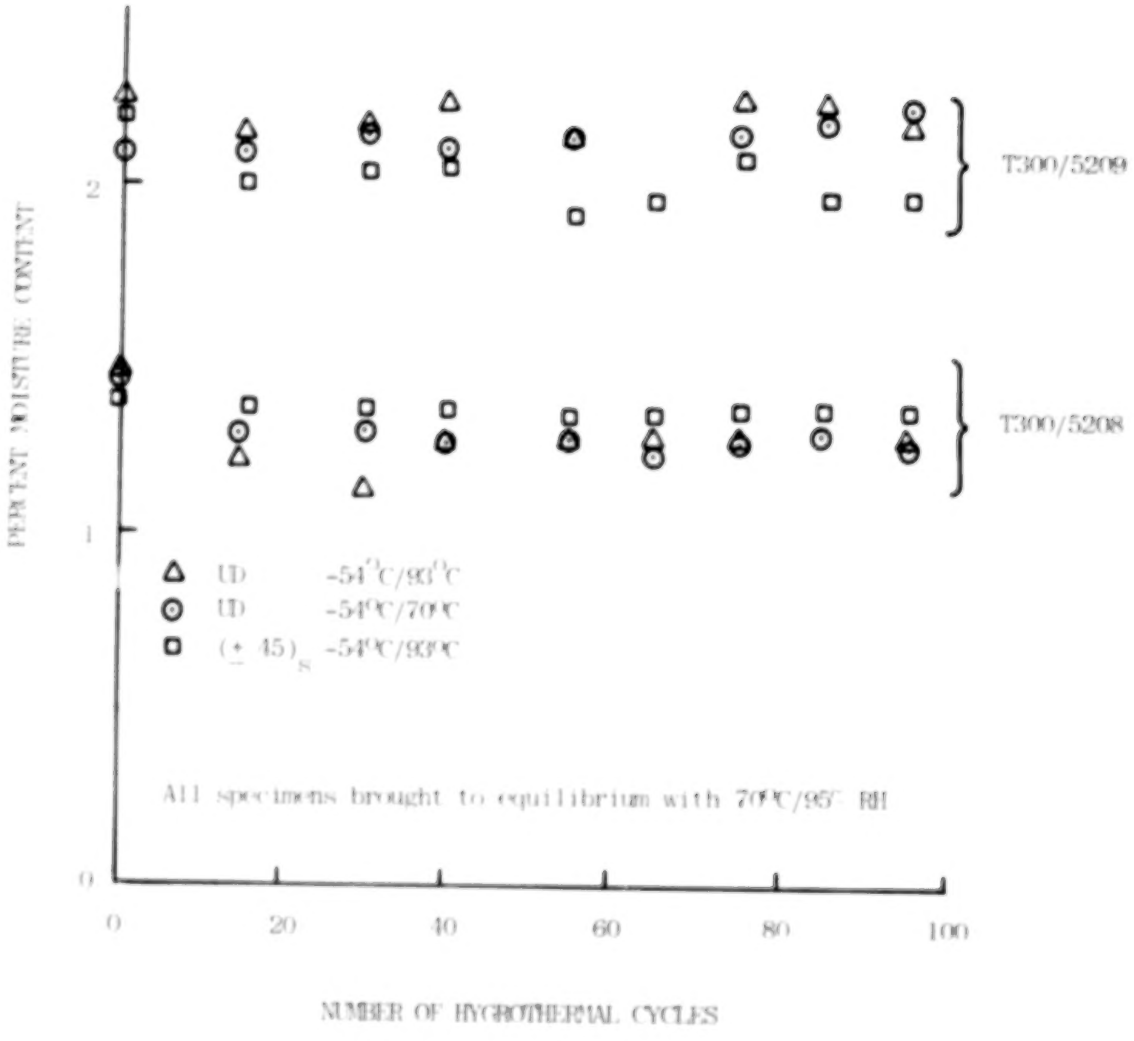

Figure 11. Effect of Hygrothermal Cycling on Equilibrium Moisture Content.

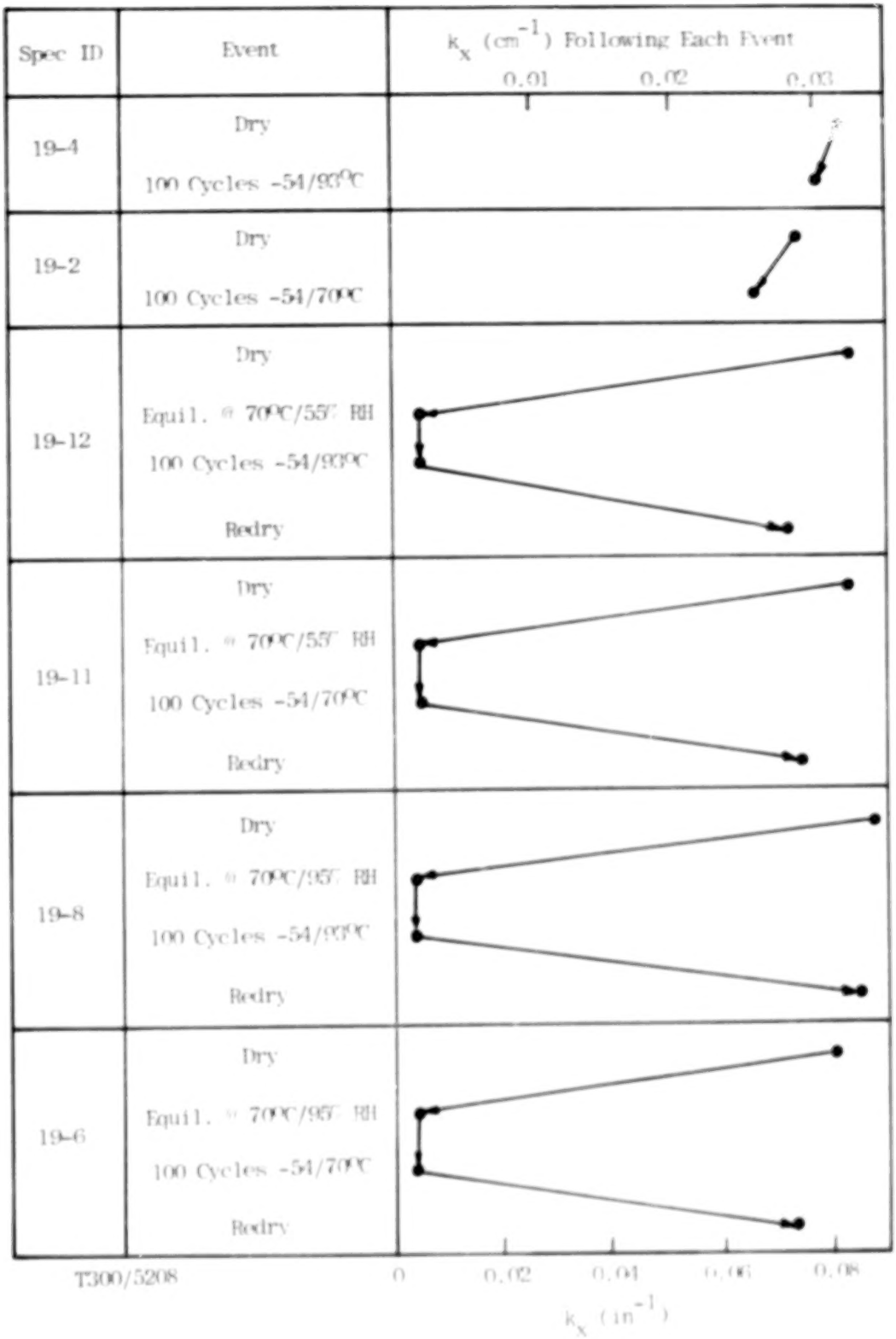

Figure 12. 25°C Curvature of T300/5208 $(0_4,90_4)_T$ Laminates as a Function of Hygrothermal History.

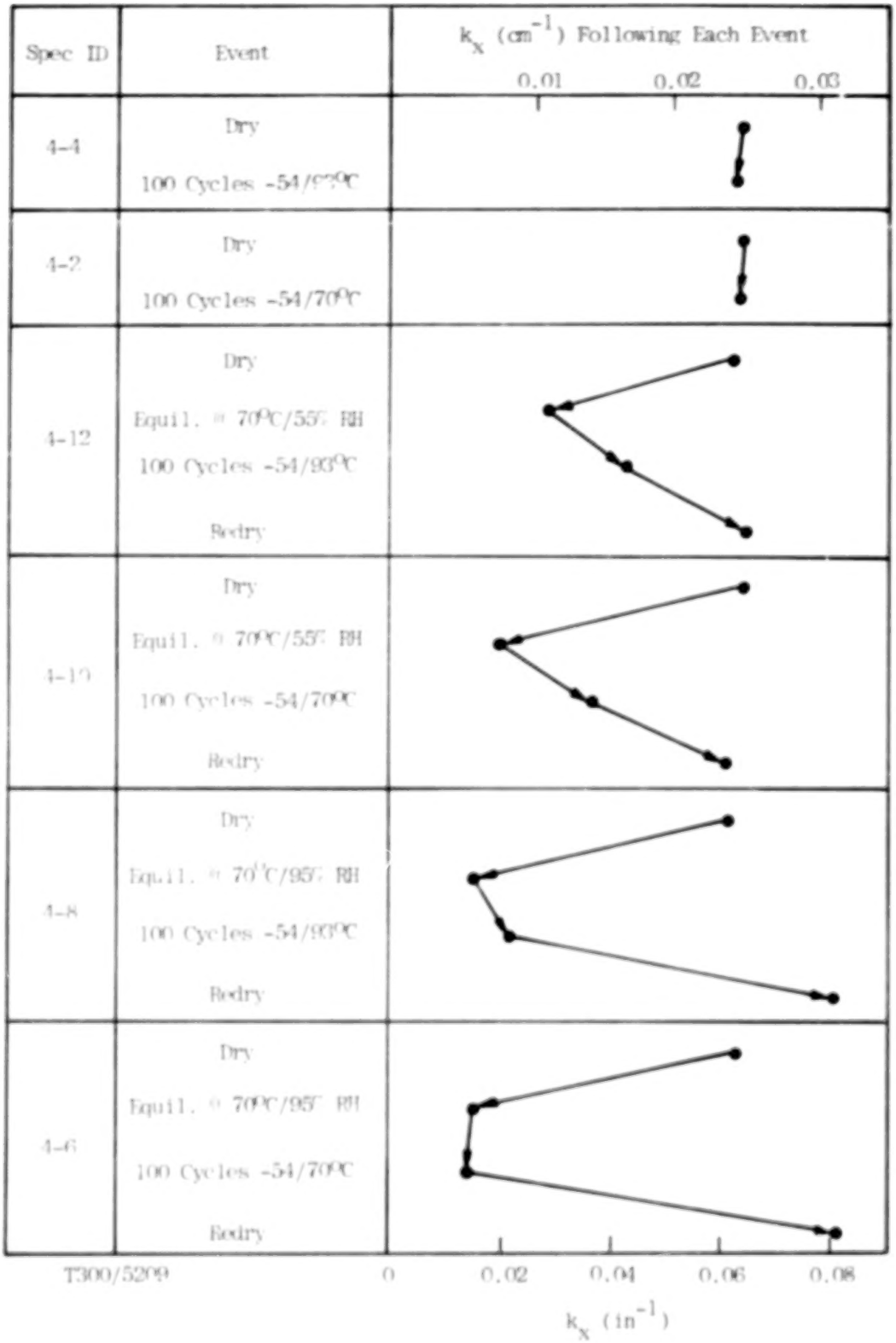

Figure 13. 25°C Curvature of T300/5209 $(0_4, 90_4)_T$ Laminates as a Function of Hygrothermal History.

CHAPTER 3

THE INFLUENCE OF HYGROTHERMAL HISTORY ON MATRIX AND INTERFACE DOMINATED LAMINATE PROPERTIES

3.1 INPLANE SHEAR TESTS

$(\pm 45_2)_s$ tensile specimens (2.5 cm wide by 7.5 cm gage length) were tested at 25, 70, and 93°C at a crosshead rate of 0.13 cm/min. Two specimens of each material were tested in four moisture conditions:

(1) Dry
(2) Equilibrated at 70°C/95% RH, then dried
(3) Equilibrated at 70°C/55% RH
(4) Equilibrated at 70°C/95% RH

Furthermore, two additional specimens in each of the four conditions listed above were cycled 100 times between -54 and 70°C and two others between -54 and 93°C prior to testing.

The specimens were tabbed with aluminum sheet stock and a 0°,90° strain gage was applied to one side of the specimen with Eastman 910 adhesive as shown in Figure 14. The figure illustrates the typical failure modes found in this test. Specimen 22-5 (T300/5208) shows a separation into two pieces and failed in a brittle manner in room temperature testing. T300/5209 specimen 7-14 shows a pattern of surface cracks parallel to the fibers but did not fail by separation. In elevated temperature testing of T300/5209 the specimens deformed in a ductile manner showing a necking down (Spec. 8-29) prior to separation due to large applied strains (Spec. 10-72). Data for all specimens tested is tabulated in Appendix B, Table 3, which provides values for the Young's modulus E_x, the Poisson ratio, ν_{xy}, the inplane shear modulus $G_{12} = E_x/(2(1+\nu_{xy}))$, and the shear strength $\tau_{12} = \sigma_x/2$. The shear strength of the majority of T300/5209 specimens

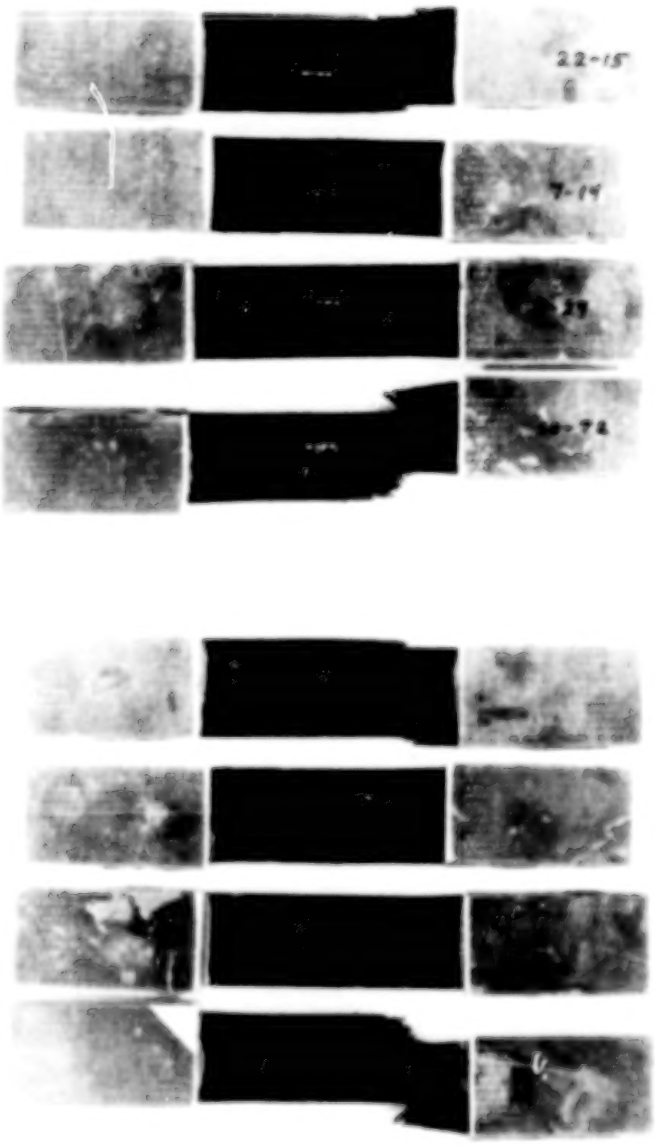

Figure 14.

Appearance of $(\pm 45_2)_s$ laminates after tensile testing.
(a) 22-15 is T300/5208 equilibrated at 70°C/95% RH, and tested at 25°C.
(b) 7-14 is T300/5209, equilibrated at 70°C/95% RH, and tested at 25°C.
(c) 8-29 is T300/5209, dry, tested at 70°C. Note necking.
(d) 10-72 is T300/5209, dry, cycled 100 times to 93°C, and tested at 93°C.

is not a well-defined quantity because of the degree of necking observed while the measured load increased very slowly with large increases in strain. In order to eliminate the need to measure the necked cross section to obtain the true net section shear stress, the shear strength tabulated in the Appendix was arbitrarily chosen as the value at a maximum applied strain ϵ_x of 3.5%.

Figure 15 and 16 show the dependence of shear strength at 25°C on the hygrothermal history of T300/5208 and T300/5209. Each data point represents a single test. The T300/5208 results in Figure 15 show no significant loss of shear strength due to absorbed moisture or hygrothermal cycling. On the other hand, T300/5209 specimens show a definite loss of 25°C shear strength as moisture content is increased. Furthermore, specimens conditioned to equilibrium moisture content at 70°C/95% RH and then dried prior to testing also suffer a slight (5 percent) loss in shear strength.

Given the scatter of data in Figures 15 and 16 for shear strength of specimens tested at a particular moisture content, the results indicate no influence of 100 hygrothermal cycles on shear strength. This conclusion is shown even more graphically in Figure 17 where the entire shear stress-strain responses of cycled and uncycled T300/5208 specimens tested at 93°C are plotted and found to be nearly indistinguishable.

Figures 18-20 provide the most comprehensive information of inplane shear response as a function of material, moisture content and test temperature. The curves are designated with D for dry, 70/55 for specimens equilibrated at 70°C/55% RH, and 70/95 for those equilibrated at 70°C/95% RH prior to testing. The material 5208 or 5209 is given in parentheses.

Certain subtle changes in plasticization of T300/5208 with added moisture content are evident in Figure 18. Note that, although the initial shear modulus and ultimate tensile strength of T300/5208 specimens is relatively independent of moisture content, the degree of nonlinear stress-strain response increases with moisture content. If we were to compare the stress

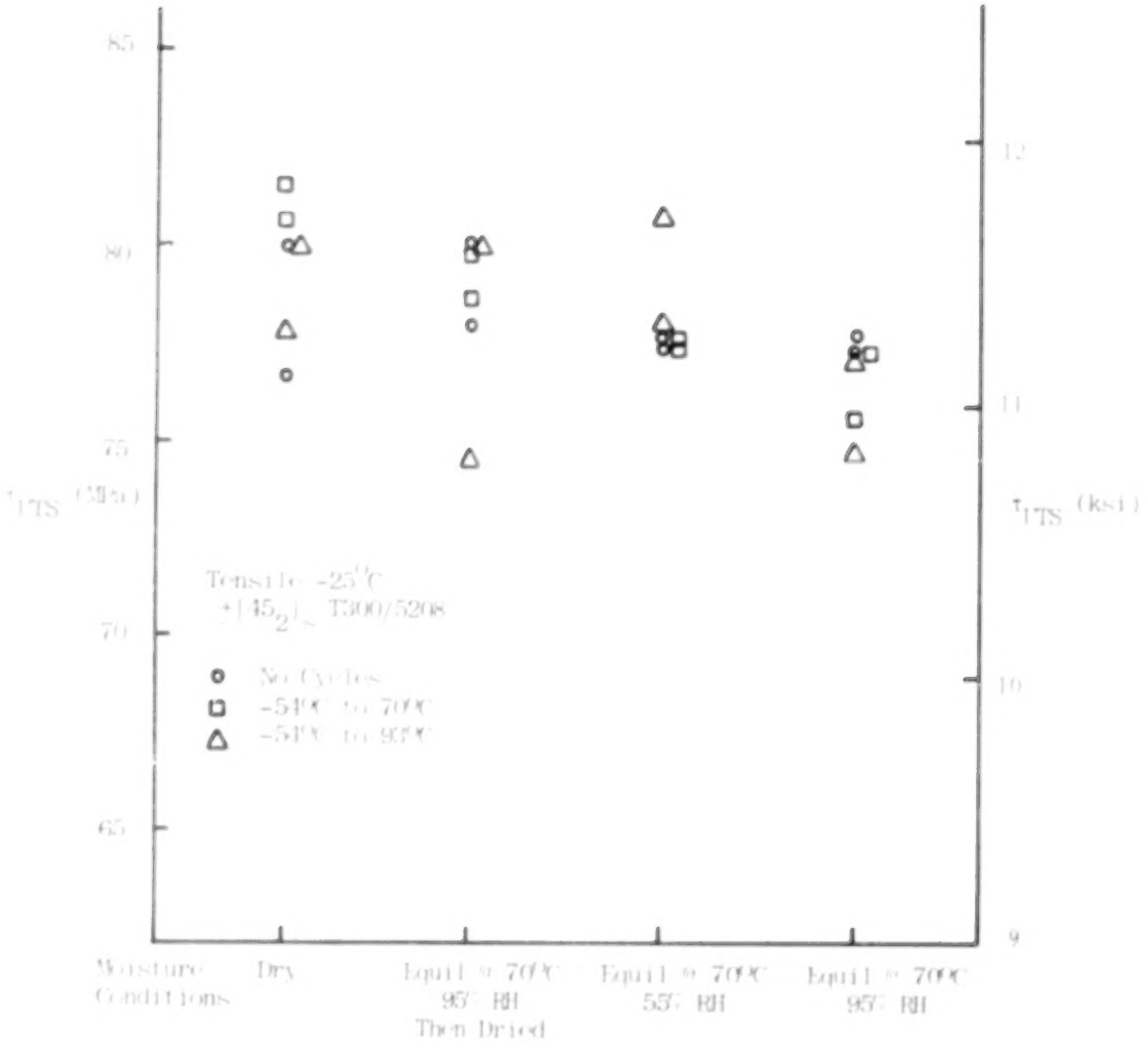

Figure 15. The Influence of 100 Hygrothermal Cycles on the In Plane Shear Strength of T300/5208 at 25°C.

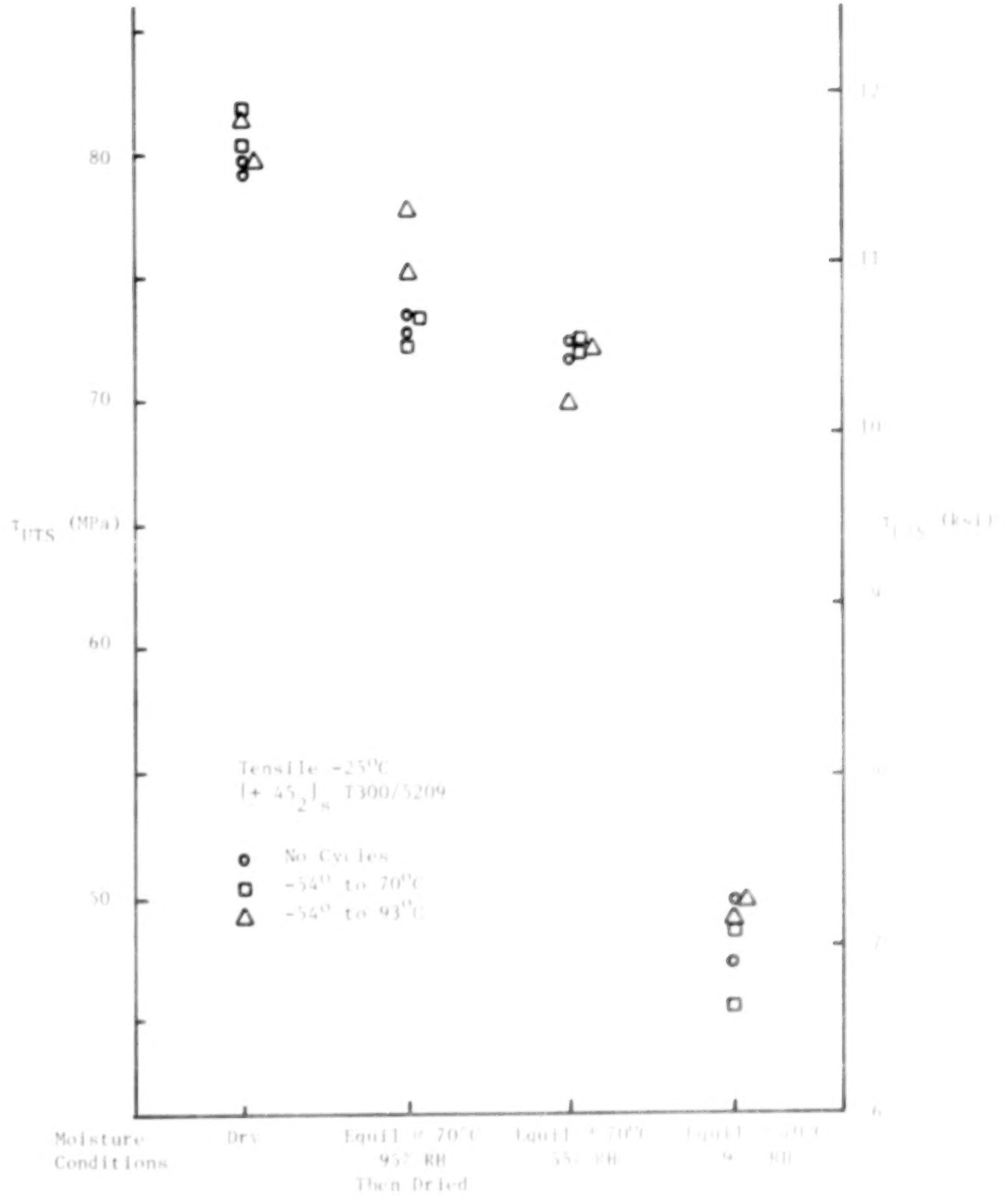

Figure 16. The Influence of 100 Hygrothermal Cycles on the In-Plane Shear Strength of T300/5209 at -25°C.

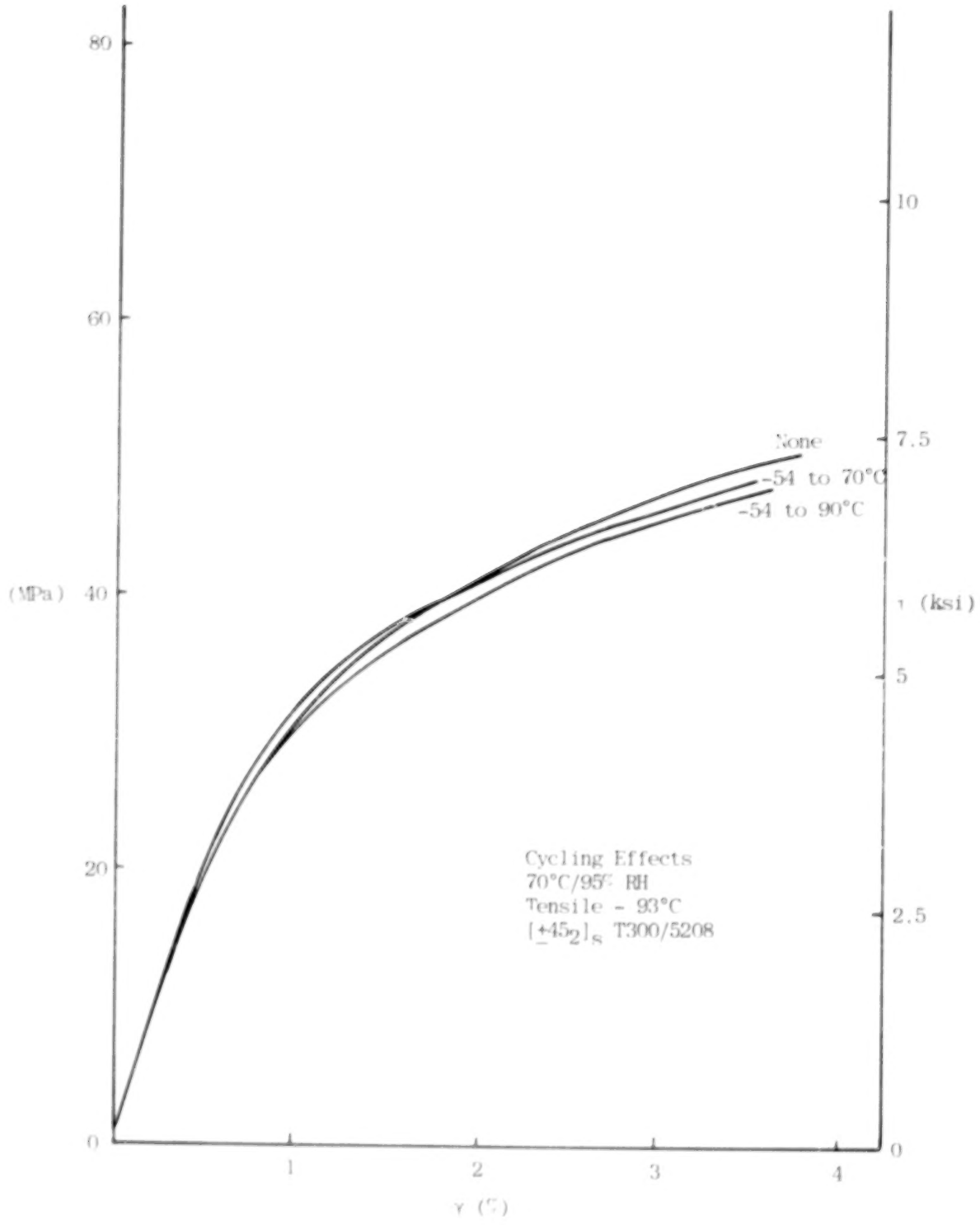

Figure 17. The Influence of 100 hygrothermal Cycles on the Shear Behavior of T300/5208 at 93°C.

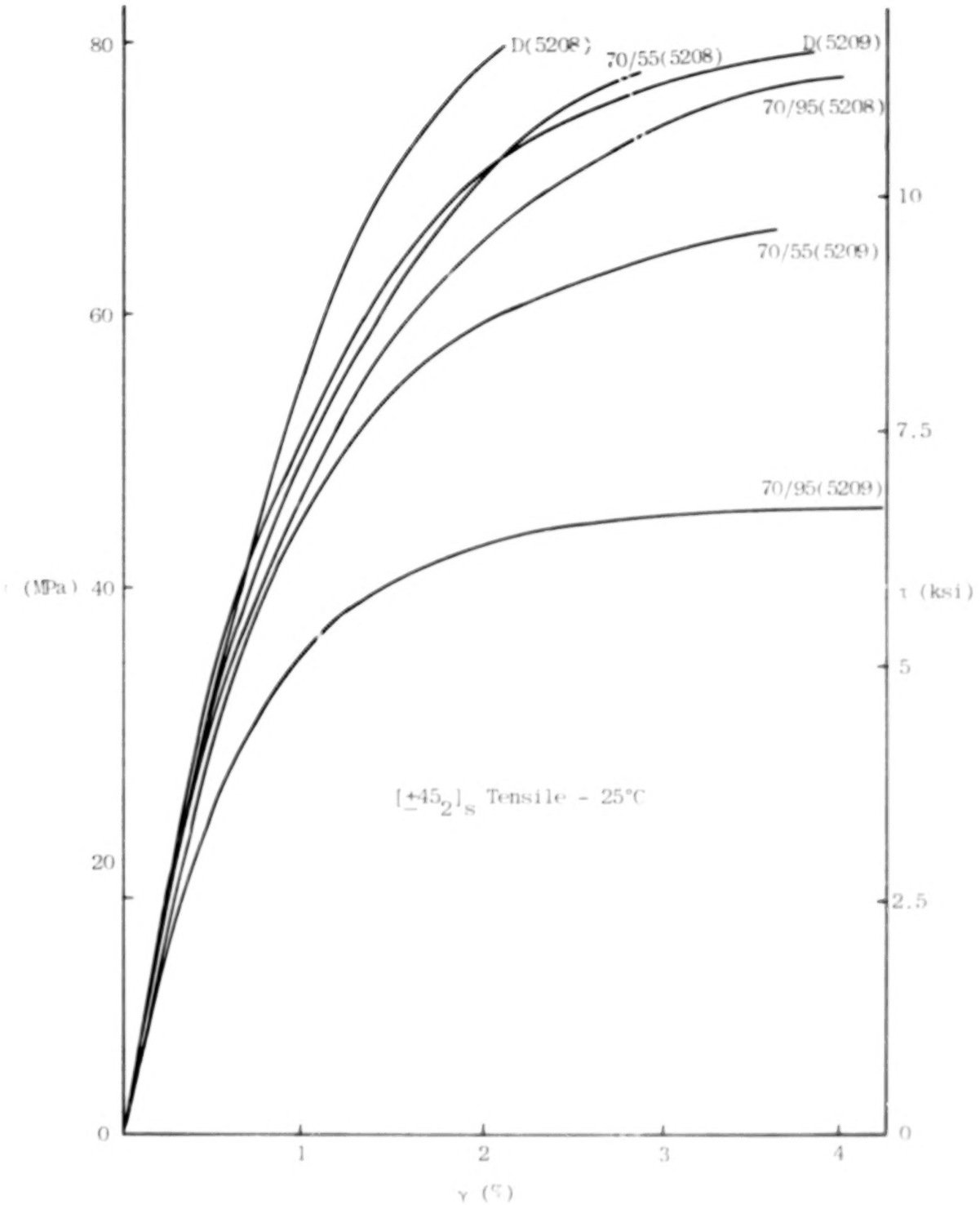

Figure 18. Representative Shear Stress-Strain Response at 25°C as a Function of Equilibrium Exposure to Moisture.

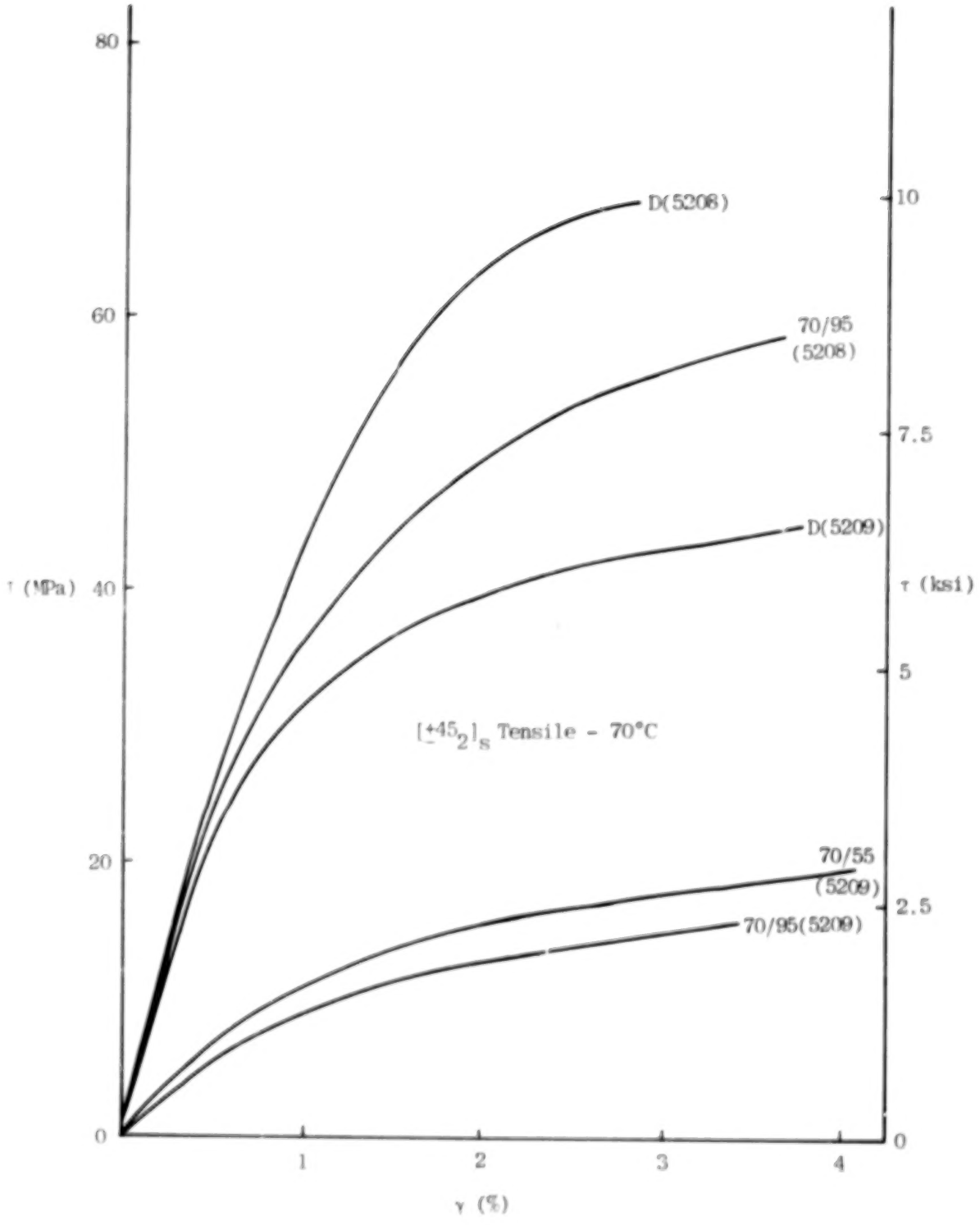

Figure 19. Representative Shear Stress-Strain Response at 70°C as a Function of Equilibrium Exposure to Moisture.

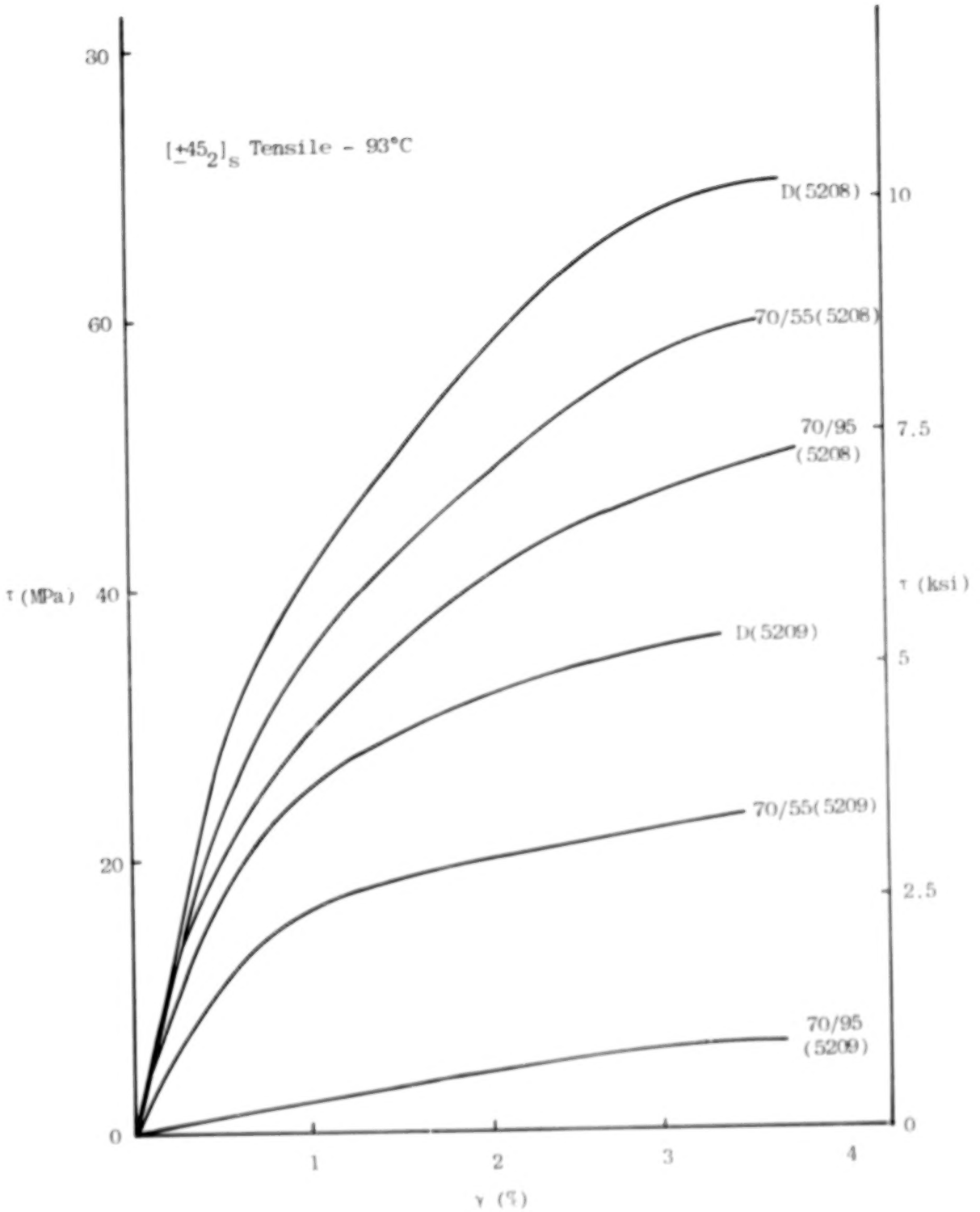

Figure 20. Representative Shear Stress-Strain Response at 93°C as a Function of Equilibrium Exposure to Moisture.

carried by specimens D(5208) and 70/95 (5208) at a shear strain of 2 percent, the moisture laden specimen suffers a twenty percent reduction in load carrying ability at this strain.

Figures 21-24 show the temperature dependence of shear modulus G_{12} and inplane shear strength in both material systems. The entire range of data for cycled and uncycled specimens is shown for each moisture conditioning state and test temperature. It is clear that the particular moisture conditioning and test temperature govern the stiffness and strength of both materials. The 5209 system is particularly sensitive to moisture induced reduction of modulus and strength at the elevated temperatures.

3.2 INTERLAMINAR SHEAR TESTS

Methods to evaluate the hygrothermal degradation of fiber-matrix bond strength were given a preliminary evaluation. Initial results from notched compression tests on T300/5209 and GY70/339 dry unidirectional composites were found to be extremely low, as noted in Table 2, and subject to large scatter. The required depth of one-half the specimen thickness, and the typical specimen thickness range of $\pm$ 2.5 x 10^{-3} cm required that a number of individual machining measurements be made on each sample.

A search for a more reliable test of interfacial shear strength uncovered a recent paper on flexural testing [42] in which T300/5208 unidirectional samples were found to fail in shear during four point bend testing. An analysis of the three and four-point bend test shows the maximum tensile stress and maximum shear stress to be related to the specimen geometry shown in Figure 26 by the following equations

$$\sigma^{T}_{max} = \frac{3P}{bh}\left(\frac{a}{h}\right)$$

$$\tau_{max} = \frac{3P}{4bh}$$

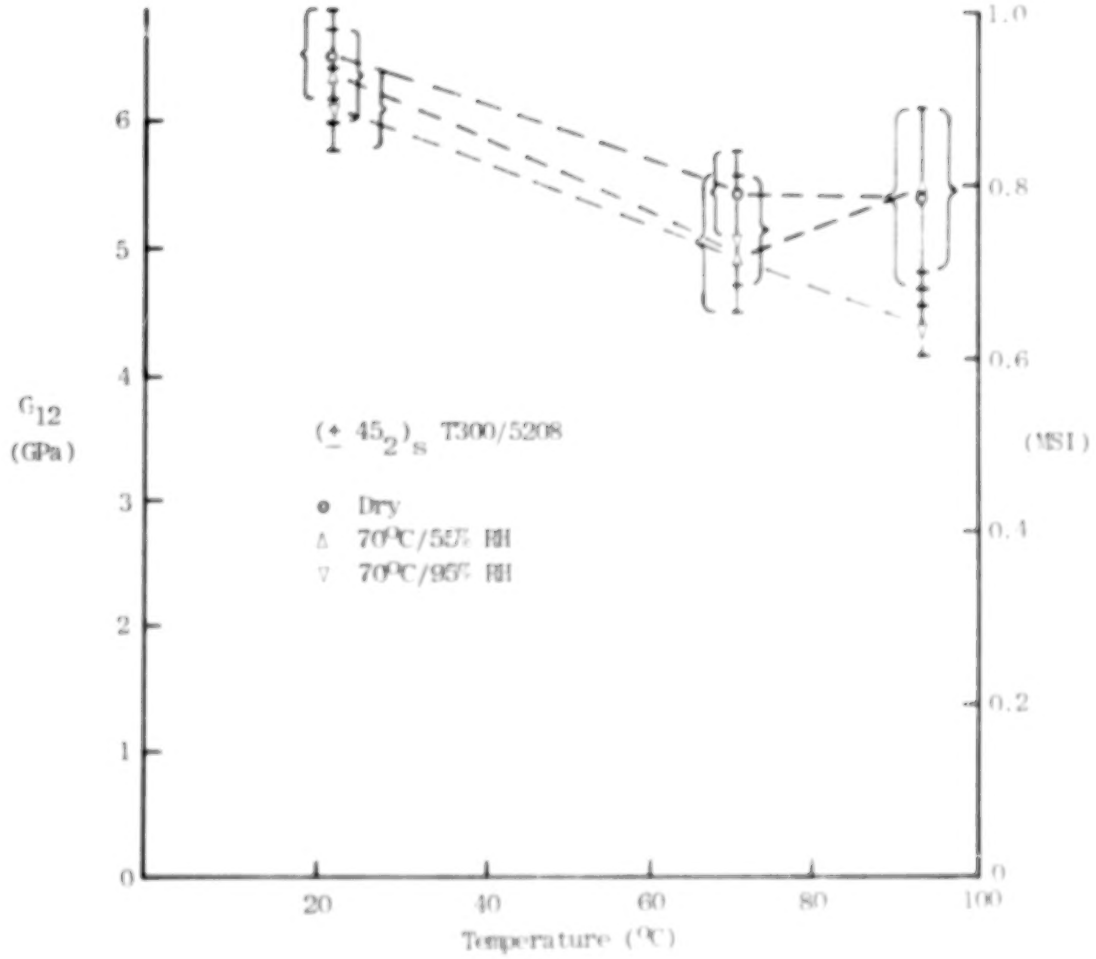

Figure 21. Shear Modulus of T300/5208 vs. Temperature. Range Bands Include Data for All Cycled and Uncycled Specimens.

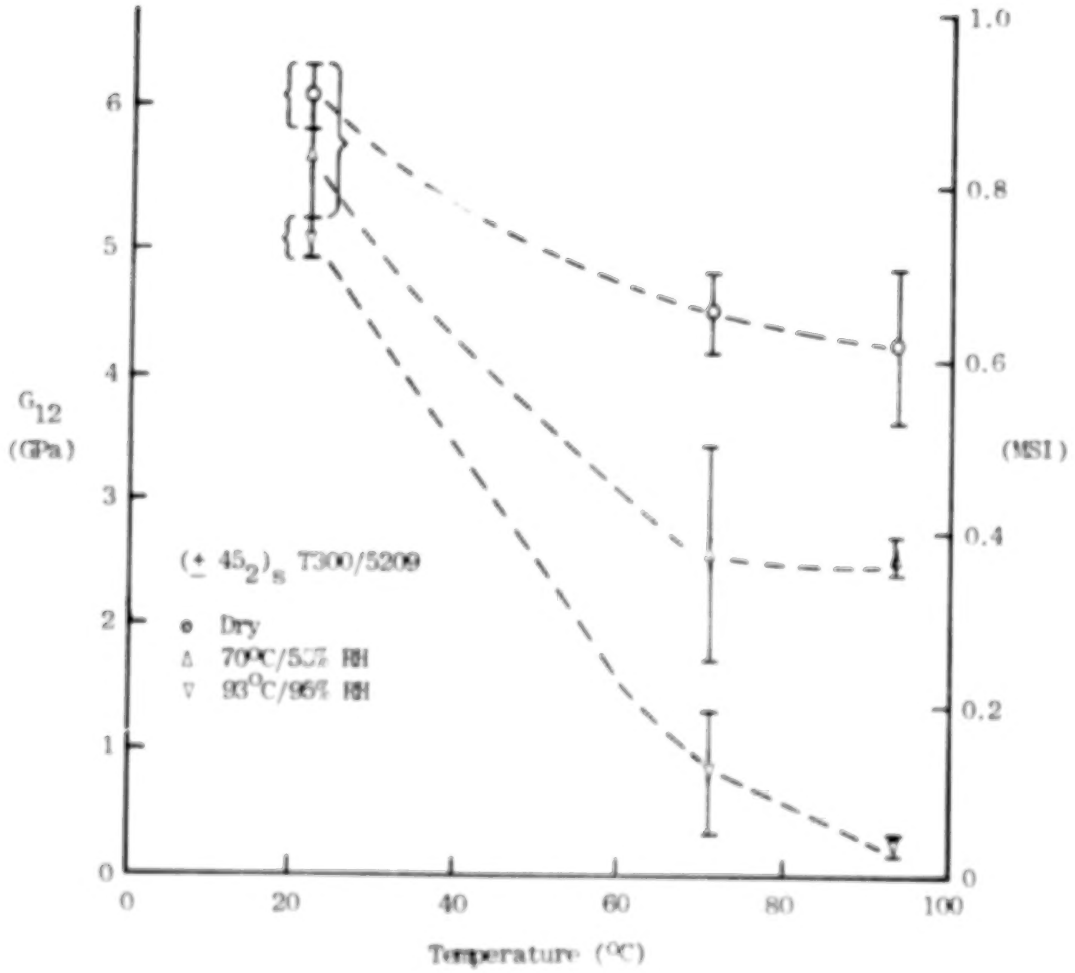

Figure 22. Shear Modulus of T300/5209 vs. Temperature. Ranges Include All Cycled and Uncycled Specimen Data.

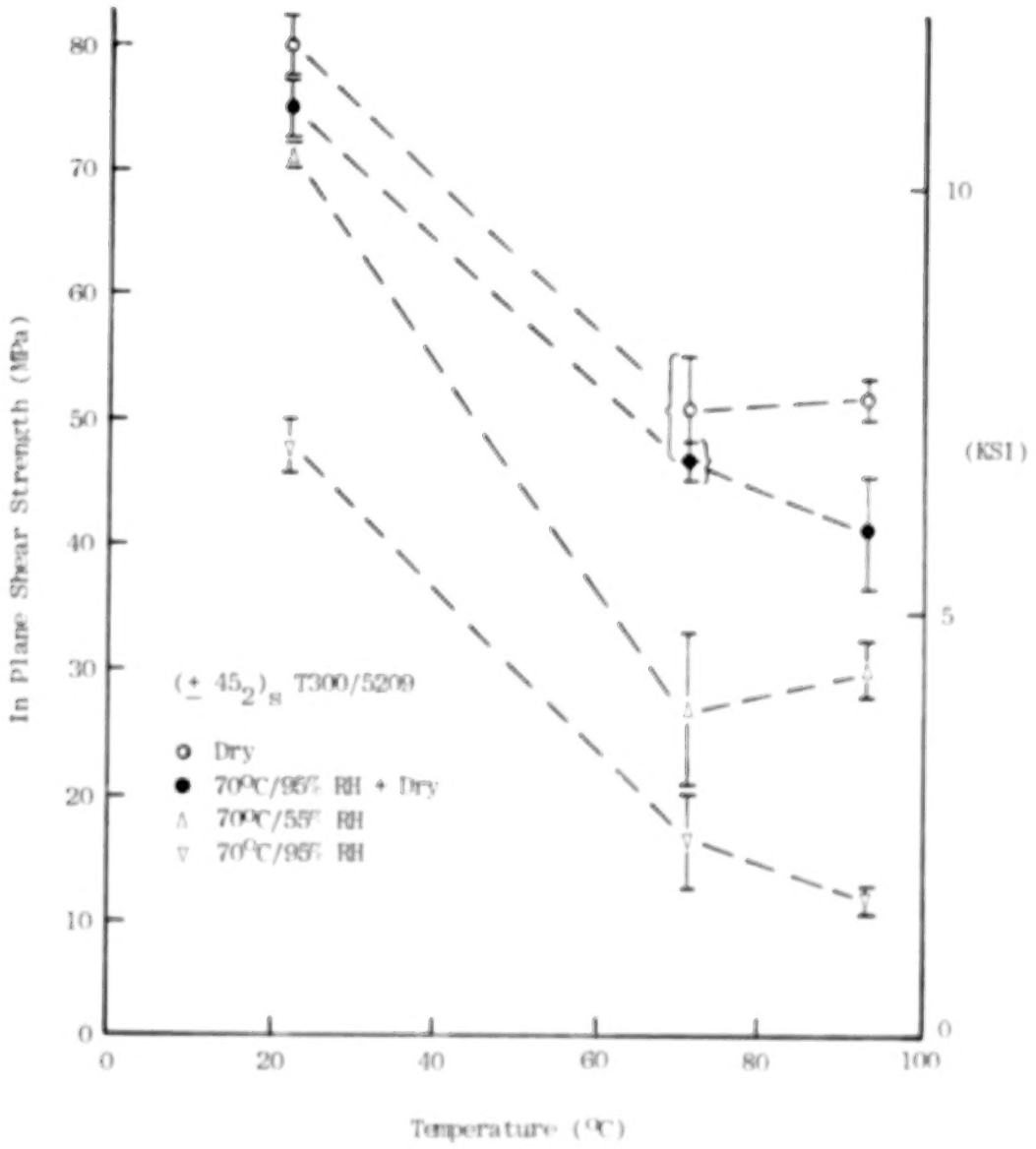

Figure 23. In Plane Shear Strength of T300/5209 vs. Temperature. Ranges Include All Cycled and Uncylced Specimen Data.

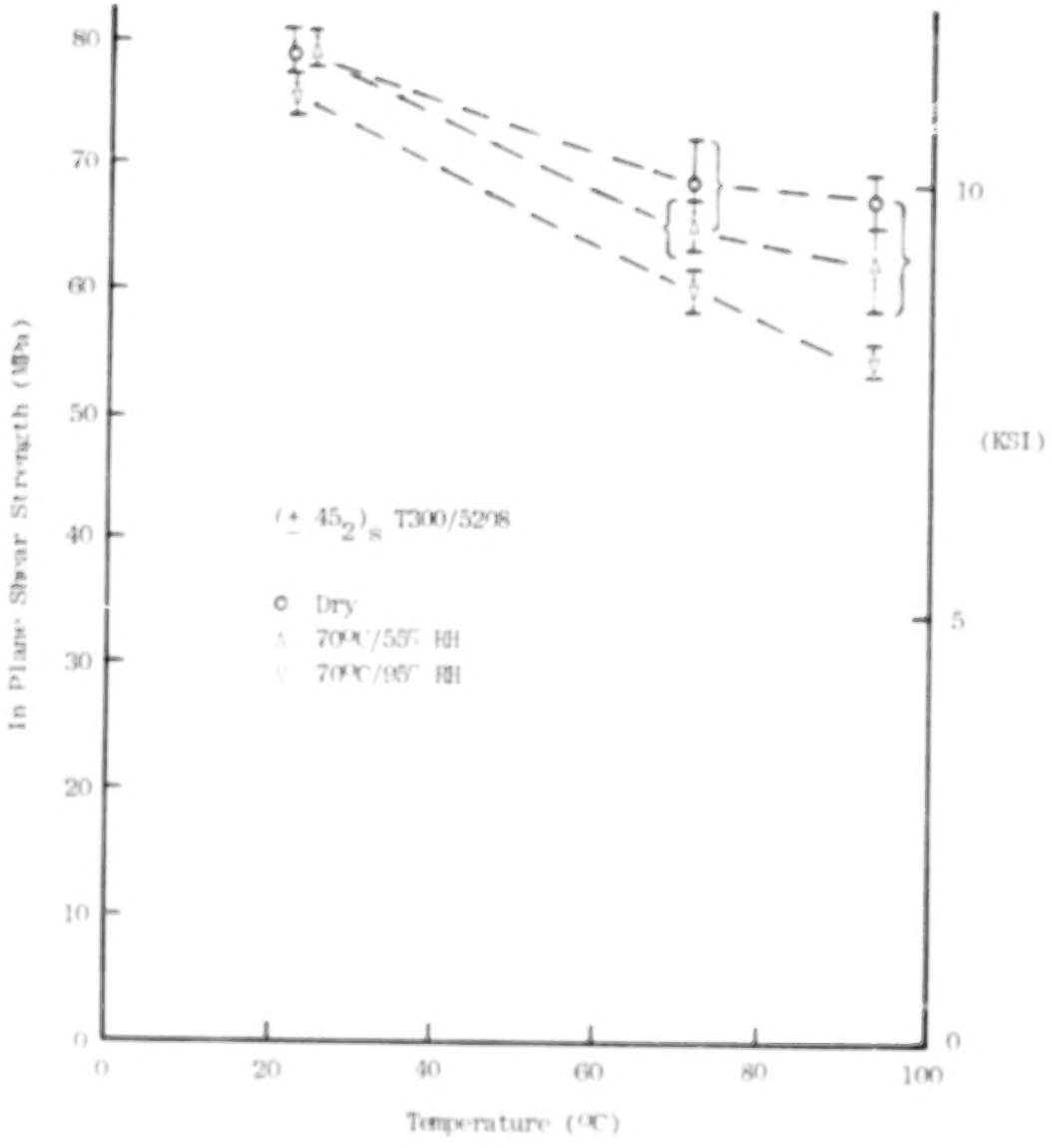

Figure 24. In Plane Shear Strength of T300/5208 vs. Temperature. Ranges Include All Cycled and Uncycled Specimen Data.

Table 2

RESULTS OF FOUR-POINT FLEXURE TESTS (s = L/3)

Material	L/h (see Fig. 3)	τ_{max} at failure MPa (ksi)	Failure Mode
T300/5209	I	69.7 (10.1)	Shear
"	I	67.6 (9.8)	"
"	I	58.6 (8.5)	"
"	II	60.7 (8.8)	"
"	II	75.9 (11.0)	"
GY70/339	I	38.6 (5.6)	Flexure
"	I	53.1 (7.7)	Flexure
"	II	63.5 (9.2)	Flex/Shear
"	III	44.1 (6.4)	Shear/Bearing
T300/5209	Notched Compression	12.4 (1.8) 6.9 (1.0)	Shear
GY70/339	Notched Compression	11.0 (1.6) 9.7 (1.4)	Compression Failure

In terms of the ratio of $\sigma^T_{max}/\tau_{max}$ in a given test geometry, one obtains the following result:

$$\sigma^T/\tau = \frac{2L}{h} \text{ in 3 point bending}$$

$$\sigma^T/\tau = \frac{L}{h} \text{ in 4-point bending where } s = L/4$$

Referring to Figure 25, lines BC and EF describe the transition from one failure mode to the other as a function of span (L) to depth (h) ratio. To the right of the lines, flexural failure is expected. To the left, shear failure should occur. However, at some small pin-spacing-to-depth ratio s/h one begins to see excessive matrix compressive bearing deformation between the loading pins. Taking s/h = 2 as the critical value, lines AB and DE are drawn in Figure 25. To the left of these lines, bearing failures are expected to dominate the response. For a particular ratio of tensile strength to shear strength, one notes that the four point bend test gives twice as large a range of L/h in which shear failure is dominant than the range available in the three point bend test. Furthermore, if the matrix or interface shear strength is reduced due to absorbed moisture, elevated temperature, or hygrothermal cycling, the new composite σ^T/τ ratio (the dashed band in Figure 25) is driven upward. Therefore, if one can choose the correct L/h ratio to give interlaminar shear failure in the initial dry condition, then all exposed samples will also fall within the shear failure window lying above DEF in the four point bend test.

Figure 26 shows the dry σ^T/τ ratios for T300/5209 and GY70/339 composites. Four point bend tests were run on both materials for span-to-depth ratios denoted by I, II and III in the diagram. In this case the distance between each set of pins was equal and s = L/3. The test data in Table 2 confirm the essential utility of the diagram in choosing the shear window. T300/5209 specimens all failed by interlaminar shear parallel to the fiber orientation at values five to ten times higher than those

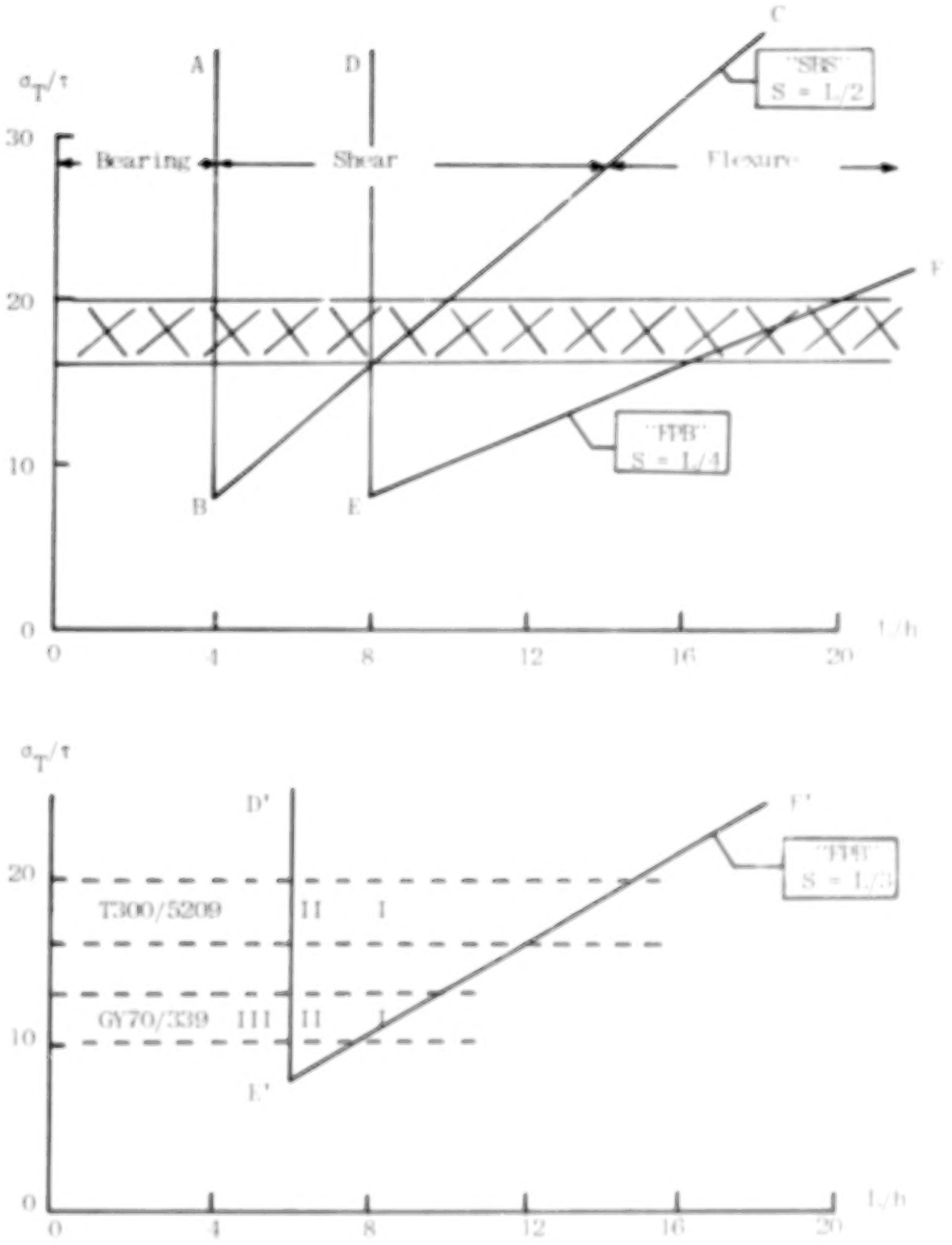

Figure 25. Analysis of Expected Failure Modes in Unidirectional Composites as a Function of Span to Depth L/h Ratio and Flexure Test Configuration (See Fig. 26).

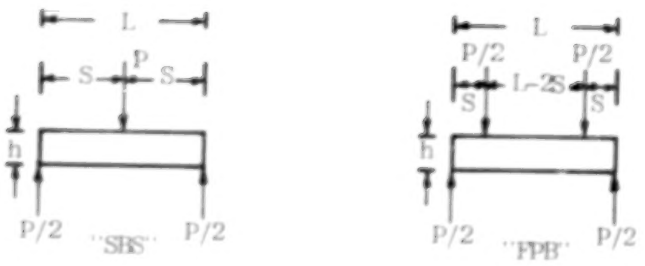

Figure 26(a). Flexural Test Geometry for Short Beam Shear (SBS) and Four-Point Bend (FPB) Tests.

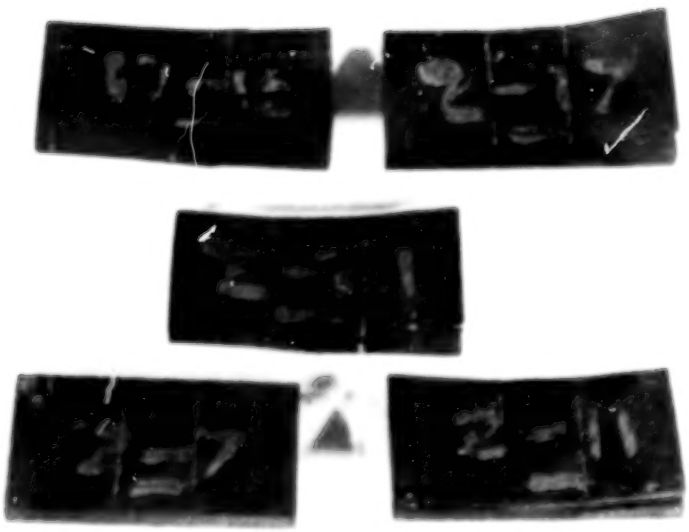

Figure 26(b). Typical Shear Failures in the Four-Point Bending (S = L/3) Fixture. See Table B4 for Specimen Hygrothermal History.

obtained in notched compression tests. The test results for GY70/339 demonstrate that for intrinsic tensile strength to shear strength ratios of ten or less it is not possible to force an interlaminar shear failure in a simple bend test. Mixed mode failures predominate as the corner (E') of the shear window is approached in testing.

These preliminary experiments, therefore, identified the four point flexure test as a simple and reliable method to examine any hygrothermally induced alteration of interlaminar shear strength in T300/5209 and T300/5208. In samples which have been exposed to cycling and subsequently dried, any reduction in shear strength will be indicative of either interfacial debonding or matrix microcracking, since effects due to matrix plasticization are considered reversible upon redrying.

Sixteen-ply unidirectional T300/5208 and T300/5209 laminates 2.54 cm (1 in.) long by 1.27 cm (0.5 in.) wide were tested under four point flexure at 25°C. The loading pins were equally spaced 0.64 cm (0.25 in.) apart over a total span of 1.91 cm (0.75 in.). The resulting span-to-depth ratio L/h = 9 insured failure of all specimens by interlaminar shear rather than by tensile or compressive failure (see Figure 26b). The interlaminar shear strength is calculated from the equation

$$\tau_{max} = 3P/4bh$$

where P is the peak load, b the specimen width, and h the specimen thickness. Figures 27 and 28 plot the interlaminar shear strength (ILS) of T300/5209 and T300/5208 as a function of the equilibrium water content absorbed by each specimen at 93°C prior to hygrothermal cycling, drying, and testing. Specimens were hygrothermally cycled 100 times over the temperature range indicated, as described in Chapter 2.

In the T300/5208 series no statistically significant change in ILS can be observed as a function of prior moisture content or hygrothermal cycling. The T300/5209 series shows a significant loss of ILS after exposure to humid-

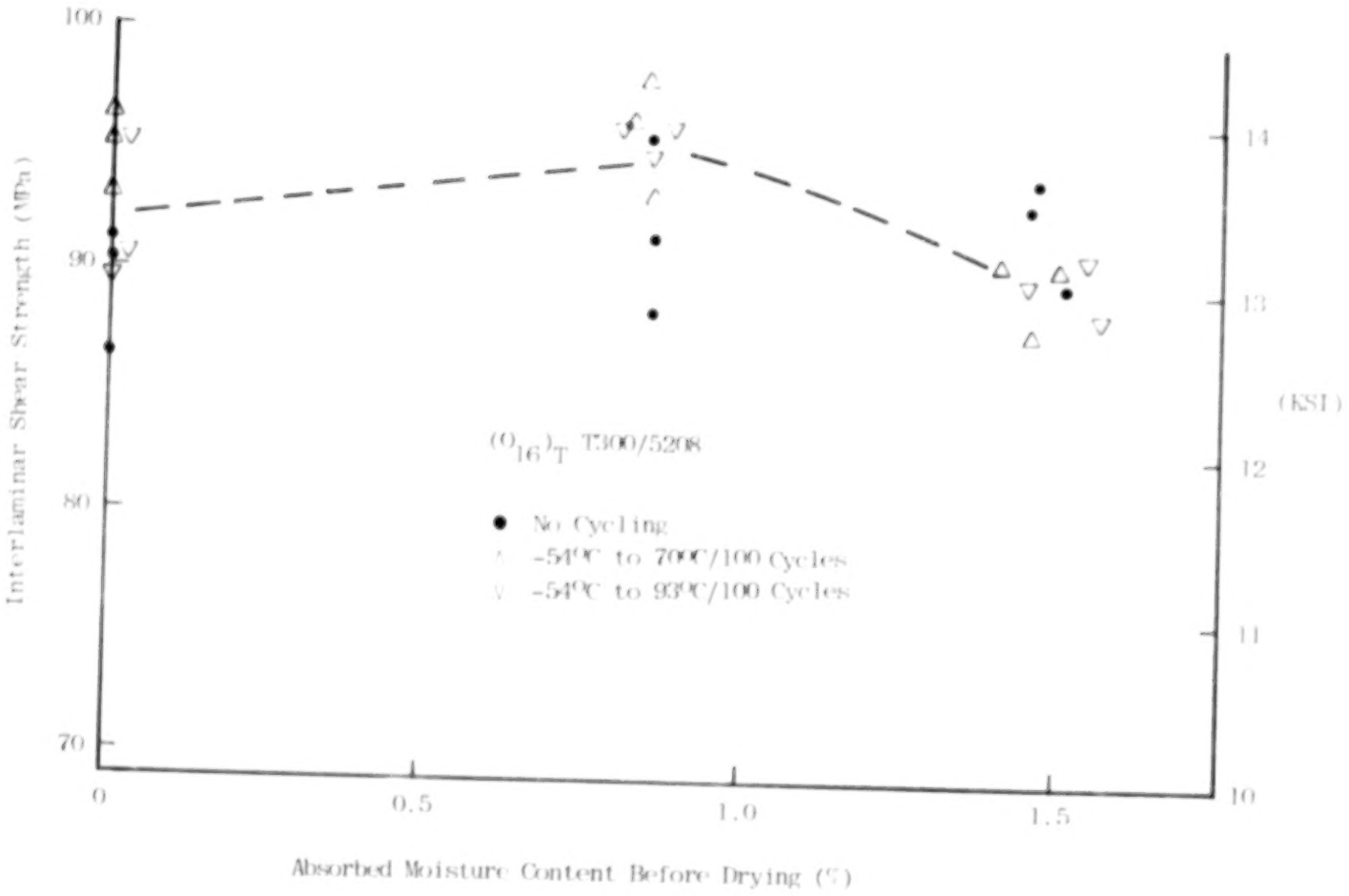

Figure 27. Interlaminar Shear Strength of T300/5208 vs. Equilibrium Moisture Absorbed Prior to Cycling, Drying and Testing.

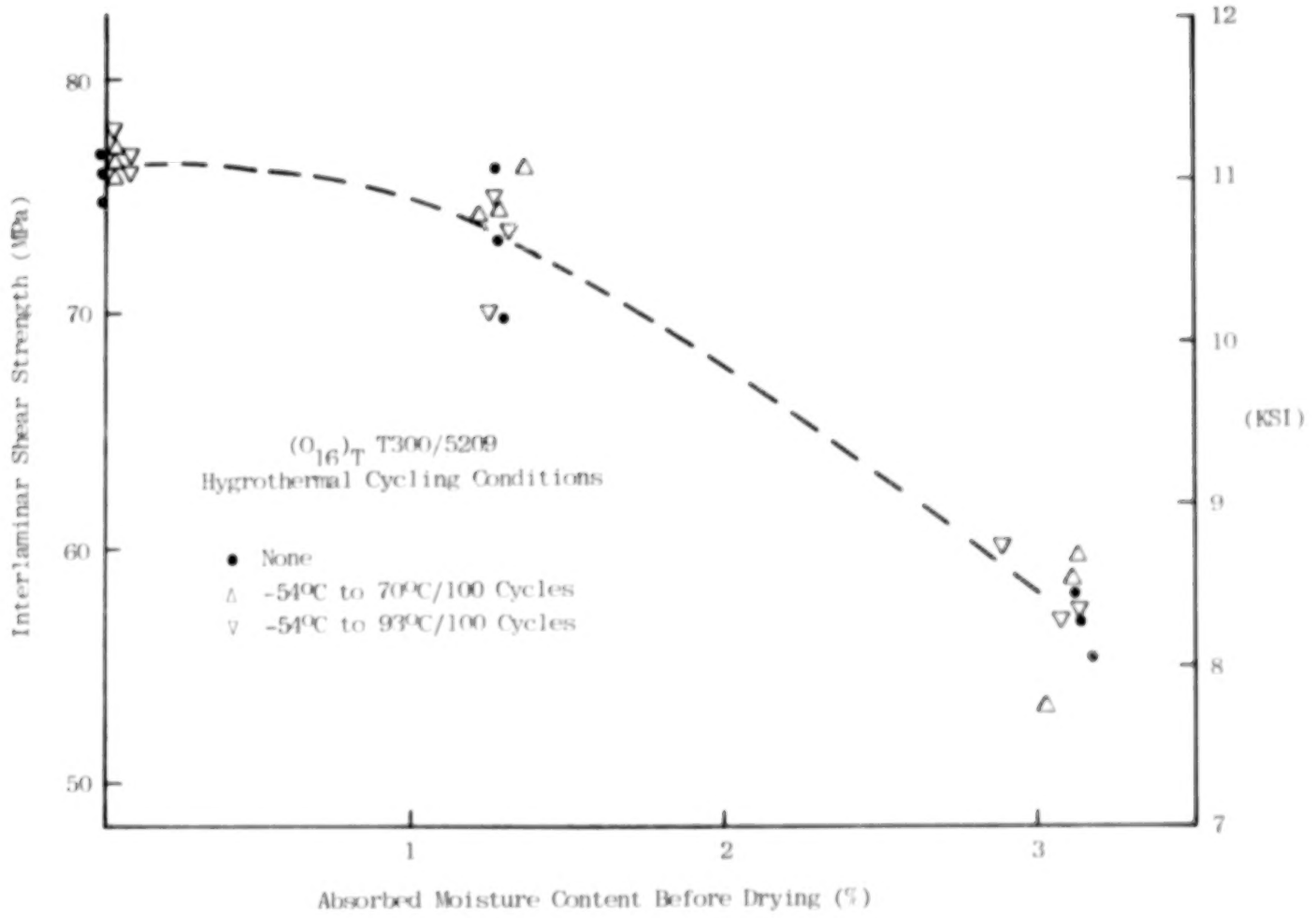

Figure 28. Interlaminar Shear Strength of T300/5209 vs. Equilibrium Moisture Absorbed Prior to Cycling, Drying and Testing.

ity at 93°C. However, the loss of strength appears to be independent of hygrothermal cycling. The large reduction in ILS for T300/5209 specimens which absorbed 3 percent moisture may be contributed to by the extreme loss of inplane shear stiffness and strength noted in this system at 93°C after exposure to 95% RH at 70°C (see Figures 22 and 23). The interlaminar shear specimens exposed to 95% RH at 93°C have been subjected to temperature greater than the wet glass transition temperature of this material. The lack of ILS loss in T300/5209 exposed to lower humidity and in all T300/5208 tests indicates the importance of not exceeding the wet glass transition temperature during accelerated moisture conditioning at elevated temperatures.

In T300/5209, accelerated moisture conditioning at temperatures near or above the wet glass transition temperature appears to cause a permanent loss of inplane shear strength (Figure 23) as well as interlaminar shear strength which accompanies those reversible losses due to moisture-induced plasticization. On the other hand, the lack of these effects in T300/5208 tests suggests that moisture conditioning at temperatures as high as 93°C can be used with this system in an accelerated test program.

CHAPTER 4

MICROSCOPIC EVIDENCE FOR DAMAGE DUE TO HYGROTHERMAL CYCLING

4.1 MICROSCOPIC EXAMINATION FOR DAMAGE AFTER TEN HYGROTHERMAL CYCLES

2.5 by 2.5 cm square specimens from eight-ply unidirectional, $(\pm 45, 0, 90)_s$, and $(90, 0, \pm 45)_s$ laminates previously brought to equilibrium at 70°C with 55 and 95 percent humidity were cycled ten times between -54°C and 70 or 93°C. Specimens were held ten minutes at each temperature and were hand carried between air circulating chambers maintained at the two temperature extremes. After five cycles, all specimens were replaced in the humidity chambers in which they were initially exposed and held overnight, in order to reintroduce moisture to the specimen surfaces and edges before the second set of five thermal cycles was completed. The specimens were sectioned as shown in Figure 29 to provide a measure of microscopic damage near the laminate free edges, surfaces and interior and to determine the depth of penetration of surface or free edge initiated damage. Macroscopic and microscopic examination of specimens showed little obvious damage after ten cycles, with the exception of $(\pm 45, 0, 90)_s$ T300/5208 laminates which contained delamination cracks at the free edge, independent of moisture content and cycling history. Based on these results, we chose to give all other specimens in the test matrix 100 cycles between -54°C and 70 or 93°C, according to the description given in Chapter 2.

4.2 MICROSCOPIC EXAMINATION FOR DAMAGE AFTER 100 HYGROTHERMAL CYCLES

From each material, specimens at three moisture contents (dry, equilibrated at 70°C/55% RH, and equilibrated at 70°C/95% RH) were exposed to 100 hygrothermal cycles from -54°C to 70 or 93°C prior to sectioning. Of the eighty specimens which were microscopically examined, very few

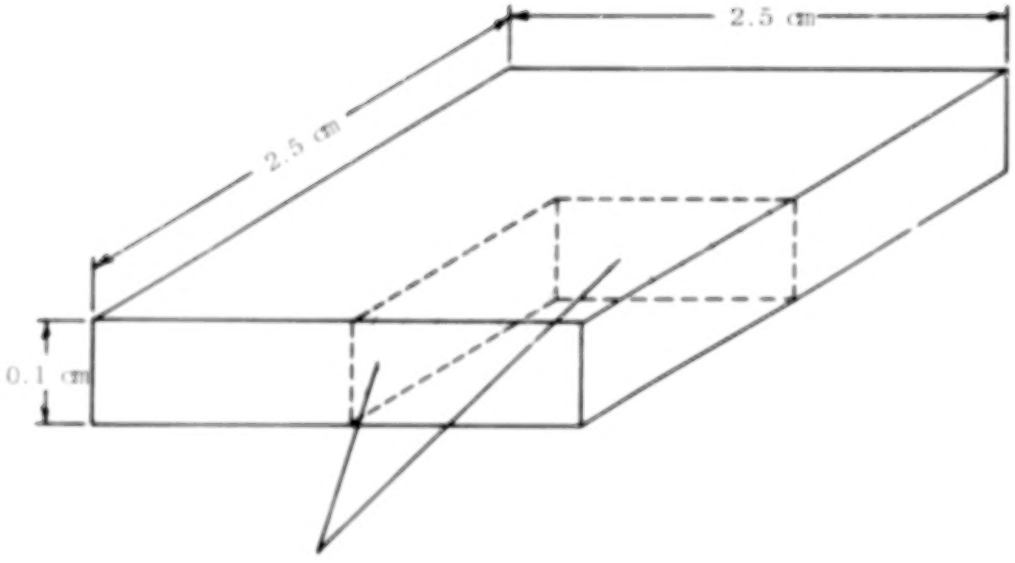

Surfaces Examined by Metallography

Procedure: Sections were cut using a thin blade diamond wheel, and mounted in acrylic cold mount. They were polished with silicon carbide paper, and then on an automatic polishing wheel ending with 0.05 micron compound.

Figure 29. Schematic of Surfaces Examined by Metallography and Metallographic Procedure.

showed any evidence that either the moisture absorption conditions or cycling conditions caused permanent microstructural damage in the form of microcracking. In those few in which microcracks were observed (with the exception of edge cracking in T300/5208 $(\pm 45, 0, 90)_s$ laminates), microcracking was localized, scattered, and very sparse and did not appear to be related to a general degradation mechanism. The micrographs which are displayed in this chapter are shown primarily to demonstrate that the metallographic techniques which were employed can indeed observe cracking when such damage exists in the laminates. They should not be considered as representative of the specimens as a whole or even representative of the particular cross-section of the specimen unless so stated in the discussion.

Figures 30 and 31 show low and high power micrographs of dry UD and quasi-isotropic T300/5209 laminates cycled to a maximum temperature of 93°C. The microstructures, Figures 30a and 31a, are indistinguishable from micrographs of the original as fabricated panels shown in Appendix A. All 5209 laminates contain rounded matrix voids with dimensions on the order of 10-30 μm. There is little evidence that these rounded voids act as microcrack iniation sites during hygrothermal cycling.

Figure 32a shows the edge of a $(\pm 45, 0, 90)_s$ T300/5209 laminate conditioned at 70°C/95% RH before cycling. Lack of edge delamination should be noted for comparison to T300/5208 laminates in Figures 35 and 36. In Figure 32b a transverse crack in the outer 45° ply is shown after exposure to 70°C/95% RH and cycling to a peak temperature of 70°C. The crack runs around fibers. The tortuous path indicates a propensity for debonding at the fiber matrix interface and a linking of interface debonding by matrix cracking. The large void to the right of the crack shows no influence on the crack. The fine "craze-like" lines in the matrix rich region at the bottom of Figure 32b are only artifacts of the sectioning and polishing procedures and do not extend to any great depth into the matrix perpendicular to the section surface.

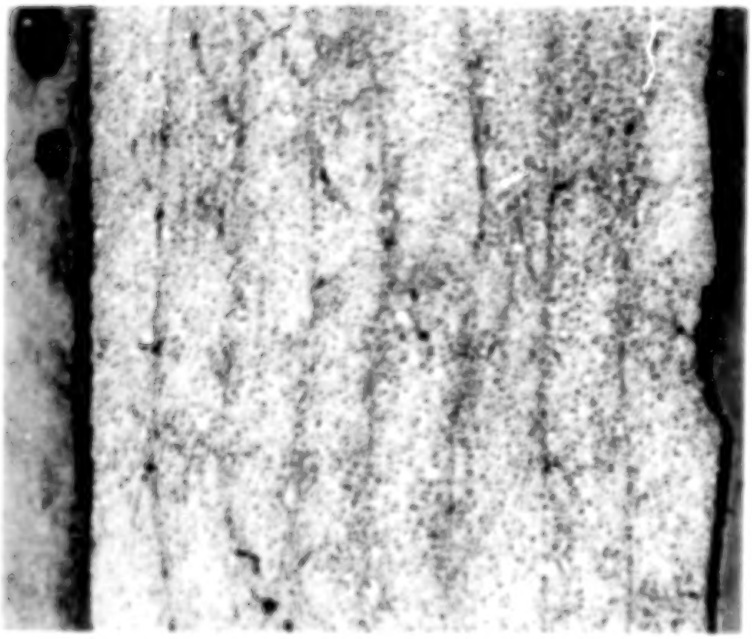

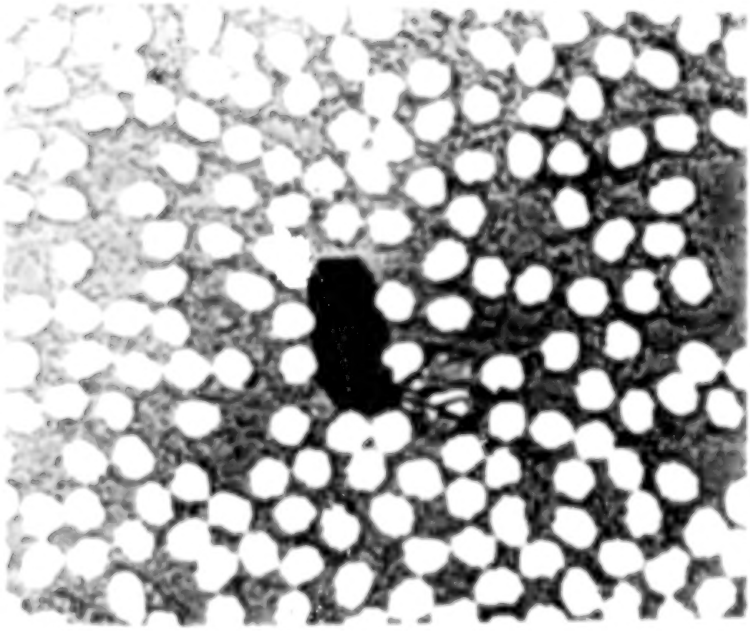

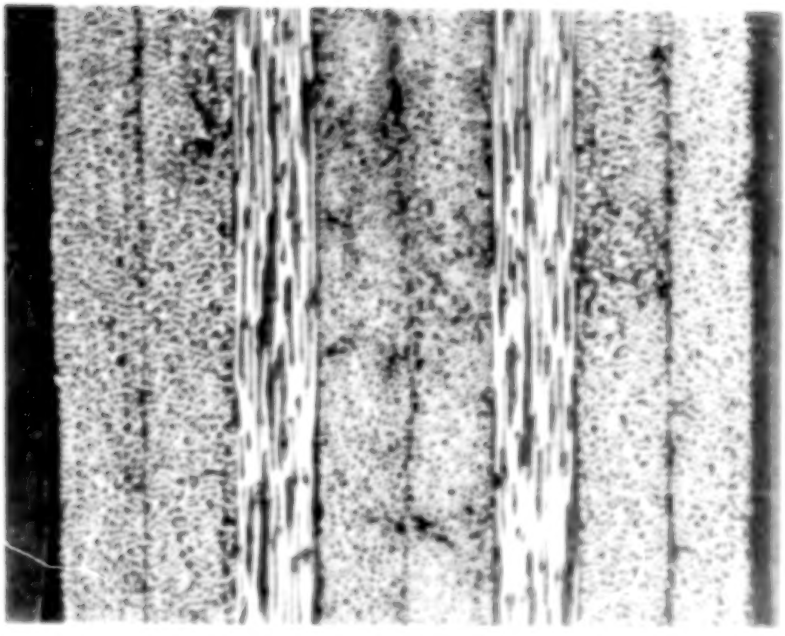

(c) Plate 0829, 100X, (0$_4$/±45/0/90)$_s$, 1000 psi, Class I, -54°C to 91°C/100 cycles.

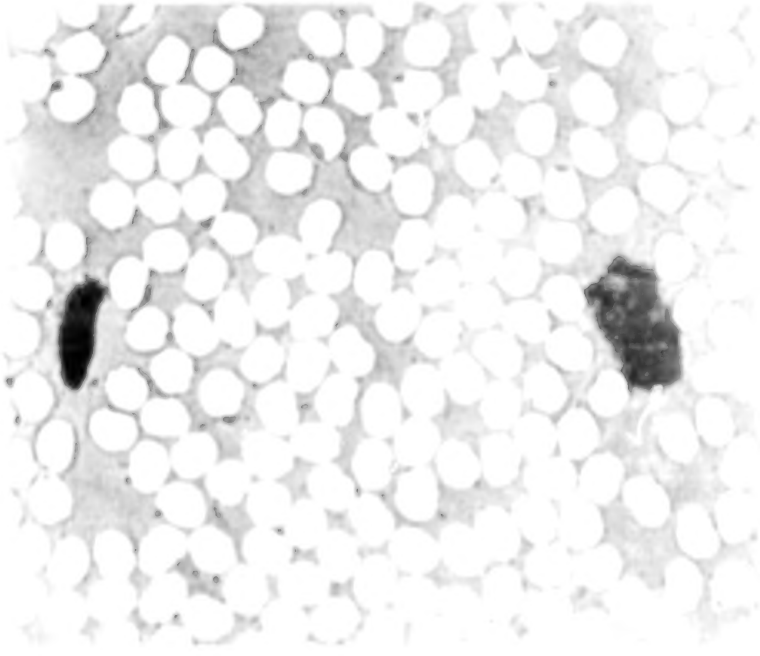

(d) Plate 0841, 100X, Sp

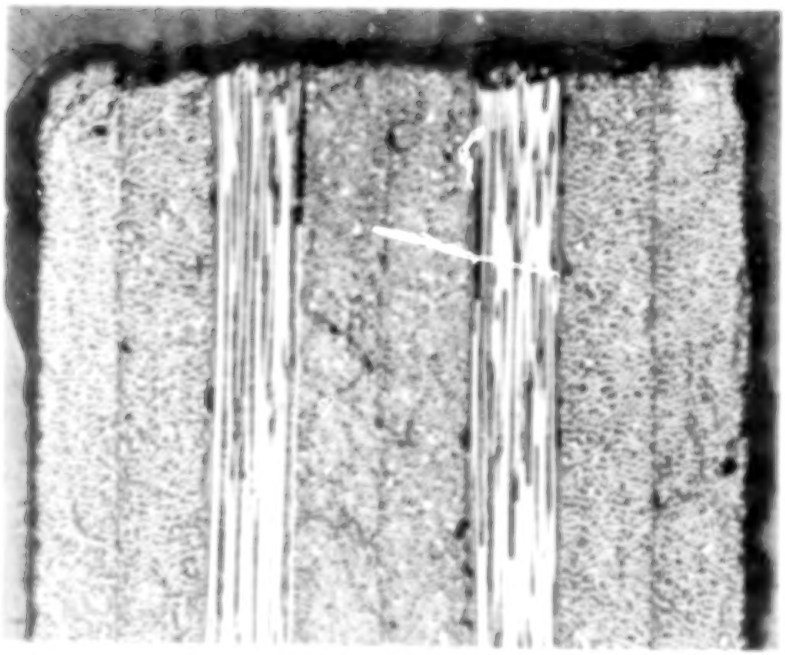

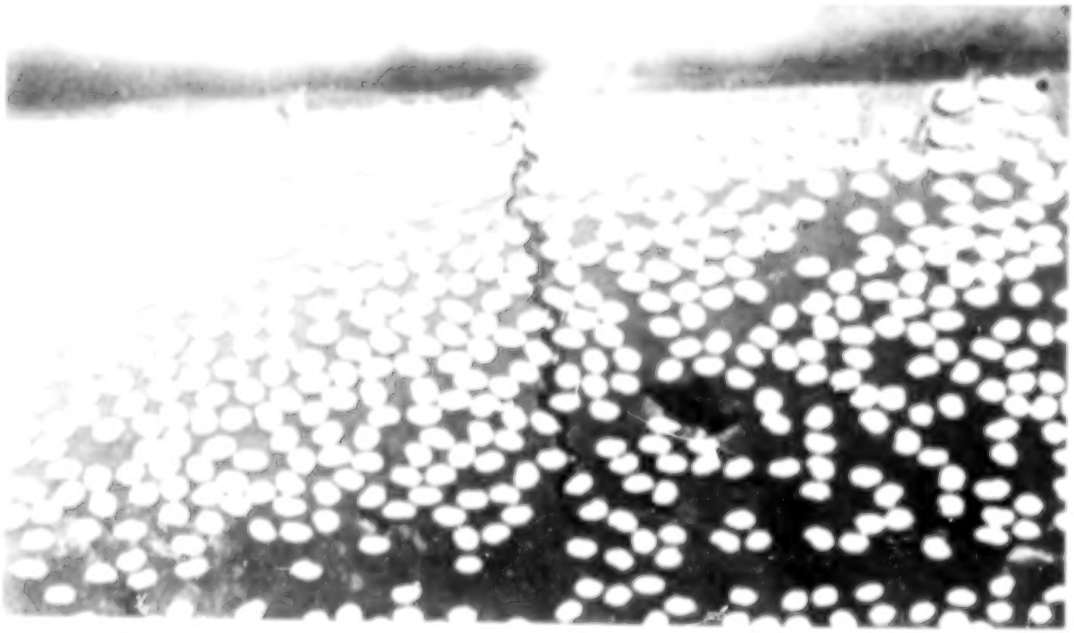

Figure 33 shows a large lenticular microvoid observed in only one other T300/5209 specimen. It is believed to have been present after fabrication and not caused by moisture absorption or cycling. However a micrograph at 500X (Figure 33b) shows microcracks ahead of the main lenticular void which may have propagated during hygrothermal conditioning and cycling. The linking up of stringer like voids and eventual delamination during moisture exposure was observed in CY70/339 exposed to water immersion or 95% RH at 82° and 93°C [14], temperatures which are well above the glass transition temperature of the 339 epoxy. The observations made here lead us to conclude that voids in laminates will contribute to enhanced hygrothermal damage only if two conditions are met: 1) that they exist in stringers between plies; and 2) that the temperature of exposure is well above the glass transition temperature of the matrix.

Figure 34 shows two more isolated microcracks in T300/5209 which extend to a depth of the surface ply. The crack in Figure 34a is especially interesting because it does not connect to the surface in this section. This may be evidence that the local tensile stress at the fiber-matrix interface (due to swelling of the matrix by moisture) is sufficiently high to initiate debonding or interface rupture during hygrothermal cycling. Alternatively, we may argue that the chemical bonding between fiber and matrix can be broken more easily when the matrix changes from a glassy to rubbery state during the absorption of moisture at high temperatures.

Figures 35 and 36 show evidence for free edge delamination of T300/5208 $(\pm 45, 0, 90)_s$ laminates after 100 cycles between -54°C and 93°C. The delamination is found primarily within or between the outer 45° plies and extends into the laminate a distance of 1 to 3 ply thicknesses. The edge cracking is just as prominent in dry specimens as those exposed to moisture. Furthermore, some delamination was observed at the opposite end of the specimen section which had been sliced by the diamond saw prior to metallographic polishing. It is suspected that the delamination observed here is caused by a combination of high thermally induced free edge stresses, as discussed in the next chapter, and some degree of stressing induced by

TABLE OF CONTENTS

Chapter	Title	Page	
	FOREWORD	i	1/A5
	ABSTRACT	ii	1/A6
	LIST OF TABLES	v	1/A9
	LIST OF FIGURES	vi	1/A10
1	HYGROTHERMAL DEGRADATION OF GRAPHITE-EPOXY COMPOSITES	1-1	1/B1
	1.0 INTRODUCTION	1-1	1/B1
	1.1 ASSESSMENT OF HYGROTHERMAL DEGRADATION - LITERATURE REVIEW	1-6	1/B6
	1.1.1 Definition of Environment	1-6	1/B6
	1.1.2 Effect of Moisture on Mechanical Properties	1-7	1/B7
	1.1.3 Effect of Hygrothermal Cycling on Kinetics of Moisture Sorption	1-10	1/B10
	1.1.4 Effect of Hygrothermal Cycling on Mechanical Properties	1-12	1/B12
	1.1.5 Assessment of Hygrothermal Degradation Mechanisms	1-12	1/B12
	1.2 PROGRAM DESCRIPTION	1-14	1/B14
	1.3 MATERIAL PROCESSING	1-19	1/C5
2	THE COUPLING BETWEEN APPLIED AND RESIDUAL STRESS AND MOISTURE SORPTION	2-1	1/C8
	2.1 DIMENSIONAL CHANGES CAUSED BY MOISTURE ABSORPTION	2-1	1/C8
	2.2 MOISTURE ALTERED RESIDUAL STRESSES	2-5	1/C12
	2.3 DESORPTION UNDER STRESS	2-9	1/D4
	2.4 INFLUENCE OF APPLIED STRESS DURING DESORPTION ON RESIDUAL STRESSES	2-17	1/E2
	2.5 HYGROTHERMAL CYCLING EXPERIMENTS	2-20	1/E7
3	THE INFLUENCE OF HYGROTHERMAL HISTORY ON MATRIX AND INTERFACE DOMINATED LAMINATE PROPERTIES	3-1	1/E12
	3.1 INPLANE SHEAR TESTS	3-1	1/E12
	3.2 INTERLAMINAR SHEAR TESTS	3-10	1/F7
4	MICROSCOPIC EVIDENCE FOR DAMAGE DUE TO HYGROTHERMAL CYCLING	4-1	1/G8
	4.1 MICROSCOPIC EXAMINATION AFTER 10 HYGROTHERMAL CYCLES	4-1	1/G8
	4.2 MICROSCOPIC EXAMINATION AFTER 100 HYGROTHERMAL CYCLES	4-1	1/G8

TABLE OF CONTENTS (continued)

Chapter	Title	Page	
5	ANALYSIS OF HYGROTHERMALLY INDUCED STRESS IN GRAPHITE-EPOXY LAMINATES	5-1	2/A10
	5.1 ANALYSIS DESCRIPTION	5-1	2/A10
	5.2 ANALYSIS OF MOISTURE INDUCED STRESSES	5-3	2/A12
	5.3 HYGROTHERMAL STRESS ANALYSIS	5-7	2/B2
6	DISCUSSION OF RESULTS	6-1	2/C14
	6.1 ASSESSING PERMANENT AND REVERSIBLE INTERFACIAL BOND DEGRADATION	6-1	2/C14
	6.2 ENERGY CONCEPTS FOR INITIATION AND GROWTH OF HYGRO-THERMAL DAMAGE	6-5	2/D4
	6.3 CONCLUSIONS	6-11	2/D10
	REFERENCES	7-1	2/D13
Appendices			
A	MATERIAL PROCESSING INFORMATION	A-1	2/E4
B	MECHANICAL TESTING TABULATION	B-1	2/F7

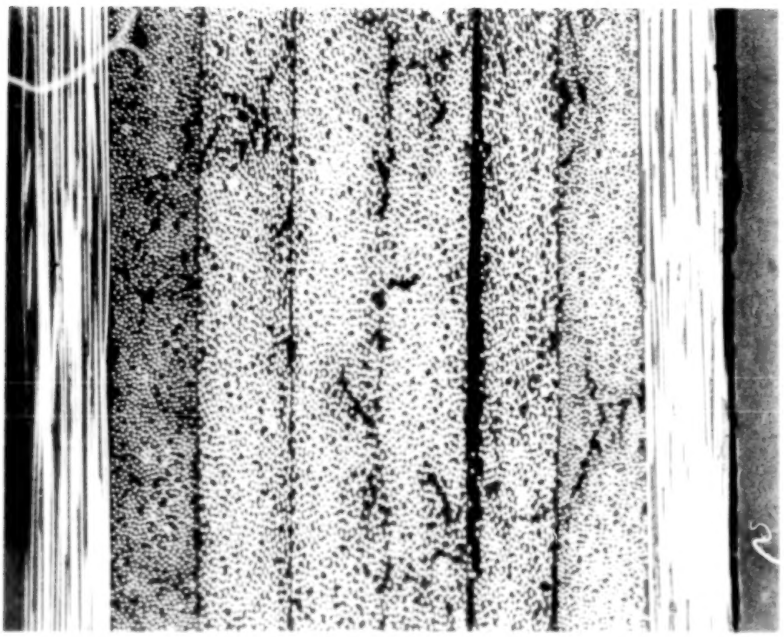

(a) Plate D2837, 100X, T300/5209, Spec 13-2, exposed 70°C/95% RH, -53°C to 70°C/100 cycles.

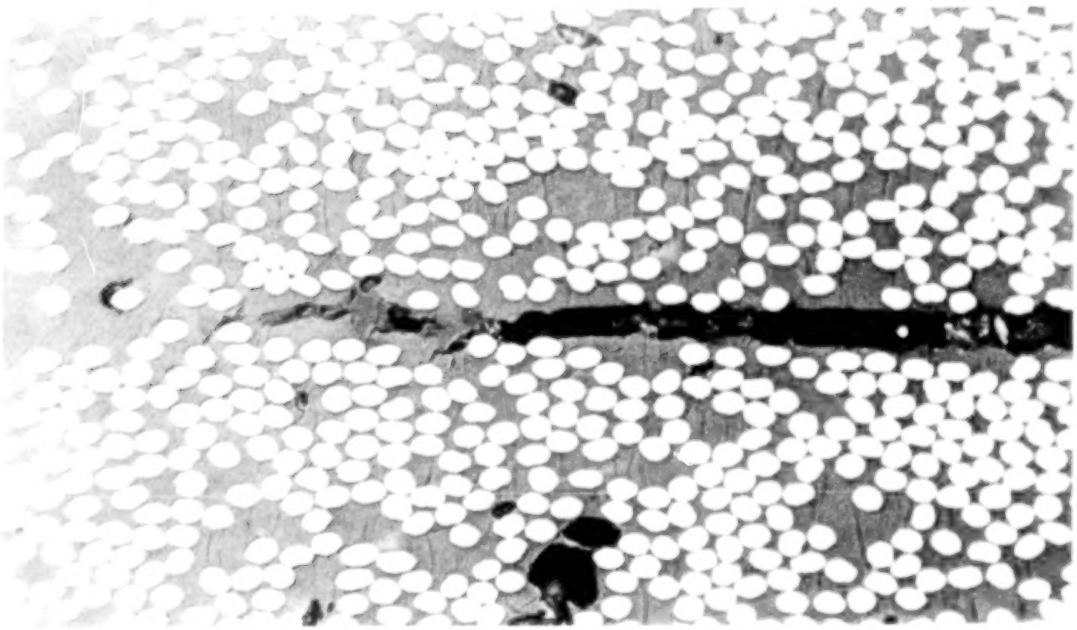

(b) Plate D2838, 500X, Spec 13-2.

Figure 33.

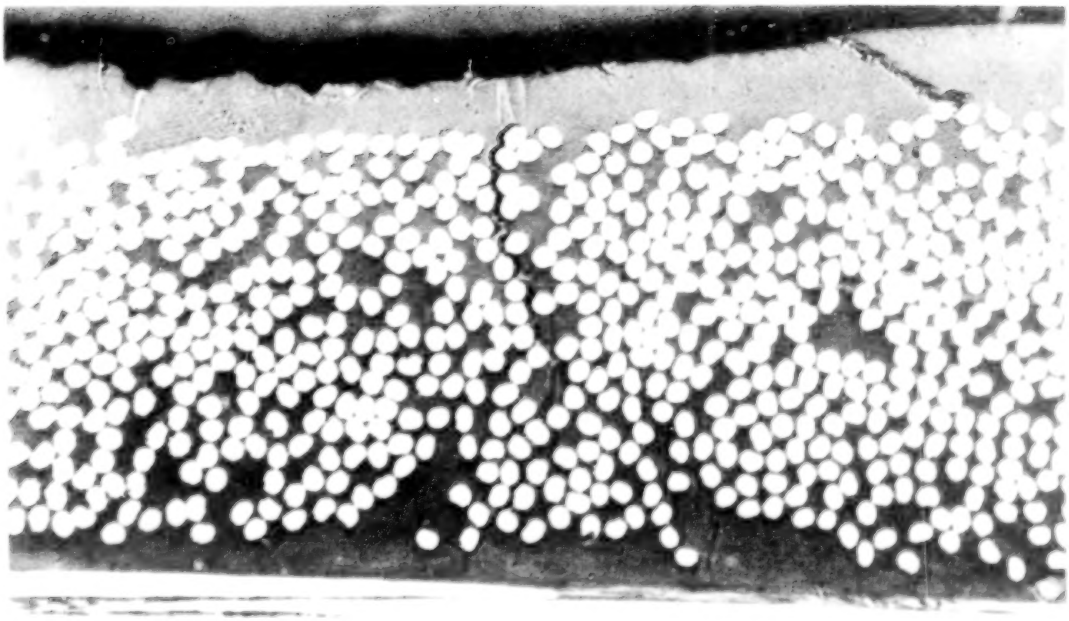

a) Plate 2836, 500X, $(90/0/\pm45)_s$ 1300/5209, Spec 15-4, exposed 70°C/95% RH, -54°C to 70°C/100 cycles.

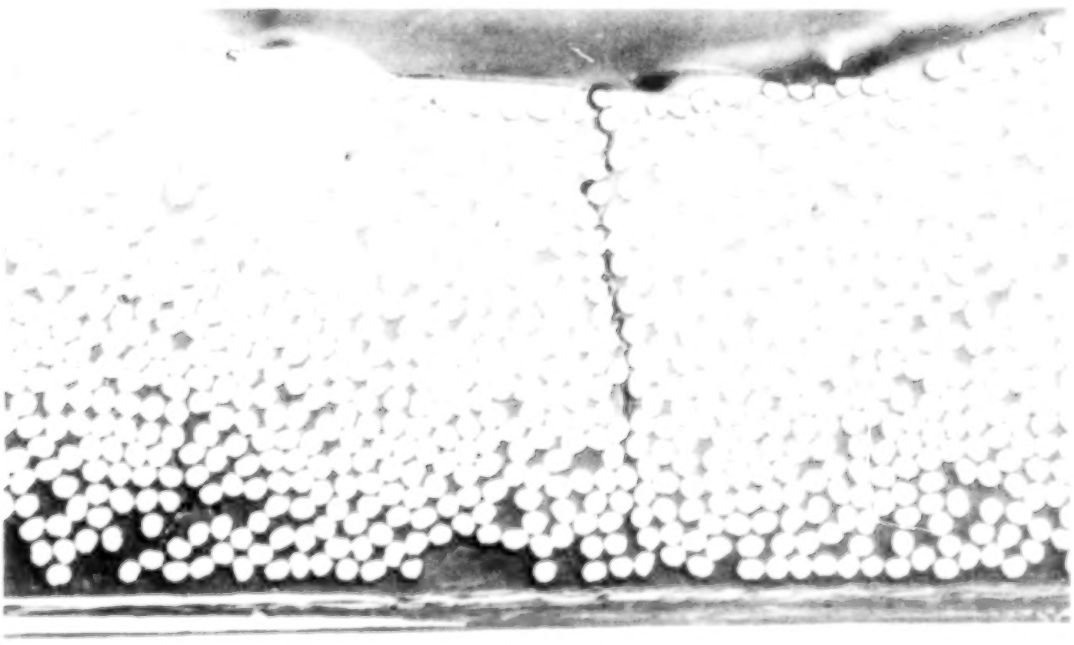

(b) Plate D2840, 500X, 1300/5209, Spec 15-4, exposed 70°C/95% RH, -54°C to 93°C/100 cycles.

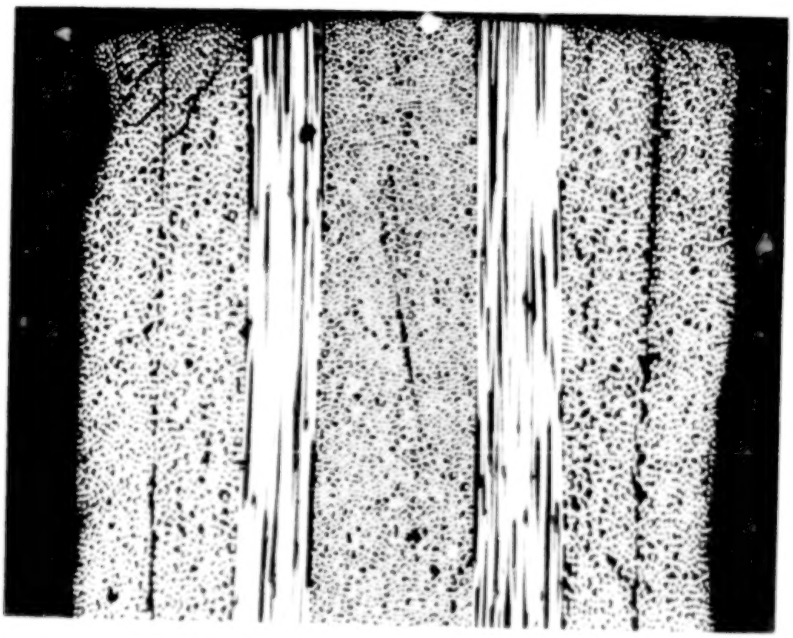

(a) Plate D2807, 100X, $(\pm 45/0/90)_s$ T300/52 8, Spec 27-4, dry, -54°C to 93°C/100 cycles.

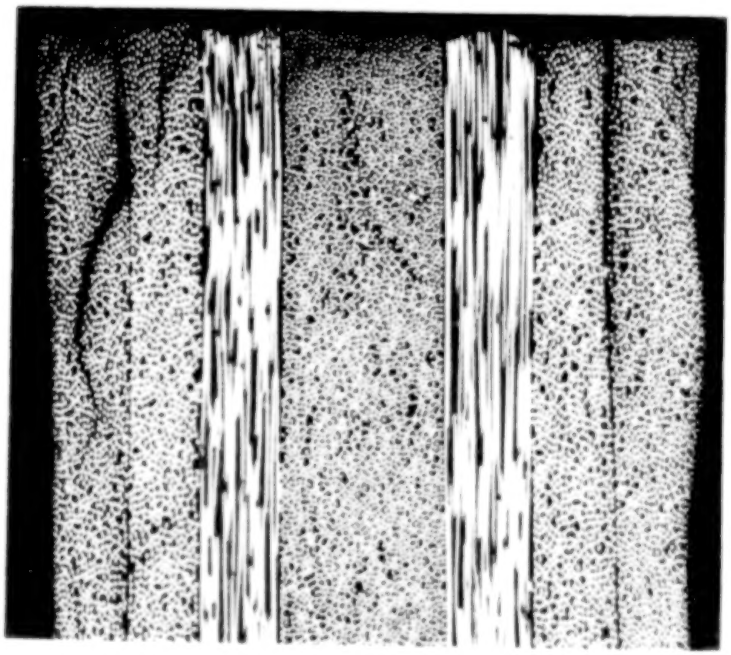

(b) Plate D2815, 100X, T300/5208, Spec 27-12, exposed 70°C/55% RH, -54°C to 93°C/100 cycles.

Figure 35.

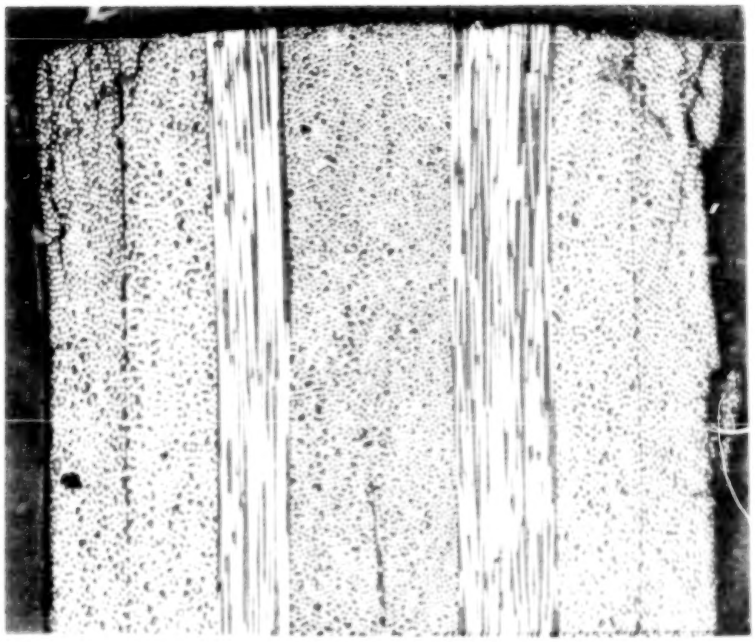

(a) Plate D2810, 100X, T300/5208, Spec 27-8, exposed [illegible] RH, -54°C to 93°C/100 cycles.

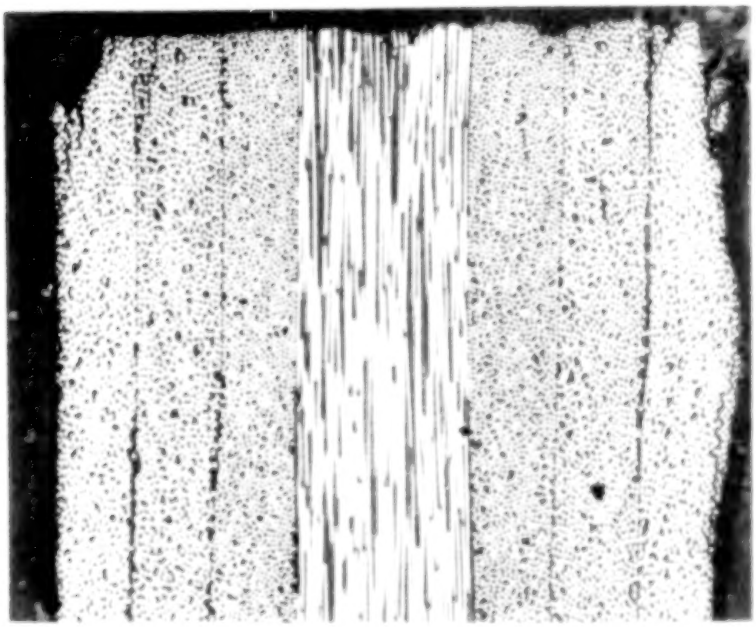

(b) Plate D2811, 100X, Spec 27-8, Section at 90° to (a).

Figure 36.

the diamond saw cutting operation. No edge delaminations were observed in any T300/5209 specimens (Figure 32) or in unidirectional and $(90, 0, \pm 45)_s$ T300/5208 specimens (Figure 37).

Figure 38 shows the only transverse cracking observed in the T300/5208 series. These specimens were taken from the panel fabricated at low pressure to develop large voids shown in Figure 38a. As in T300/5209, the rounded voids do not act as crack initiation sites during hygrothermal cycling. The transverse cracks appear to initiate at surface irregularities and extend only through the surface ply. At higher magnification in Figure 38b, there is evidence of fiber splitting and less evidence for the smooth matrix-fiber interface debonding typical of the T300/5209 system. Observations of transverse cracks in the thicker (0.14 cm) "voidy" T300/5208 laminate, but not in the thinner (0.10 cm) standard processed T300/5208 laminates is perhaps similar to observations by Hedrick and Whiteside [20] that thin laminates or neat resin specimens showed little or no evidence of surface cracking after hygrothermal cycling, while thicker laminates exposed to identical conditions exhibited surface cracks.

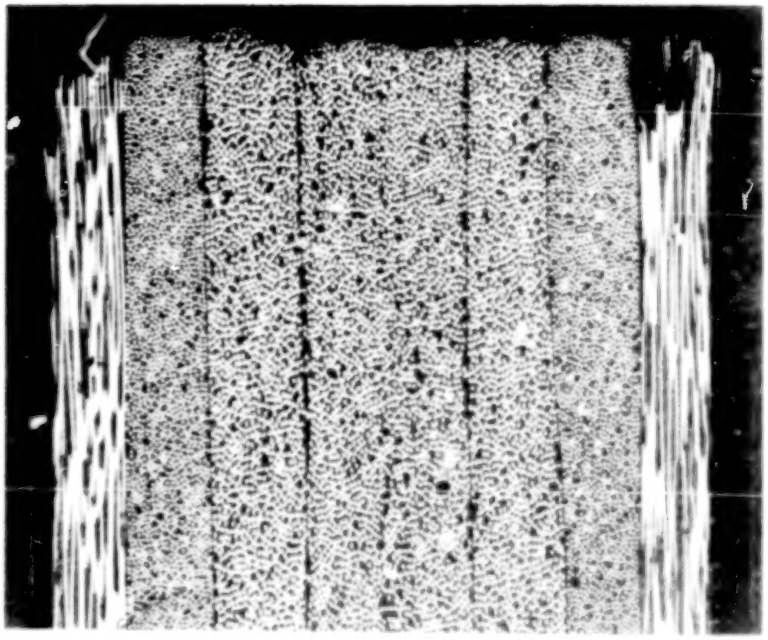

(a) Plate D2817, 100X, $(90/0/45/-45)_S$ T300/5208, Spec 30-2, dry, -54°C to 70°C/100 cycles.

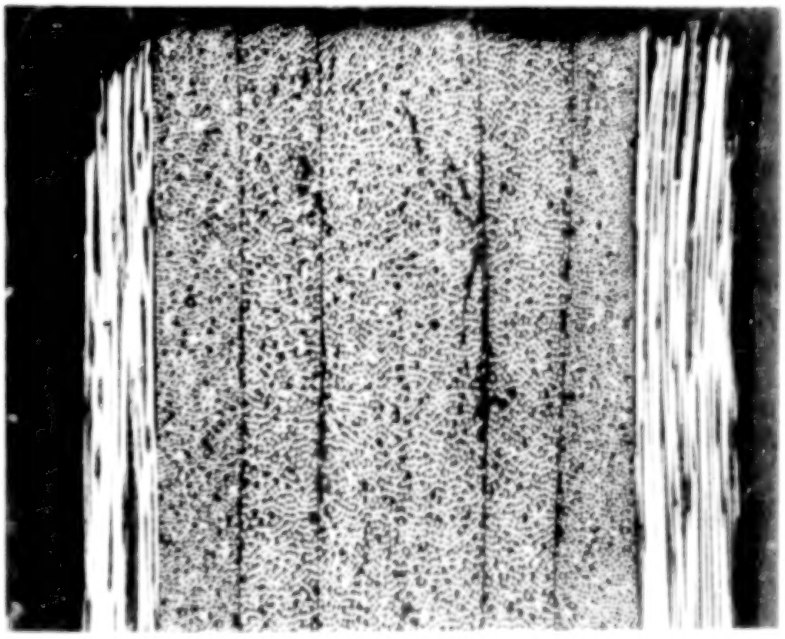

(b) Plate D2843, 100X, T300/5208, Spec 30-8, exposed to 70°C/95% RH, -54°C to 93°C/100 cycles.

Figure 17.

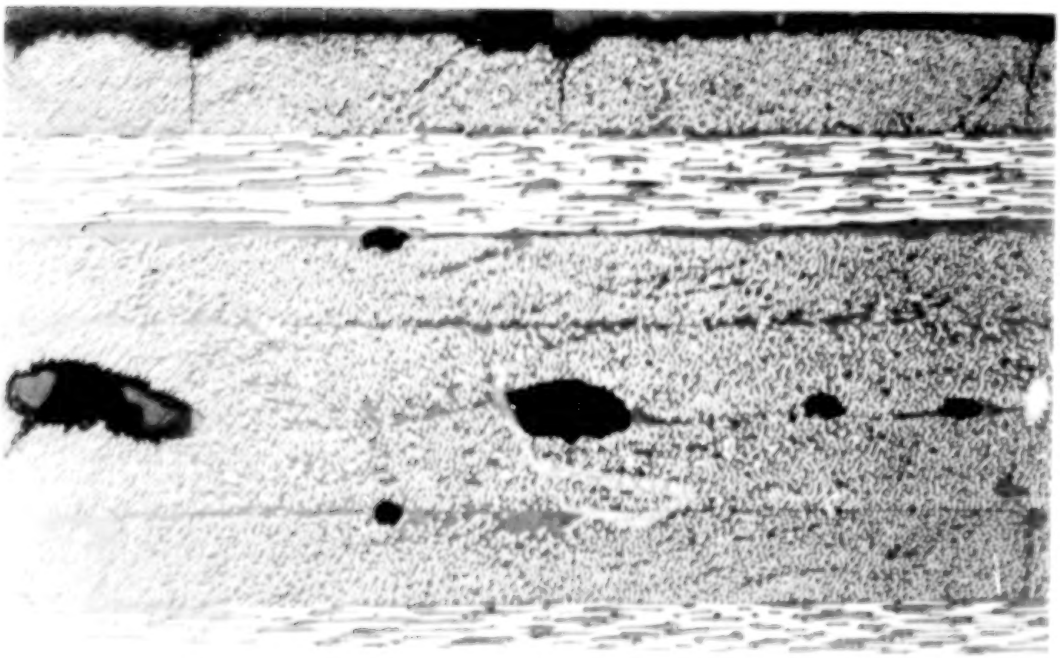

(a) Plate 32844, 50X, $(90/0/\pm45)_s$ T300/5208, Spec 28-4, exposed to 70°C/95% RH,

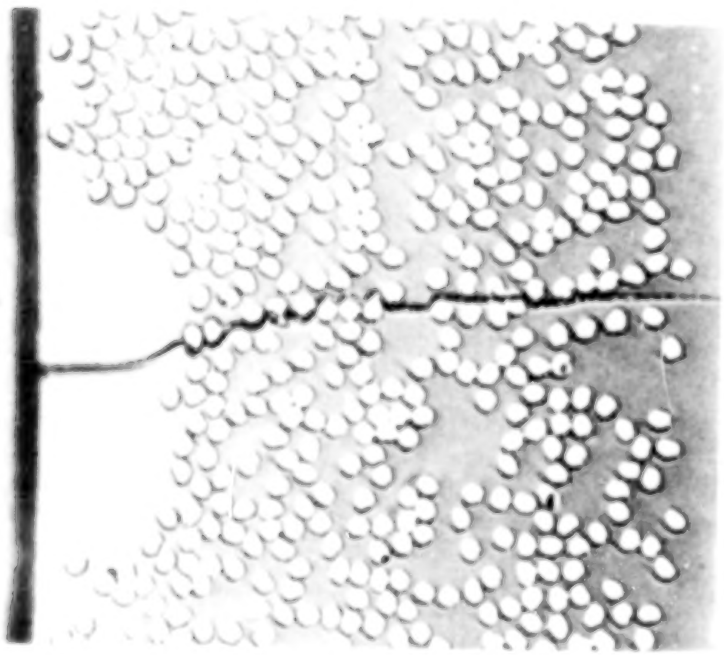

(b) Plate 32844, 500X, Spec 28-4.

Figure 38.

CHAPTER 5

ANALYSIS OF HYGROTHERMALLY INDUCED STRESS IN GRAPHITE-EPOXY LAMINATES

5.1 ANALYSIS DESCRIPTION

The hygrothermally induced stress state near the edge of composites of $(\pm 45, 0, 90)_s$, $(90, 0, \pm 45)_s$ and $(0_8)_T$ configurations were calculated by the elastic finite element modeling procedures which have been described in a series of papers [19,43-45] by Wang and Crossman. The details of the mathematical treatment used in the code FREE*EDGE for stress and mass diffusion analysis are provided in References 19, 43 and 45 and will not be repeated here.

Figure 39 shows the cross-section of an eight-ply laminate of thickness L = 8h and width 2b = 32h which is assumed to be infinitely long in the x direction. With this geometry of a flat composite coupon, we assume a state of generalized plane strain exists; i.e., that the strain ε_x is uniformly the same at all positions in the yz cross-sectional plane and is independent of the x coordinate. Warping of the yz plane due to shear is permitted in the model. The discrete model shown in Figure 39b consists of constant strain triangular finite elements concentrated near the free edge where stress gradients are expected to be greatest. Because of symmetry about the y and z axis only the upper right-hand quadrant of the cross-section must be modeled to obtain the stress state over the entire cross-section.

The elastic properties of the unidirectional plies in the laminate model were those chosen in previous papers to analyze free edge stresses in crossply laminates [19,43,44]. Using subscripts L, T, and Z to refer to longitudinal, transverse, and thickness directions of the individual ply we have assumed

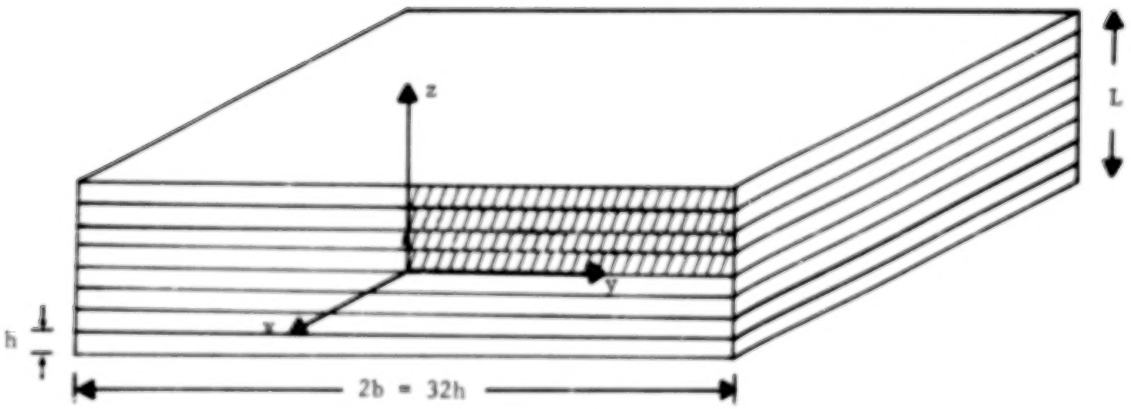

(a)

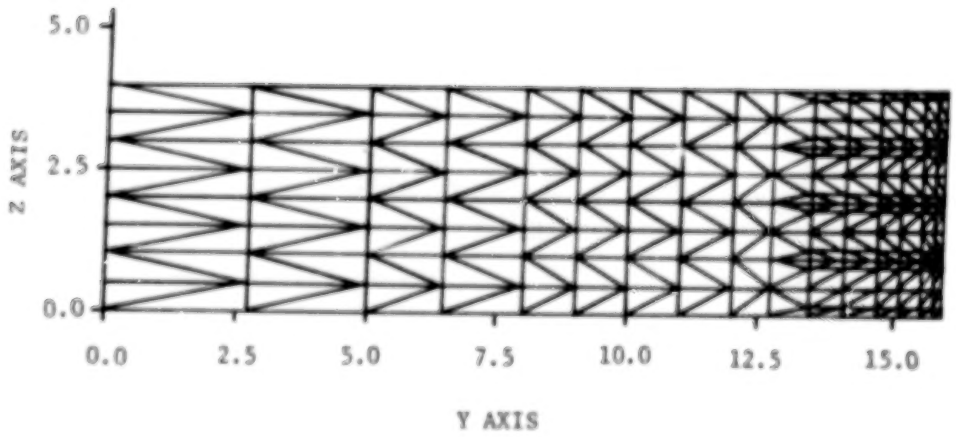

(b)

Figure 19. (a) Geometry of Symmetric 8-Ply Laminate
(b) Finite Element Grid

E_L = 138 GPa (20 x 10^6 psi)

$E_T = E_Z$ = 14.5 GPa (2.1 x 10^6 psi)

$\nu_{LT} = \nu_{TZ} = \nu_{LZ}$ = 0.21

$G_{LT} = G_{TZ} = G_{LZ}$ = 5.96 GPa (0.85 x 10^6 psi)

β_L = 0

$\beta_T = \beta_Z$ = 5000 x 10^{-6}/% Moisture

α_L = -0.36 x 10^{-6}/°C

α_T = 28.8 x 10^{-6}/°C

$D_L = 3\,D_T = 3\,D_Z$

where E is the Young's modulus, ν is the Poisson ratio. G is the shear modulus, β is the moisture expansion coefficient, α is the thermal expansion coefficient, and D is the moisture diffusion coefficient. A comparison of these properties to those measured for T300/5208 and T300/5209 in Table 1 of Appendix B shows that they are representative. However, the experimentally measured transverse modulus E_T is some 30% less than the assumed value in this analysis and has some bearing on the discussion of results. The through thickness constants E_Z, ν_{TZ}, ν_{LZ}, G_{TZ}, β_Z, and D_Z have been assumed equal to their inplane components because of the lack of experimental data or, in the case of β_Z, because of the large scatter observed in Figure 1. Recent experiments by Rajapakse and Sumsion [46] indicate that the shear modulus G_{LZ} is as much as 30% to 40% less than G_{LT}. Therefore the calculations of stresses developed in this chapter should not be taken as providing a truly absolute measure of stress magnitude but more as a means to assess what combinations of hygrothermal and mechanical loading are most critical in the initiation and growth of damage.

5.2 THE ANALYSIS OF MOISTURE INDUCED STRESSES

Figure 40a shows a plot of average moisture content in laminate of thickness, L, much less than width and length. Moisture is assumed to enter from both sides and the average water content M approaches its equilibrium value M_s at a nondimensionalized time $t^* = D_T t/L^2 \approx 0.75$, where D_T is the transverse moisture diffusion coefficient, L is the laminate thickness and t is the time. The infinite series solution for average moisture content as a function of time presented by Shen and Springer [13] can be approximated to within less than one percent error by the equations

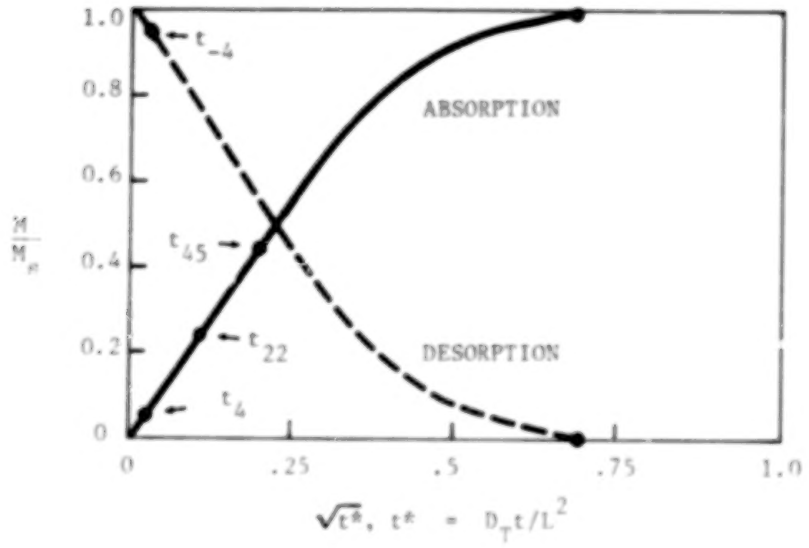

(a)

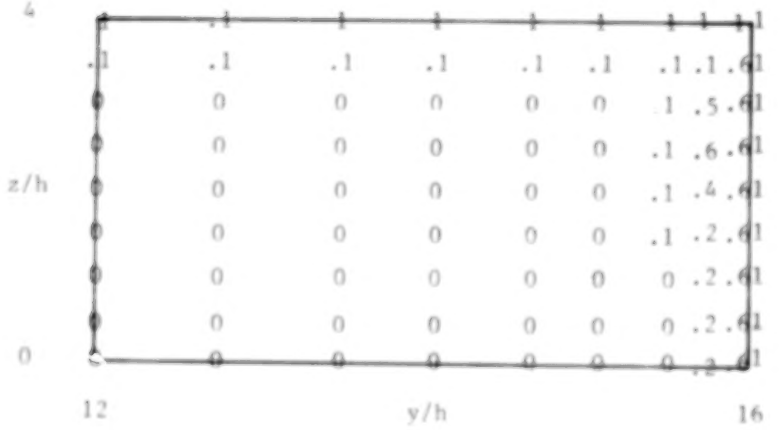

(a)

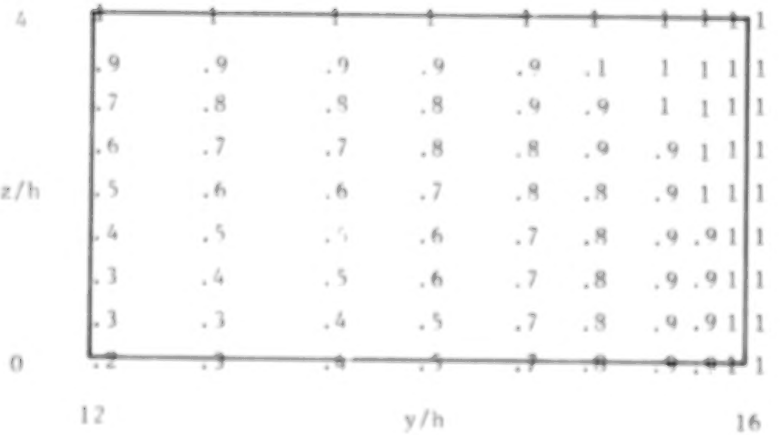

(c)

Figure 40. (a) Average Weight Gain (Loss) during Absorption (Desorption) Relative to the Equilibrium Moisture Content M_s
(b) Moisture Concentration C/C_s after Absorption Time t_4 ($M/M_s \approx 4\%$)
(c) Moisture Concentration C/C_s after Absorption Time t_{45} ($M/M_s \approx 45\%$)

$$\frac{M}{M_s} \cong \frac{4}{\sqrt{\pi}} \sqrt{t^*} \quad \text{for} \quad 0 \leq \frac{M}{M_s} \leq 0.7$$

$$\frac{M}{M_s} \cong 1 - \frac{8}{\pi^2} \exp(-\pi^2 t^*) \quad \text{for} \quad 0.4 \leq \frac{M}{M_s} \leq 1.0$$

The equations assume that D is independent of moisture concentration and that desorption is obtained from the same function f(t) on the right-hand side of the equations above by the solution of $M/M_s = 1 - f(t)$. The times designated t_4, t_{22} and t_{45} in Figure 40 refer to times at which 4, 22, and 45 percent of the total equilibrium water content has been absorbed. t_{100} will be used to designate the time at which 99.9 percent of equilibrium moisture content is reached. Negative subscripts such as t_{-4} refer to the desorption time required to lose 4 percent of the average moisture content after starting from an equilibrium moisture content M_s at t = 0.

Figure 40b is a plot of the moisture concentration calculated at each nodal position near the free edge in the finite element model of Figure 39 after an absorption time of t_4 in a $(90_2, 0_2)_s$ laminate. Only nodes for $12 \leq y/h \leq 16$ are shown and the y scale is expanded by a factor of two greater than the z scale to facilitate plotting of the local moisture concentration at each nodal position. Boundary conditions were M = 0 in the interior at t = 0 and $M = M_s$ on the surface at $t \geq 0$. Notice that moisture is diffusing faster from the y = 16h free edge in the 90° plies which are located between z = 2h and z = 4h in this analysis. The longitudinal diffusion coefficient for diffusion parallel to fibers has been assumed to be three times higher than the transverse coefficient. It is clear from the large differences in moisture concentration over very short distances from the free edge, that large moisture concentration gradients exist at short absorption times. At a longer time, t_{45}, the moisture gradient in both y and z is clearly reduced as moisture penetrates deeper into the composite.

After the moisture concentration is determined at each node point for a particular sorption time, the elastic analysis of moisture-induced stresses

proceeds. In this process the swelling strains due to the average moisture concentration in each element are calculated and the effect of these strains (which vary from element to element) on the overall response of the finite element system is calculated in a manner analogous to the calculation of the effect of thermally induced expansional strains [19].

The analysis determines all six stress (strain) components in each finite element. Previous papers have shown that at distances greater than the laminate thickness, L, from the edge the components τ_{xz}, τ_{yz}, σ_z tend to zero and the plane stress state, assumed in classical laminated plate theory and employed in Chapter 2, is rapidly approached. Pipes et al [18] have calculated the effect of a moisture gradient on the stress distribution in a thin composite laminate using classical laminated plate theory and one-dimensional moisture diffusion. Our aim in this analysis is to concentrate on the edge effects caused by the two-dimensional diffusion field.

The existence of non-zero through thickness stress components near the free edge has some effect on the inplane components. For example, the stress σ_x near the edge of 90° plies in quasi-isotropic laminate experiencing a tensile strain ε_x is some 35 percent higher than the plane stress value far from the edge [43]. The stress τ_{xz} peaks at the free edge in what appears to be a singular manner under applied tensile strain ε_x. However, the τ_{xz} caused by thermal stresses built in during cooling from the stress free cure temperature to ambient conditions are found to be of opposite sign to those caused by tensile loading and tend to cancel each other under combined thermomechanical loading [45]. The stress τ_{yz} is found to peak at a position $y = 0.98b$ but must drop rapidly to zero at $y = b$ to satisfy the boundary condition at the free edge [44]. Furthermore, the elastic analysis of shear stress components τ_{xz}, τ_{yz} and even τ_{xy} ignores the highly nonlinear nature of the shear stress-strain curve (as shown in Figures 17-20) and clearly will overestimate the actual level of stress which exists, particularly if the out-of-plane shear behavior is found to be less stiff than the easily measured inplane behavior [46].

Because of these considerations our study of free edge effects under hygrothermal loading will concentrate on alterations in the through thickness normal stress component σ_z which is considered to be the main cause of edge delamination in polymer matrix composites [47].

5.3 HYGROTHERMAL STRESS ANALYSIS

Figure 41 shows the distribution of σ_z in a unidirectional laminate which has been brought to moisture equilibrium at M_s = 1 percent and which is then desorbed. Because of the assumed homogeneous continuum nature of the unidirectional laminate, a uniform distribution of moisture $M = M_s$ or $M = 0$ results in a zero stress state at the laminate level of analysis. On a finer microstructural scale large stresses exist locally around each fiber and matrix [48] but average to zero across the laminate under the stress free boundary conditions in this analysis.

The σ_z distribution is shown as a function of position z along the free edge at y = 0.999b in Figure 41a. The distribution at several desorption times is shown. In Figure 41b σ_z at the z = 0 midplane of the composite is plotted vs. position y. In this figure the y scale is inverted to place the free edge at the left-hand side. The symbols used in the two plots are placed at positions occupied by the finite element centroids; and it is clear that the "free edge" stresses in Figure 41a are, in reality, located at a finite distance from the edge as shown in Figure 41b. The desorption conditions depicted in this figure show that a high tensile σ_z exists over a large portion of the edge at short desorption times. As moisture diffuses outward from greater depths, the moisture gradient decreases (as in Figure 40) and the stress peak at the edge decreases as well. We will use plots of σ_z vs. position z very near the edge at y = 0.999b in our analysis of combined mechanical, thermal, and hygroscopic stresses, because this type of plot allows us to examine the peak stress σ_z in each of the laminate plies.

The combined effects of hygrothermal and mechanical loading are studied by first analyzing individually the σ_z stresses caused by a unit change in

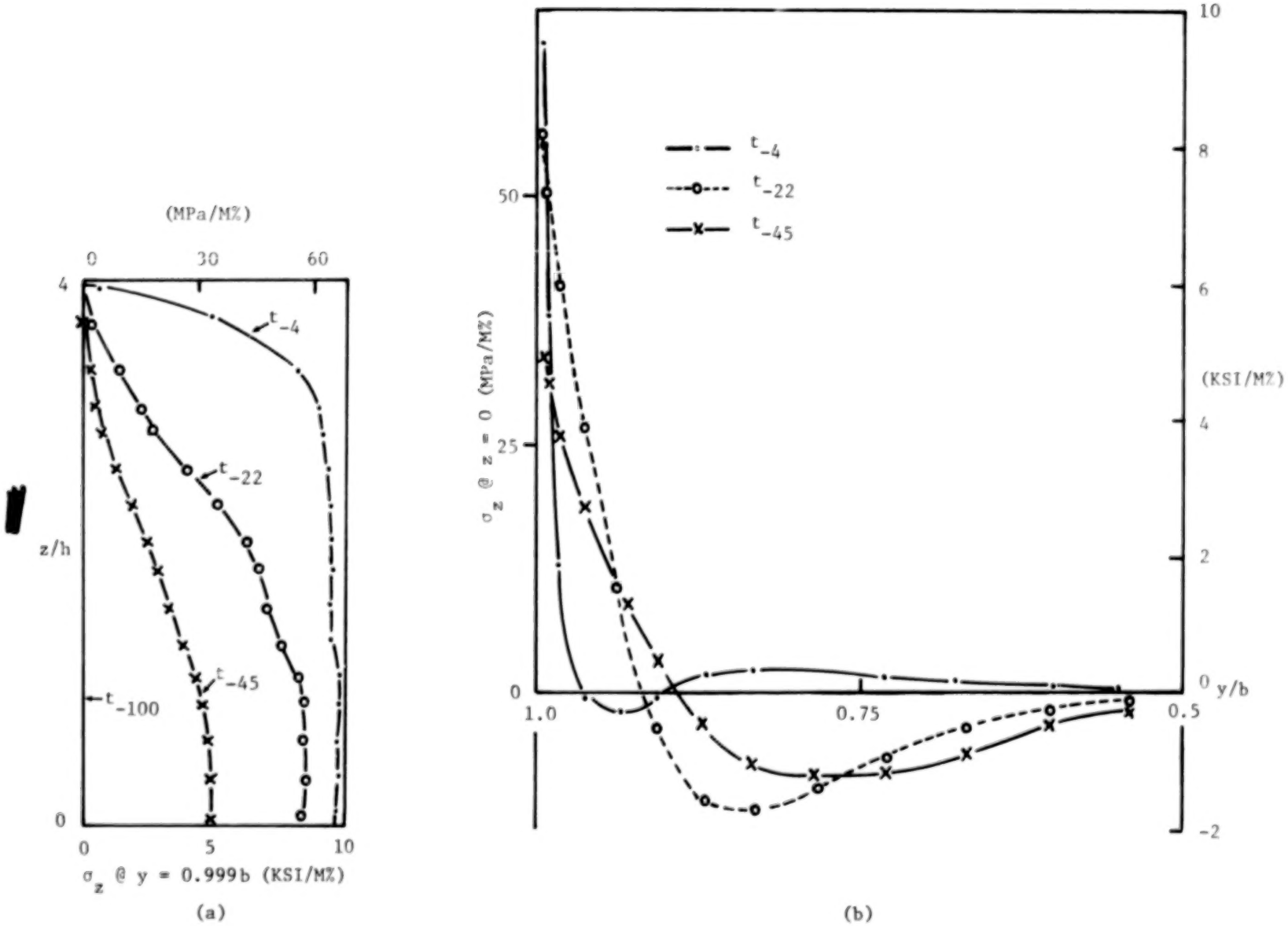

Figure 41. (a) σ_z Through Thickness Distribution near Free Edge of Unidirectional 8-Ply Laminate during Desorption from Equilibrium Moisture Content M_s.
(b) σ_z Distribution along Midplane of Unidirectional 8-Ply Laminate during Desorption

tensile strain ($\mu\varepsilon_x$), temperature (°C), and moisture (%) at several sorption times. For simplicity we choose to determine σ_z due to moisture at sorption times t_4 and t_{100} only. The resulting plots of σ_z (y = 0.999b) vs. z are shown in Figures 42 and 43 for the two quasi-isotropic laminates examined in this study. The horizontal lines at z = 0, 1, 2, 3, 4h are the ply interfaces and the particular fiber orientation with respect to the x axis is shown at the right-hand edge of each figure. A moisture equilibrium content of M_s = 1 percent is assumed throughout this analysis. Because the analysis ignores the threshold phenomenon noted in Figure 1 in the transverse moisture expansion, this level of swelling is equivalent to that seen in T300/5208 laminates at 1.4 percent moisture, a value obtained under 95% RH exposure conditions. A short time absorption of water (t_4) leaves the free edge in a state of compression, while the state of stress after absorption to equilibrium is strongly dependent on the stacking sequence of the plies. The thermal stress pattern and that at moisture absorption time t_{100} are nearly identical in shape because both are caused by expansions due to an uniform change in either temperature and moisture. Note finally that the σ_z stress at the midplane of the composite due to tensile straining is negative for the $(90, 0, \pm45)_s$ laminate but positive for the $(\pm45, 0, 90)_s$ laminate.

Figure 44 shows the σ_z stress state which develops during simulated hygrothermal cycling of the two quasi-isotropic laminates of T300/5208 used in this study. The plots have been derived from Figures 42 and 43 by assuming a stress-free temperature of 170°C (Figure 2), an equilibrium moisture content of 1.4 percent, followed by a short desorption period t_4, which causes a large tensile stress to develop at the free edge in the same manner as noted in Figure 41 for the unidirectional laminate. The circles indicate the stress pattern at the low temperature end of the thermal cycle, while the squares denote the pattern at the maximum temperature during the cycle. The peak σ_z stress occurs in the 0° plies of both stacking sequences at the high temperature end of the cycle. However, in the $(\pm45, 0, 90)_s$ laminate, the peak stress in the 90° ply at -54°C is nearly as high. The

BLANK

PAGE

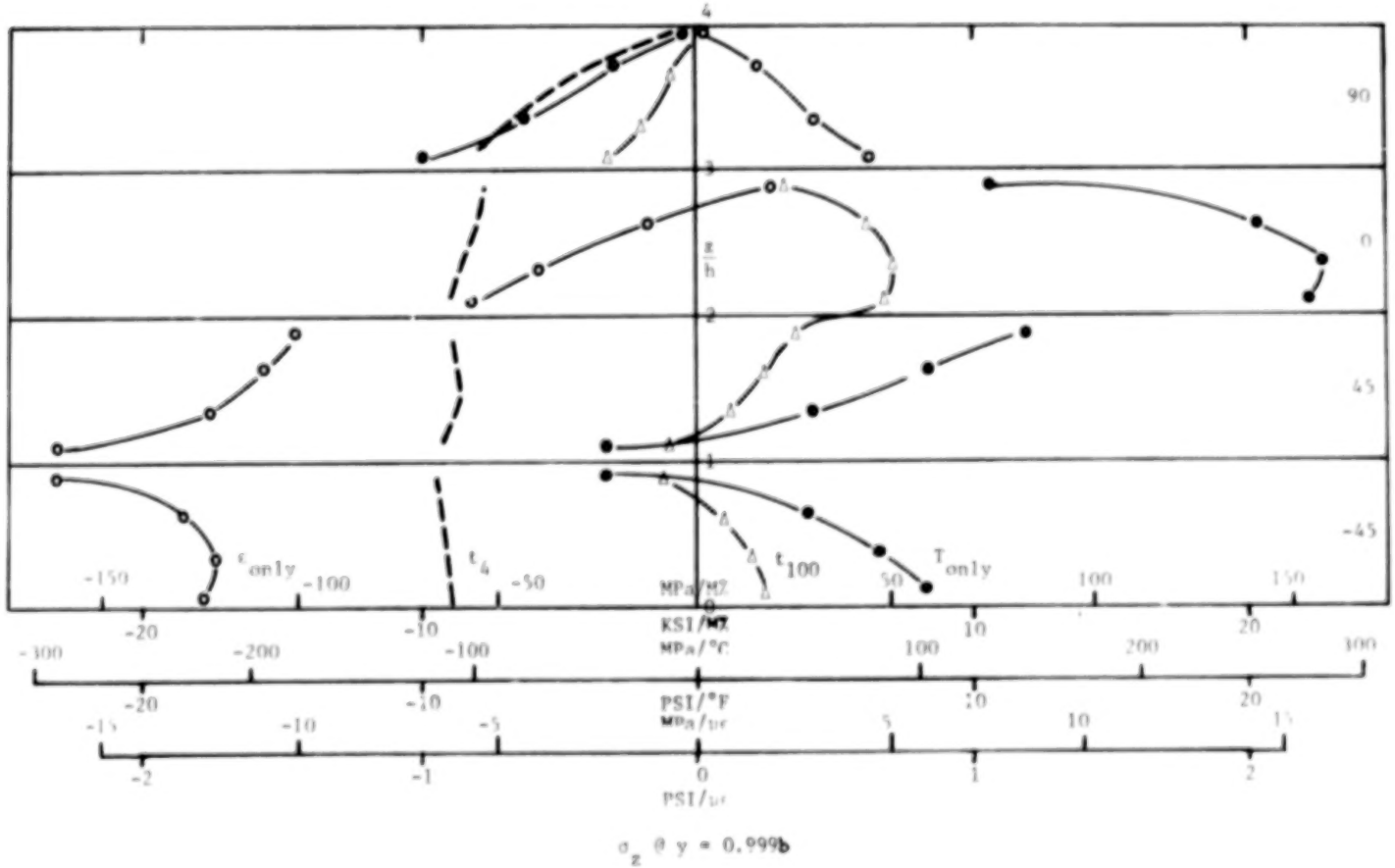

Figure 42. σ_z Through Thickness Distributions in $(90, 0, 45, -45)_s$ Laminate due to Temperature, Moisture, and Tensile Strain

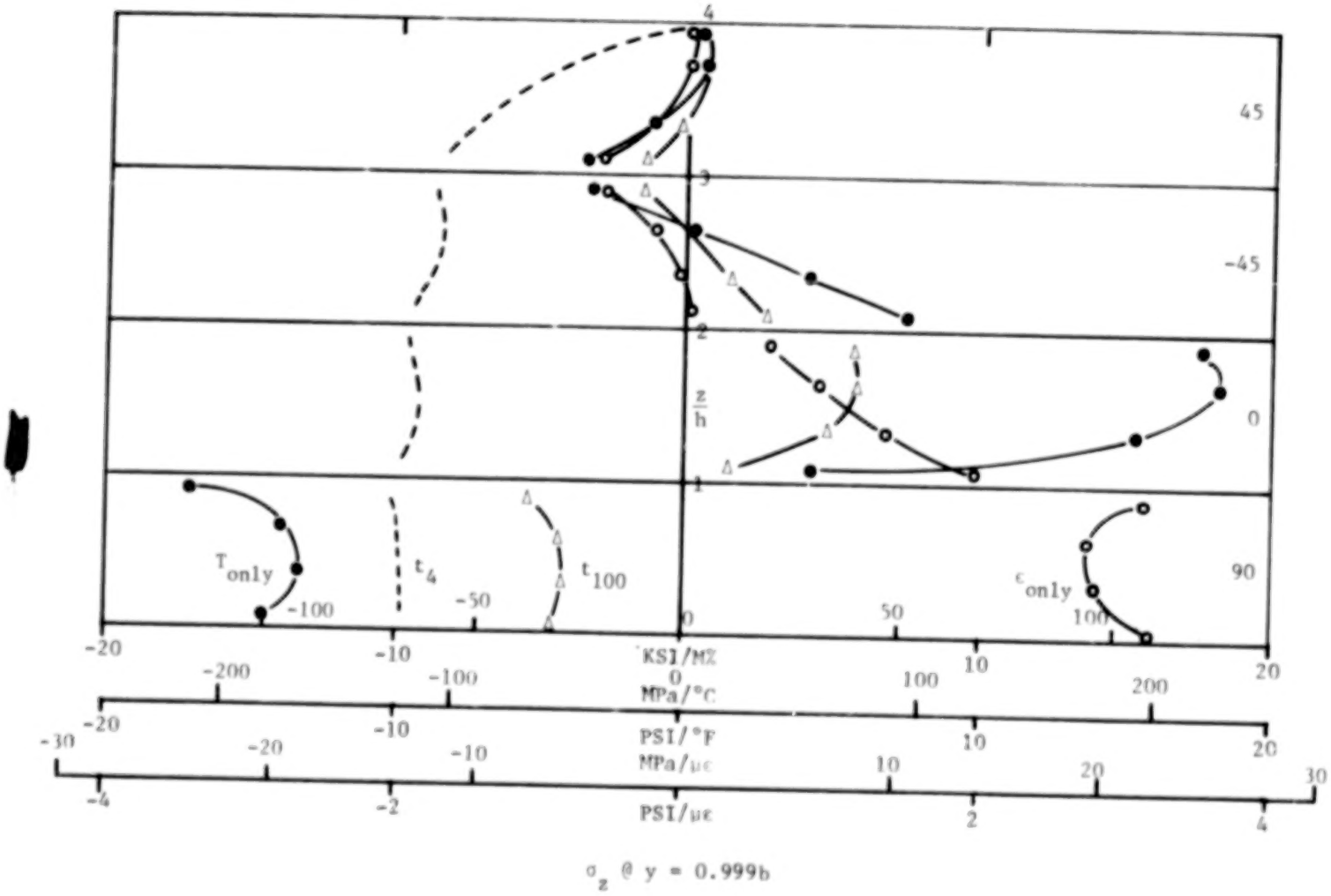

Figure 43. σ_z Through Thickness Distributions in $(45, -45, 0, 90)_s$ Laminate due to Temperature, Moisture, and Tensile Strain

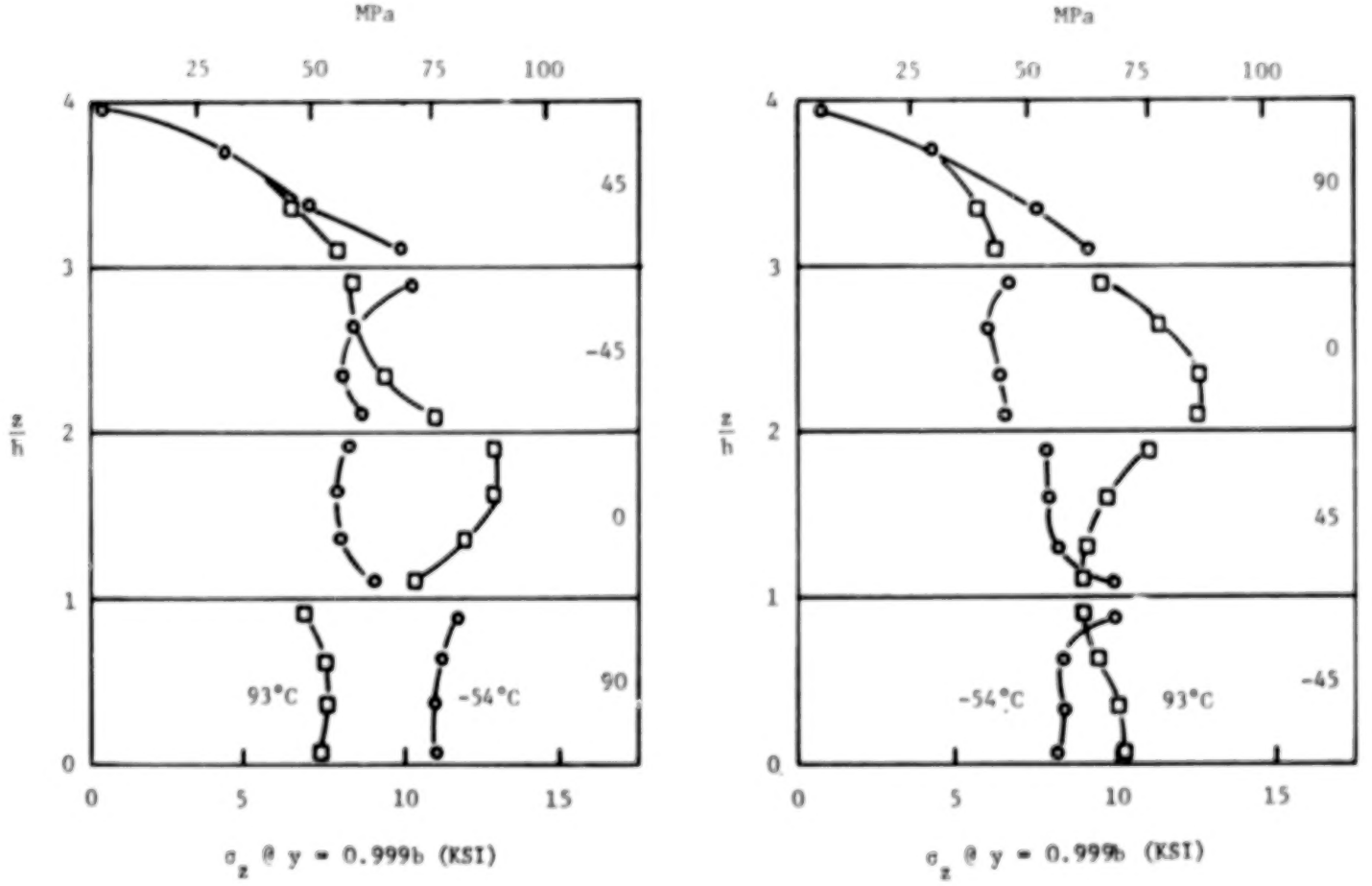

Figure 44. σ_z Through Thickness Distributions in $(\pm 45, 0, 90)_s$ and $(90, 0, \pm 45)_s$ Laminate at Temperatures Indicated Following a Desorption Time t_{-4} from Equilibrium Level M_s

variation of stress with temperature appears less important in these laminates than the tensile stress caused by desorption itself. In both laminates the level of stress in all plies exceeds the commonly observed 50 MPa transverse tensile strength of T300/5208 [26]. One would expect edge delamination between several of the plies caused by hygrothermal cycling in both of these laminates.

Published distributions of σ_z (at y = 0.999b) vs. z in crossply laminates under thermal [44] and hygroscopic loading [19] were used to investigate the combined hygrothermal stress distribution in $(90_2, 0_2)_s$ and $(0_2, 90_2)_s$ laminates to determine if crossplied laminates were more susceptible to edge delamination than the quasi-isotropic laminates.

Figure 45 shows the individual σ_z stress distributions due to short time absorption at t_4, equilibrium moisture absorption at t_{100}, and thermal stress at -54°C. The combined effect of termperature at -54°C and equilibrium moisture absorption at t_{100} is also shown to illustrate that edge stresses due to moisture sorption nearly cancel those due to thermal residual strains.

Figure 46 shows the σ_z stress distribution at the temperature extremes used in the hygrothermal cycling experiments described in Chapter 2. As in the quasi-isotropic analysis we find that stress levels as high as 100 MPa (15 ksi) are calculated at the two temperature extremes after a desorption time of t_{-4}; however, the location of the peak stress moves from the 90/0 ply interface at -54°C to near the composite midplane at 93°C.

Figure 47 shows similar calculations for the $(0_2, 90_2)_s$ laminate. In this laminate, unlike the results for $(90_2, 0_2)_s$ and quasi-isotropic laminates, we find that the thermal stress at low temperatures (-54°C) has a large influence on the peak stress which develops under short time desorption (t_{-4}). The combined hygrothermal σ_z stress is projected to exceed 150 MPa at the 0/90 interface, while the stresses at 93°C are found to be proportionately lower at all positions along the free edge.

BLANK

PAGE

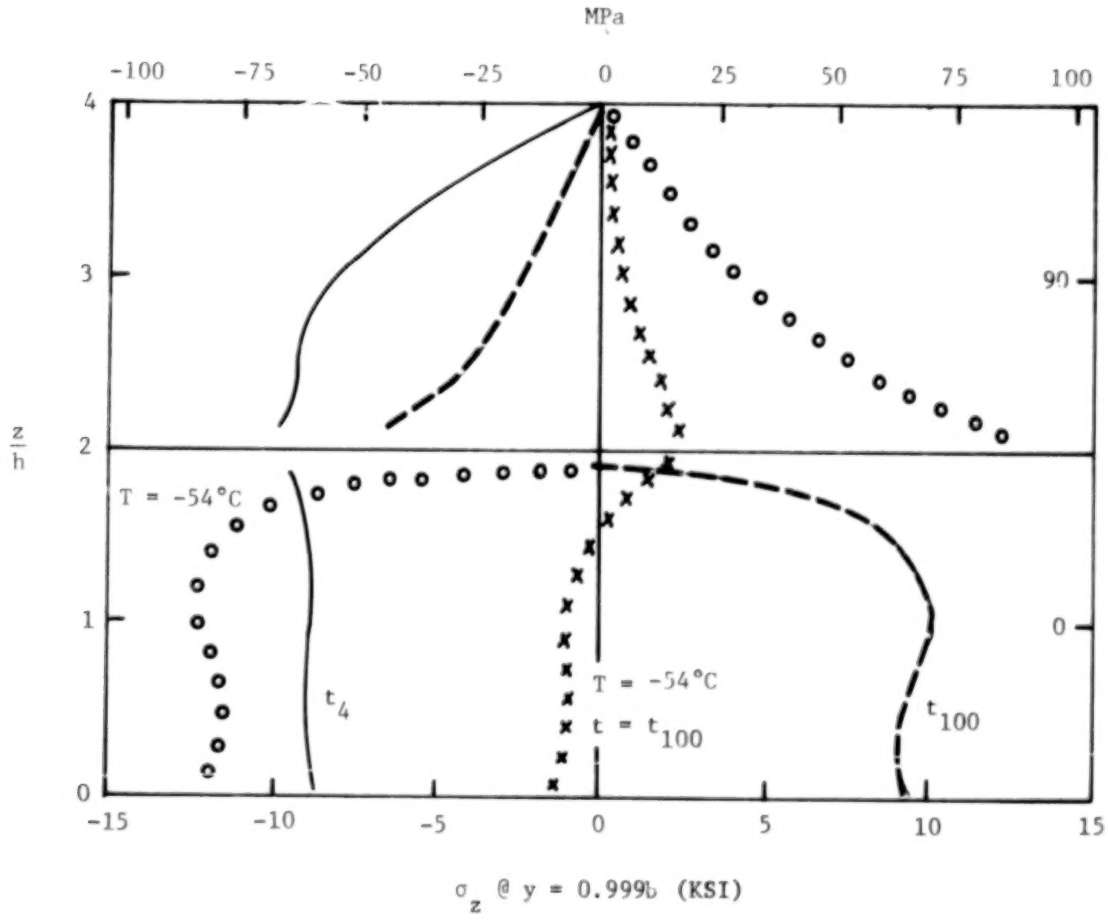

Figure 45. σ_z Through Thickness Distributions in $(90_2, 0_2)_s$ Laminate Due to Temperature and Moisture

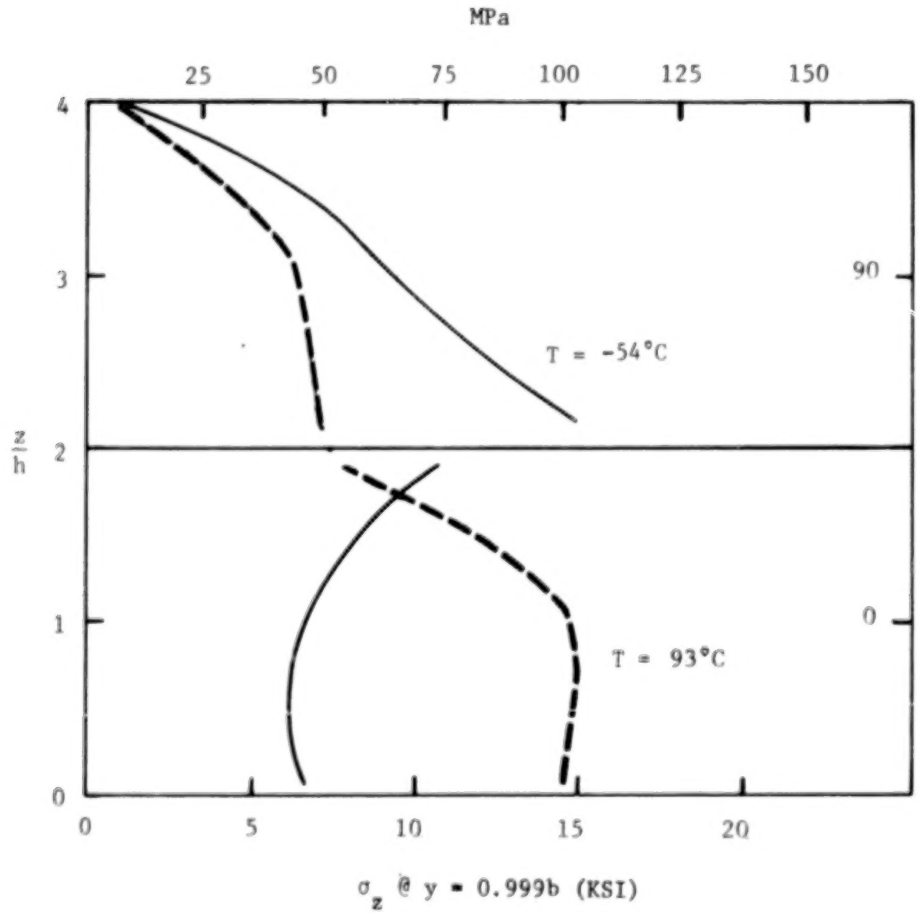

Figure 46. σ_z Through Thickness Distributions in $(90_2, 0_2)_s$ Laminate after Desorption Time t_{-4} Following Saturation at Moisture Content M_s

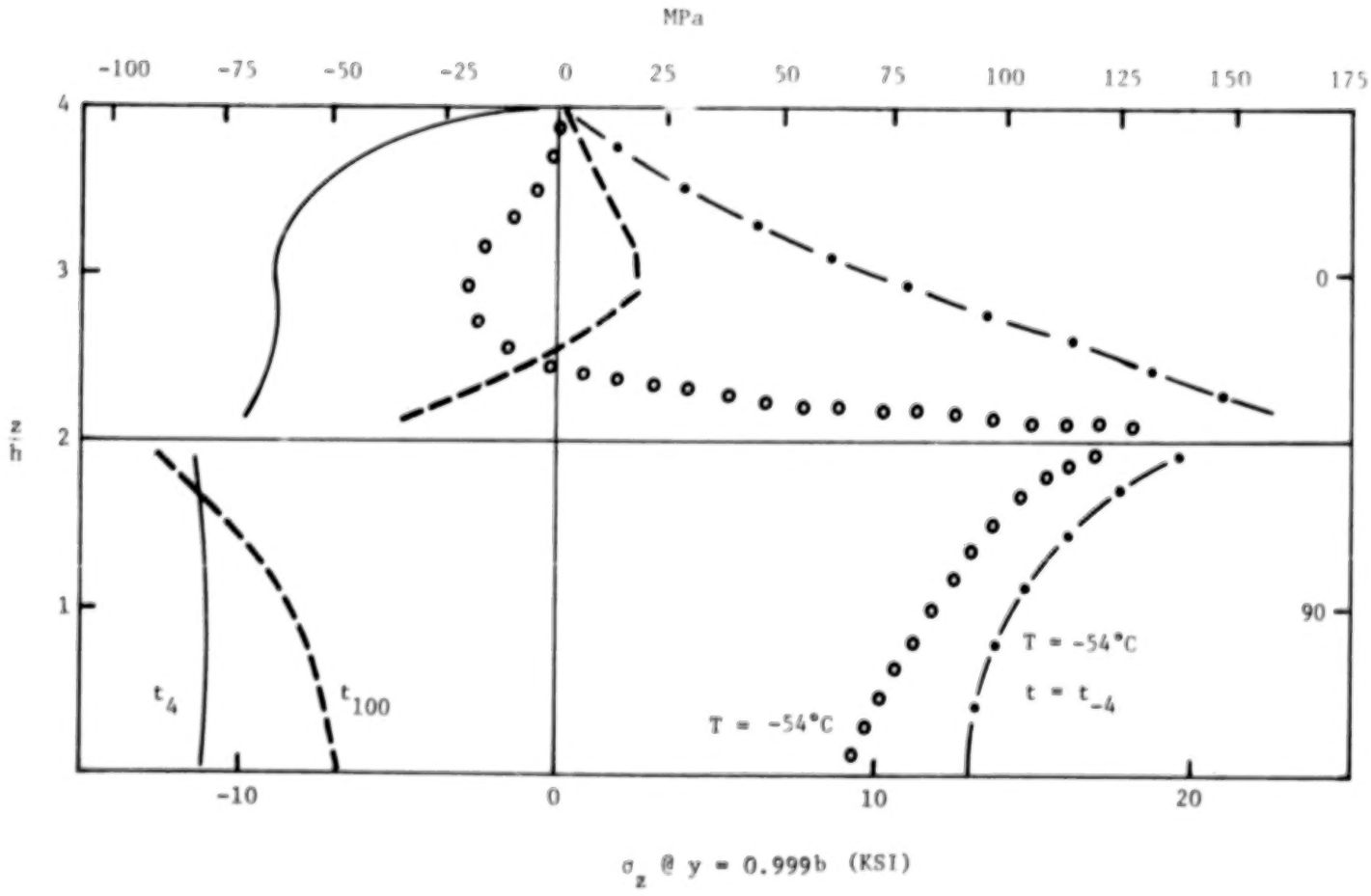

Figure 47. σ_z Through Thickness Distributions in $(0_2, 90_2)_s$ Laminate due to Temperature and Moisture

We have seen in the analysis of crossplied and quasi-isotropic laminates that the peak σ_z stress due to hygrothermal conditioning is calculated to be $1\frac{1}{2}$ to 3 times greater than the transverse tensile strength of T300/5208 composites, yet microscopic examination of these laminates in Chapter 4 showed a surprising lack of microcracking and edge delamination. A previous analytical and experimental study of coupled thermal and mechanical loading of quasi-isotropic laminates has shown that the onset of observed edge delamination correlates with a calculated peak σ_z stress on the order of 80 to 100 MPa [45]. The values obtained for hygrothermal cycling are in this range for the crossplied laminates and only slightly below for the quasi-isotropic and unidirectional laminates, and yet we have observed little microscopic damage. The high rate of viscoelastic stress relaxation in T300/5209 certainly reduces the stress level calculated here on the basis of elastic theory, but T300/5208 does not show a significant viscoelastic response over the times and temperatures we are concerned with in this program.

The discrepancy between the predicted onset of edge delamination and the experimental results can be understood when we examine the magnitude of the stress σ_z as a function of y rather than z. The right-hand plot in Figure 41 shows that σ_z drops rapidly from the edge, at y = b toward the center of the laminate at y = 0. Far from the edge a state of plane stress is found which meets the assumptions of laminated plate theory. Three profiles are shown corresponding to desorption times resulting in weight losses of 4, 22, and 45 percent of the equilibrium moisture content. It is clear that at time $t = 0_+$ the infinitely steep gradient of moisture concentration near the edge will cause a stress singularity.

However, we must realize that these stresses are calculated on the assumption of a homogeneous, anisotropic continuum. At distances from the edge or surface on the order of the graphite fiber diameter these assumptions are not valid. On this fine scale, a micromechanical analysis of

fiber and matrix like that of Adams and colleagues [48] is necessary. Figure 48 plots the time dependence of the σ_z stress at several positions near the laminate edge. Note that the peak stress at a given position decreases with distance from the edge. The edge stresses σ_z given in Figures 44-47 are those calculated at position y = 0.999b and only 7 μm from the specimen edge. The T300 fiber diameter is on the order of 7 μm as well. The assumption of a homogeneous continuum clearly should not be made over such a small distance. If the material behaves homogeneously over a distance of approximately 5 fiber diameters, then the peak σ_z stress is on the order of 40 MPa rather than 70 MPa calculated only 7 μm below the surface. Similarly the peak hygrothermal σ_z stresses given in Figures 44-47 would be proportionately lower if they were plotted at a distance of several fiber diameters from the edge. The calculated σ_z stresses may be reduced even further if we assume a lower transverse modulus in the analysis which is closer to the experimental value for T300/5208 and T300/5209 and if we were to carry out an incremental analysis, taking into account the nonlinear elastic or viscoelastic character of the shear and transverse stress-strain response.

Given these considerations we must conclude that the level of σ_z stress calculated by elastic analysis for the hygrothermal history examined in the experimental study is marginally below that level needed to initiate edge delamination. However, the analysis of edge cracking in reference 45 suggests that edge stress induced hygrothermal damage at specimen edges or surfaces will be significant under <u>combined</u> hygrothermal and mechanical loads. Figure 49 shows the combined effect of tensile strain ϵ_x = 0.5 percent on the σ_z stress distribution at -54°C and 93°C after a desorption time of t_{-4}. In the $(\pm 45, 0, 90)_s$ laminate, we find a two-fold increase in σ_z above the level due to the hygrothermal state (Figure 44) alone. On the other hand, the σ_z edge stress in $(90, 0, \pm 45)_s$ laminates is lowered by tensile straining.

The results of the finite element analysis of hygrothermal stresses near laminate-free edges presented in this report lead one to conclude that

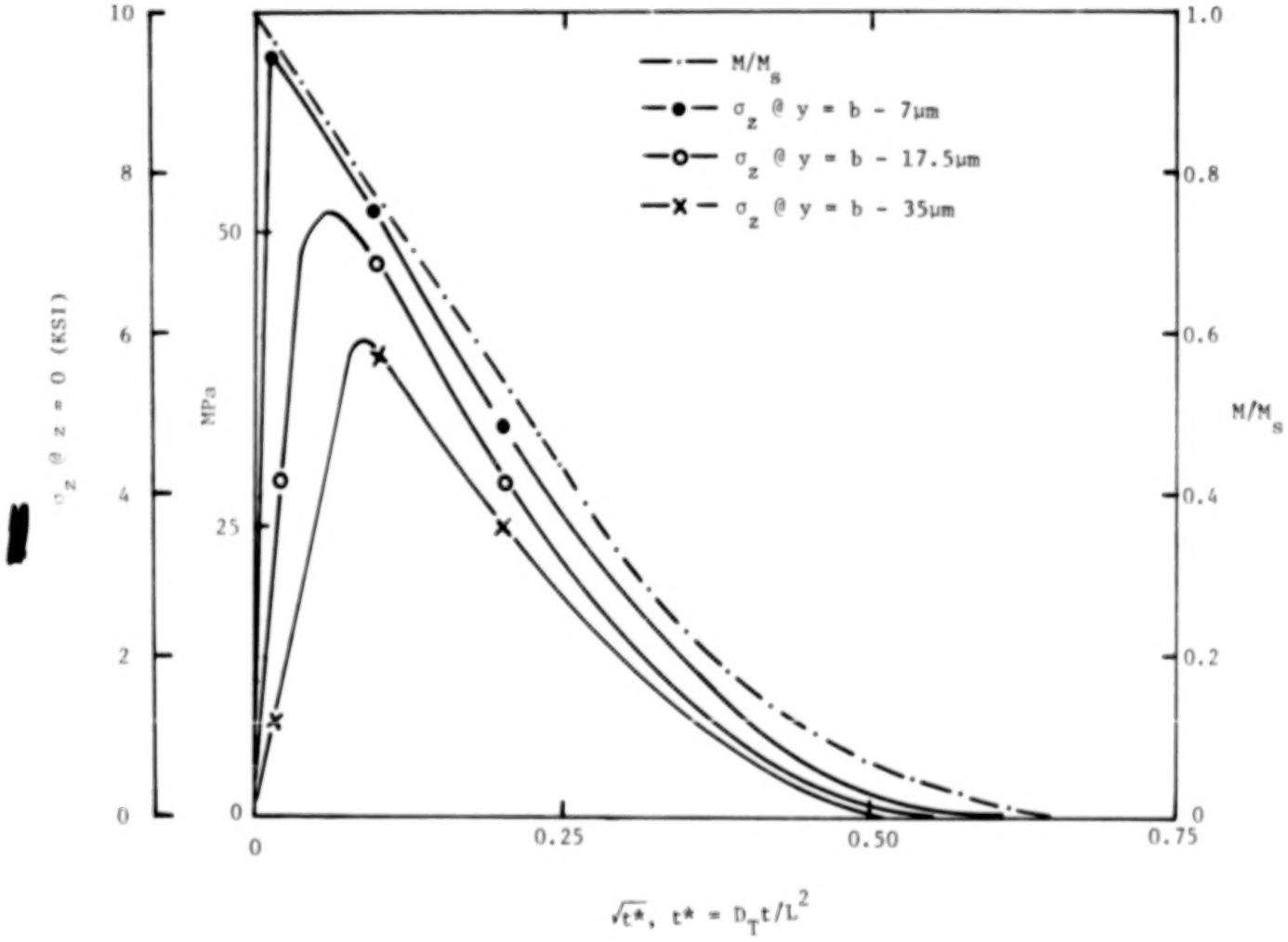

Figure 48. The Time Dependence of σ_z ($z = 0$) during Desorption in 8-Ply Unidirectional Laminate at Three Positions near the Free Edge ($y = b$). Moisture Content during Desorption Also Plotted

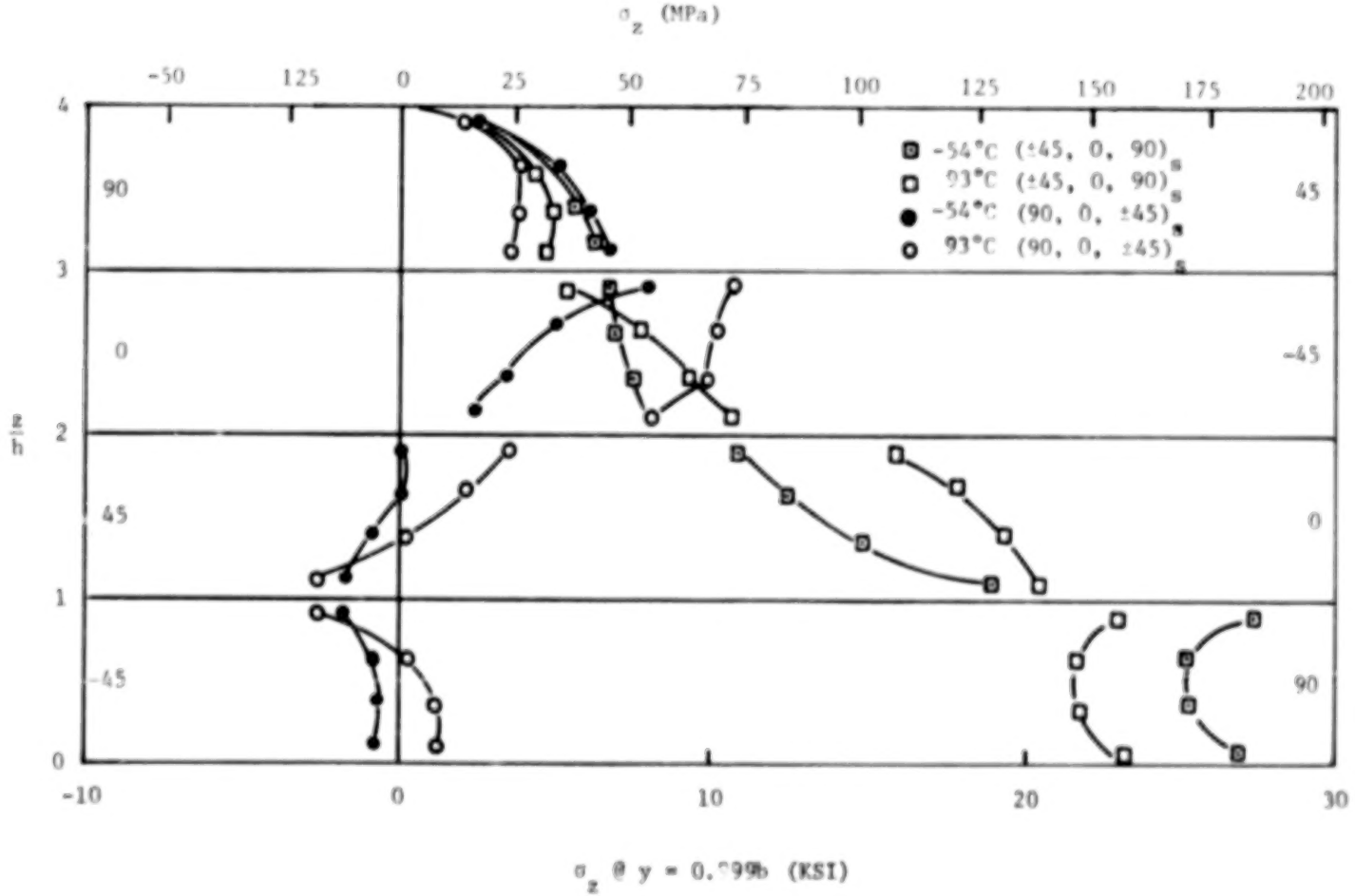

Figure 49. σ_z Through Thickness Distributions in $(\pm 45, 0, 90)_s$ and $(90, 0, \pm 45)_s$ Laminates after a Desorption Time t_{-4} Following Saturation to M_s and under an Applied Tensile Strain of 5000 μin/in

the contribution of moisture absoption/desorption gradients to development of delamination at the free edge is less important than the thermal and mechanical contributions. During absorption we have found experimentally as well as analytically that moisture lowers the residual stresses. While desorption creates large tensile stresses near the edge, the distance over which these stresses are high is on the order of several fiber diameters or less, where the homogeneous continuum model breaks down. Based on these results, we would recommend that experimental and analytical studies of hygrothermal degradation due to environmental cycling should concentrate more on the combined effects of hygrothermal and mechanical loads.

CHAPTER 6
DISCUSSION OF RESULTS

6.1 ASSESSING PERMANENT AND REVERSIBLE INTERFACIAL BOND DEGRADATION

The interlaminar shear tests reported in Chapter 3 for moisture exposed and dried T300/5208 indicated that the interfacial bond strength in the dry material was unaffected by prior sorption of equilibrium moisture content at 93°C up to 95 percent relative humidity. In T300/5209 prior exposure to 93°C/55% RH resulted in no degradation in the interlaminar shear strength of the dried material, while exposure to 93°C/95% RH caused a significant reduction in strength as seen in Figure 28. The cause of the bond degradation during exposure to temperatures well above the wet glass transition temperature of 5209 is not clear. Browning [2] has proposed a stress rupture mechanism which predominates when the matrix is in a leathery or rubbery state at elevated temperature. By this process the existence of tensile stress normal to the fiber-matrix interface may be sufficient to cause chemical bond breaking. Miller and Adams [17] have shown that matrix swelling due to moisture absorption will cause a tensile stress to develop normal to the fiber-matrix interface along the line of closest approach of fibers distributed in an idealized square array. However, at a given temperature and moisture content, the interface stress which develops is due to the combination of thermal contraction of matrix and moisture induced swelling of the matrix.

Tensile interface stress will be most prominent at high temperature where the compressive thermal residual stress is minimized and at high moisture content where the tensile hygroscopic residual stress is maximized. Because the level of thermal stress is less in 5209 composites due to the lower cure temperature, one can argue that higher tensile interface stress

is developed during absorption to equilibrium at a particular temperature. Furthermore, 5209 is also found to pick up significantly greater amounts of moisture than 5208 and the interface stress component due to matrix swelling will be proportionately greater.

These predicted interface stresses have been based on the assumption of elastic behavior. It is clear from Figure 3 that the alteration of residual stress by absorbed moisture in T300/5209 laminates is much less than that predicted by elastic analysis. In fact, if one uses the plots of $(0_4, 90_4)_T$ T300/5209 laminate curvature as a function of temperature in Reference 15, one finds that if the curvature of the T300/5209 laminate exposed to 93°C/95% RH was measured at 93°C, it would be essentially zero. This implies that the zero stress state has moved from 137°C in the dry material to 93°C in the moisture equilibrated material by a stress relaxation mechanism. This balance between thermal and hygroscopic stresses on a ply-by-ply laminate level also implies that the local fiber-matrix interface stress is close to zero. In the absence of applied mechanical stress, it is thus difficult to account for permanent fiber-matrix bond degradation by a stress rupture mechanism due to the plasticization of the matrix, since plasticization has the simultaneous effect of reducing the hygrothermal stresses at the interface by viscoelastic stress relaxation. Although we have demonstrated that such extreme exposures will cause permanent interface damage in T300/5209, more experimental studies are required to account for the loss.

Reversible interfacial bond degradation was not examined experimentally in this study but can contribute to mechanical property loss which at first glance one might attribute strictly to matrix plasticization. The cleanest example of this coupling is the transverse tensile response of unidirectional composites. As noted by Verette [36] the transverse tensile strength of AS/3501 composites is reduced by nearly forty percent after absorption of moisture, while transverse modulus itself is reduced by only ten percent. Adams and Miller [48] used a micromechanical analysis to simulate a transverse tensile test of graphite-epoxy, taking into account hygrothermal

stresses and moisture altered nonlinear stress-strain response of the epoxy matrix. Yet the predicted transverse strength of the wet composite was essentially identical to the dry composite when a maximum effective matrix shear stress failure criterion was used. Chiao et al. [49] showed that the transverse tensile strength of a series of flexibilized S2 glass-epoxy composites was much less sensitive to the degree of matrix plasticization than was originally postulated. The decrease in the initial modulus of the epoxy correlated well with the observed decrease in transverse strength, while a large increase in strain to failure as a measure of matrix flexibility (or plasticization) did not result in a proportionate increase in transverse tensile strain or stress.

These analytical and experimental results appear to indicate that transverse tensile strength is an interface strength dominated property. If we postulate that transverse failure occurs when the most highly stressed point on the fiber-matrix interface reaches some critical tensile stress we can use Adams' calculations to estimate the loss of transverse strength of graphite-epoxy composite due to the absorption of moisture. In his analysis the peak interface normal stress in transverse tension is 1.7 times the average applied stress. The thermal residual normal stress, σ_i^{Th}, at 20°C is -32 MPa (-4.6 ksi) at this same point. Taking 55 MPa (8 ksi) as a typical transverse tensile strength, $\bar{\sigma}_T$, of the dry composite at room temperature we calculate the interface bond strength, σ_i^F, to be

$$\sigma_i^F = 1.7\,\bar{\sigma}_T + \sigma_i^{Th} = 62 \text{ MPa (9 ksi)}$$

For a wet composite the combined thermal and hygroscopic residual interface stress, σ_i^{Th+wet}, is calculated by Adams to be 16.5 MPa (2.4 ksi). The wet transverse tensile strength, $\bar{\sigma}_T^{wet}$, at the point of interface debonding is then calculated to be

$$\bar{\sigma}_T = \frac{1}{1.7}\left[\sigma_i^F - \sigma_i^{Th+wet}\right] = 27 \text{ MPa (3.9 ksi)}$$

and the percent reduction of transverse tensile strength due to absorbed moisture is (27/55) x 100 or 49 percent.

While it appears that altered residual stress at the fiber-matrix interface is sufficient to account for the observed reduction in transverse tensile strength, Kaelble [16] has offered a second mechanism based on a reduction of the fiber-matrix surface energy γ by the absorption of water. Kaelble employs the Griffith fracture equation $\sigma_c \propto \sqrt{\frac{E\gamma}{a^*}}$ where E is the effective modulus, a* is the apparent defect size, and σ_c is the critical stress which must be exceeded for a crack of size a* to propagate unstably. Kaelble determined the dispersive and polar contributions to the surface free energy of HTS/epoxy composites and predicted reductions in interface strength of 50 to 70 percent after absorption of moisture to the fiber-matrix interface. Observed reductions of interlaminar shear strength measured by notched compression shear tests ranged from 40 to 55 percent, but the degree of plasticization of the matrix on the shear test results was not examined in that study.

The discussion of interfacial bond degradation has centered around three mechanisms: (1) irreversible bond rupture at high temperature/moisture content; (2) hygrothermally altered interface residual stresses which are only partially reversible if the matrix is viscoelastic; and (3) reversible moisture altered interface surface energy. The effect of the first mechanism on mechanical response is most easily assessed by comparing the original dry response vs. the exposed and dried behavior as we have done in Chapter 3. The effect of the latter two mechanisms must be assessed in moisture-laden specimens where the response may be marked by the simultaneous plasticization of the matrix.

The ability to vary the residual stresses in T300/5209 laminates by proper choice of humidity level and exposure temperature, as noted in Figure 3 and discussed in Chapter 2, provides a means to distinguish between interface bond strength degradation mechanisms which involve either (1) altered surface energy or (2) altered residual stresses. Consider the following experimental

program. Expose two sets of T300/5209 unidirectional laminates to 70°C/55% RH and to 93°C/20% RH until equilibrium moisture content is reached. From Figure 3 both sets of laminates should contain approximately the same moisture content (0.85 percent), but the 93°C exposed specimens will contain nearly twice the level of residual stress. Furthermore, the 93°C exposed specimens will have a residual stress very nearly equal to the level found in dry laminates cooled from the cure temperature.

We have chosen exposure conditions at low enough combinations of temperature and moisture that permanent degradation in interface bond strength by mechanism 1 will not be expected. If surface energy controls the interface bond strength then both sets of moisture lader specimens should show similar cransverse strength reduction compared to the dry value. However, if residual stress controls the effective interface strength, then the transverse tensile strength of 93°C exposed specimens will lie close to the initial dry value, while that of specimens exposed at 70°C will show a significant reduction compared to the initial dry value. Similar experiments could be designed to determine the dependence of compression strength and inplane and interlaminar shear strength on interfacial bond strength following those same hygrothermal exposures. The level of residual stresses could be followed by exposing $(0_4, 90_4)_T$ laminates to the same temperature/humidity conditions. The proposed experiments provide for the first time a means to assess interface dominated degradation of mechanical properties independent of matrix plasticization, by making use of the moisture-altered viscoelastic character of the material.

6.2 ENERGY CONCEPTS FOR INITIATION AND GROWTH OF HYGROTHERMAL DAMAGE

In Section 5.3 calculations were made to determine the through thickness normal stress near laminate free edges due to mechanical, thermal and hygroscopic loading. The additional effect of a steep moisture gradient was particularly emphasized. While the level of through thickness

normal stress σ_z was calculated to be 1½ to 3 times higher than transverse tensile values, it was argued that the peak stresses due to a moisture gradient acted only very close to the free edge over a distance of 1-5 fiber spacings, where the assumption of a homogeneous continuum must be re-examined. It was noted that the delamination of tensile loaded $(\pm 45, 0, 90)_s$ laminates was observed experimentally under conditions which correlated with a calculated peak stress, σ_z, of 80-100 MPa while observed transverse tensile strength was only 50 MPa [45]. While the calculated hygrothermal stresses in quasi-isotropic and cross-plied laminates were found to reach 80-100 MPa levels only very near the surface, where the continuum model breaks down, we also noted in Section 6.1 that the expected transverse tensile strength of moisture laden composites may be as much as 50 percent less than the dry value due to interfacial strength loss. Therefore the distance over which a wet transverse tensile strength of 25-35 MPa is exceeded near the free edge of the unidirectional composite in Figure 41 is on the order of 5-10 fiber diameters, where the assumption of a homogeneous continuum may indeed be adequate for the calculation of stress. It is the purpose of this section to discuss an alternate explanation for the observed lack of hygrothermal damage during cycling.

The continuum mechanical analysis provides us with a measure of stress magnitude and direction but not with a criterion for initiation and propagation of fracture. It is well established from studies of metals, glasses and ceramics that the fracture criterion involves not only a stress level, but also a material specific property, G (the crack extension force or energy release rate), which refers to the level of energy dissipated during an incremental opening of an advancing crack in the medium. The critical value of stress σ_c at which a pre-existing flaw in the material begins to grow is given by the Griffith fracture equation

$$\sigma_c = f_G \sqrt{\frac{EG_c}{a^*}}$$

where f_G is a constant related to geometry and stress state, E, is the effective stiffness, a* is the characteristic dimension of the largest pre-existing flaw, and G_c is the critical energy release rate (which takes the place of the crack surface free energy, γ, in materials where the creation of additional crack surface requires more energy than that needed to break a monolayer of chemical bonds on the crack surface).

In a complex structure like that of a composite laminate, reaching the critical stress, σ_c, in the vicinity of a flaw does not in itself lead to catastrophic failure by unstable growth of the flaw. The growth of the crack alters the compliance or stiffness of the overall structure. If the energy release rate G during the extension of the crack from a* to a*+da decreases below G_c, the critical value for initiation, the crack will run stably and require additional work be done on the structure to supply energy for the crack to extend. If the energy release rate, G, during crack growth from a* to a*+da is greater than G_c, the crack extends unstably as the structure feeds the necessary energy to the crack to allow extension. A third case involves a crack of length a* which grows stably as G decreases with increasing crack length a*+da. If at some critical length, a_{crit}, the energy release rate begins to increase with increasing crack length, the crack will begin to grow unstably because the structure can feed enough energy to the crack to allow extension, even though the actual value of G is less than G_c. For a more complete description of fracture mechanics concepts applied to composite materials, the reader is referred to a review by Kanninen et al. [50].

Rybicki, Schmueser, and Fox [51] have recently calculated the energy release rate of $[(\pm 30)_2 / 90/\overline{90}]_s$ Boron-epoxy laminate which was observed to delaminate in a stable manner as tensile load was increased. By finite element modeling, energy release rate was calculated to decrease initially with depth of the midplane delamination and then to increase as the depth exceeded approximately three ply thicknesses. The energy release rate continued to increase slowly with depth to 17-ply thicknesses (one ply thickness = 0.018 cm) without exceeding its initial value at small delamination lengths. Experiments determined that the midplane delamination grew

in a stable manner to a depth of 15 ply thicknesses before laminate tensile failure. Calculations based on finite element modeling and experimental observation of delamination depth resulted in an estimate for G_c of 175 J/m^2. Observations of the strain at which delamination initiated led to an effective initial flaw size of one ply thickness based on the fracture equation $a^* = EG_c/\sigma_c^2\pi$ for an edge notched specimen. In the above relation the delamination stress σ_z near the free edge must exceed σ_c to a depth of a^* before the delamination crack will propagate inward. However, the microscopic evidence for flaws of size a^* existing near the edge of boron-epoxy or graphite-epoxy has not been shown.

To understand the mechanism for the initiation of an edge delamination, it is necessary to consider fracture mechanics applied on the micromechanical level [50]. A series of papers by Garrett and Bailey and colleagues [52-54] have recently appeared which examine the onset of transverse cracking of 90° glass-epoxy plies in a $(0, 90, 0)_T$ crossplied laminate tensile loaded in the 0° direction. By maintaining a constant thickness 90° layer and by increasing the thickness of 0° plies, the strain at which transverse failure was initiated increased from 0.6% to greater than 1.6%. The explanation for such behavior, although stated differently in the papers, relates to the value for G, the energy release rate, which depends upon the relative proportion of 0° and 90° plies.

The authors postulate that transverse cracks initiate at or near the fiber-matrix interface in regions where the random fiber packing has resulted in a locally high effective fiber volume fraction. At a 70% fiber volume fraction the local strain magnification factor can be on the order of 20 for a matrix modulus of 3.5 GPa typical of 175°C cured epoxy [53]. Alternatively we could choose to look at the local stress concentration in the fiber matrix interface region in the manner of Miller and Adams [17]. Since it is clear that locally the stress (strain) concentration is high enough to cause fracture, the next stage in the fracture process is the linkup of these microcracks across several fiber spacings and eventually across the entire transverse ply. Here the concept of G_c, the critical energy release rate and a property of the material, becomes important.

Consider the case of a 90° ply sandwiched between two 0° plies and loaded in tension parallel to the 0° direction. It is possible to determine the energy release rate G during the linkup and propagation of a potential transverse crack across the 90° plies. One may use a micromechanics approach like that of Garret and Bailey [53] or a finite element approach like Rybicki et al. [51] to analyze the process. If the energy release rate is less than the critical value G_c for the material, then the potential crack will not be supplied sufficient energy to cause transverse fracture. Garrett and Bailey found that by increasing the volume fraction of 0° plies relative to the 90° ply, less energy was released during the fracture process. The growth of the transverse crack in the 90° ply places a greater stress locally in the 0° plies and the composite as a whole sees an extension of $\delta\ell$. If the 0° plies are much thicker than the 90° ply then $\delta\ell$ will be proprotionately smaller and the energy released ($G = F_c \delta\ell$ where F_c is the tensile load on the composite) may be less than the critical value G_c required for propagation of the transverse crack.

Let us now return to the problem of the energy criterion for free edge delamination of graphite-epoxy laminates due to hygrothermal environment. Curtis et al. [55] have measured a value for G_c of 154 J/m^2 in a HTS epoxy composite double edge notched tensile specimen. Using the equation

$$a^* = \frac{E^* G_c}{\pi \sigma_c^2}$$

where E* will be taken as the transverse modulus 14.5 GN/m^2 as assumed in our analysis, we can determine the depth a* to which a delamination crack will initiate if the stress $\sigma_z \geq \sigma_c$ from the edge to depth a*. For example, let us choose a stress level of 35 MN/m^2 typical of the wet transverse tensile strength. If this stress is exceeded to a depth of a* = 0.058 cm below the free edge, then a crack of that length will form at the edge. In Figure 41 σ_z is plotted versus the depth y for desorption times of t_{-4}, t_{-22}, and t_{-45} in a unidirectional laminate. Assuming a ply thickness, h, of 0.013 cm for the graphite-epoxy composite and noting that the half-width b is taken at 16h in the

finite element model, we can determine the actual depth to which a particular stress is exceeded in the desorption process. From Figure 41, the assumed critical stress of 35 MPa is found to be exceeded to a depth of 0.002 cm at t_{-4}, 0.006 cm at t_{-22}, and 0.001 cm at t_{-45}. Since these depths are all less than a*, the crack will not initiate during desorption in the eight-ply laminate analyzed here.

The stress field in a 64-ply unidirectional laminate is identical to that shown in Figure 41 because of the independence of the continuum mechanics solution from the actual size of the structure being analyzed. However, because the physical dimensions (h, b, etc.) of the 64-ply model are increased by eight times, the actual depth to which the stress exceeds 35 MPa also increases by a factor of 8. Now we find for a desorption time of t_{-22} that this stress level is exceeded to a depth of 0.048 cm which approaches the critical depth a*. Thus, under the same hygrothermal conditions, the thick laminates may delaminate at the edge while the thin laminates cannot.

The consideration of the energy release rate as well as the level of stress thus indicates that hygrothermal damage in the form of delamination cracking is sensitive to the thickness of the laminate. Hedrick and Whiteside [20] observed cracks in thick laminates and neat resin samples after hygrothermal cycling, but found no evidence for cracks in laminates less than 0.25 cm thick exposed to identical conditions. These observations are consistent with the energy criterion for fracture discussed here.

These results have important implications to development of a realistic accelerated test methodology for assessing hygrothermal degradation in graphite-epoxy laminates. It is clear that tests which concentrate on the standard 8- or 16-ply laminates in studies of hygrothermal effects could underestimate the level of surface or edge damage in laminates of thicker construction and overestimate the level of damage in even thinner laminate constructions. Additional studies of the effect of laminate thickness on the level of hygrothermal surface damage, especially around holes and cutouts are recommended to resolve the importance of the energy

concept of fracture on these micromechanical damage processes.

6.3 CONCLUSIONS

T300/5209 and T300/5208 graphite-epoxy laminates were studied (1) to determine the coupling between applied stress, internal residual stress and moisture sorption kinetics, (2) to examine the microscopic damage mechanisms due to hygrothermal cycling, (3) to evaluate the effect of absorbed moisture and hygrothermal cycling on inplane shear response, (4) to determine the permanent loss of interfacial bond strength after moisture absorption and drying, and (5) to evaluate the three-dimensional stress state in laminates under a combination of hygroscopic, thermal, and mechanical loads. Specimens were conditioned to equilibrium moisture content under steady exposure to 55 or 95% RH at 70°C or 93°C. Some specimens were tested subsequent to moisture conditioning and 100 cycles between -54°C and either 70°C or 93°C. Based on results of the experimental and analytical studies, the following conclusions were reached:

1. Transverse expansion of unidirectional T300/5209 and T300/5208 due to absorbed moisture is linearly proportional to the equilibrium moisture content minus a 0.4 percent threshold level below which no expansion is observed.

2. Through thickness expansion of unidirectional composites is greater than the inplane transverse expansion and exhibits no threshold phenomenon.

3. Expansion due to absorbed moisture alters the laminate residual stress. In T300/5208 the alteration can be predicted by elastic classical laminated plate theory. In T300/5209 the residual stress state is strongly dependent on hygrothermal conditioning history and requires a viscoelastic analysis to predict the altered stress state.

4. The desorption coefficient of T300/5208 and T300/5209 at 70°C was found to be independent of initial moisture concentration and the level of internal or applied stress.

5. Hygrothermal cycling 100 times between -54°C and 93°C caused no significant microstructural cracking of eight-ply unidirectional and quasi-isotropic laminates and no change in the inplane or interlaminar shear response.

6. While the inplane shear properties of T300/5208 and T300/5209 were found to be independent of hygrothermal cycling history they were found to be quite sensitive to moisture content and test temperature. Shear stress-strain curves at 25, 70, and 93°C for each material and moisture condition are provided. T300/5209 suffered a five percent degradation of inplane shear strength at room temperature when previously equilibrated at 70°C/95% RH and dried prior to testing.

7. Only T300/5209 specimens previously exposed to 93°C/95% RH showed any permanent reduction in dry room temperature interlaminar shear strength.

8. Residual stresses in dry T300/5209 laminates increased by 35 percent after exposure to 70°C/95% RH, 100 hygrothermal cycles and desorption to the dry state. T300/5208 laminates typically suffered a 5-10 percent loss of residual stress after hygrothermal cycling.

9. Finite element analysis of free edge stresses in unidirectional, cross-plied and quasi-isotropic laminates due to hygroscopic, thermal and mechanical loads showed that stress levels were most severe during the initial desorption period

following absorption to equilibrium moisture content. However, arguments based on fracture mechanics concepts indicate that edge delamination due solely to a severe moisture gradient during desorption near the free edge will only initiate in thick laminates of approximately 64 plies or greater in thickness. However, thinner laminates will be susceptible to moisture enhanced delamination under combined hygrothermal and mechanical loads.

10. A test methodology is proposed which makes use of the viscoelastic character of T300/5209 to determine, independently of matrix plasticization, the mechanism for the reversible loss of fiber-matrix bond strength in the presence of absorbed moisture.

REFERENCES

1. J. Hertz, J. L. Christian, and M. Varlas, et al., "Advanced Composite Applications for Spacecraft and Missiles," Phase I, Final Report, AFML-TR-71-186, Vol. II, General Dynamics-Convair Division, San Diego, California (March 1972).

2. C. E. Browning and J. T. Hartness, "Effects of Moisture on the Properties of High-Performance Structural Resins and Composites," Proceedings of the Third Conference on Composite Materials, ASTM (1974), pp. 284-302.

3. C. H. Shen and G. S. Springer, "Effects of Moisture and Temperature on the Tensile Strength of Composite Materials," Journal of Composite Materials, Vol. 11 (Jan. 1977), pp. 2-16.

4. C. H. Shen and G. S. Springer, "Environmental Effects on Elastic Moduli of Composite Materials," Journal of Composite Materials, Vol. 11 (July 1977), pp. 250-264.

5. K. H. G. Ashbee and R. C. Wyatt, "Water Damage in Glass Fibre/Resin Composites," Proceedings of the Royal Society of London, Series A, Vol. 312 (1969), pp. 553-564.

6. Proceedings of the Air Force Workshop on "Durability Characteristics of Resin Matrix Composites," Battelle Columbus Laboratory, Columbus, Ohio (October 1975).

7. J. R. Vinson, R. B. Pipes, William J. Walker and Donald R. Ulrich, "The Effects of Relative Humidity and Elevated Temperature on Composite Structures," presented at Workshop on the Effects of Relative Humidity and Elevated Temperature on Composite Structures, Delaware University, Newark, NJ (1976).

8. E. L. McKague, Jr., J. E. Halkias, and J. D. Reynolds, "Moisture in Composites - The Effect of Supersonic Service on Diffusion," Journal of Composite Materials, Vol. 9, Jan. 1975, p. 2-9.

9. D. H. Kaelble, P. J. Dynes, E. H. Cirlin, J. Adhesion, Vol. 6 (1974), pp. 23-48.

10. R. J. Delasi and J. B. Whiteside, "Effect of Moisture on Epoxy Resins and Composites," Proceedings of the Symposium on Advanced Composite Materials, ASTM (1978), p 2-20.

11. C. E. Browning, G. E. Husman, and J. M. Whitney, "Moisture Effects in Epoxy Matrix Composites," Composite Materials: Testing and Design (Fourth Conference), ASTM-STP 614 (1977).

12. Y. Weitsman, "Diffusion with Time-Varying Diffusivity, With Application to Moisture-sorption in Composites," Journal of Composite Materials, Vol. 10, (July 1976), pp. 193-204.

13. C. H. Shen and G. S. Springer, "Moisture Absorption and Desorption of Composite Materials," Journal of Composite Materials, Vol. 10 (January 1976), p. 2-20.

14. R. E. Mauri, F. W. Crossman, and W. J. Warren, "Assessment of Moisture Altered Dimensional Stability of Structural Composites," SAMPE Symposium, Vol. 22 (1978), pp. 1202-1217.

15. F. W. Crossman, R. E. Mauri, and W. J. Warren, "Moisture-Altered Viscoelastic Response of Graphite/Epoxy Composites," Proceedings of the ASTM Symposium on Advanced Composite Materials, ASTM, 1978, p. 205-220.

16. D. H. Kaelble, P. J. Dynes, L. W. Crane, and L. Maus, "Interfacial Mechanisms of Moisture Degradation in Graphite-Epoxy Composites," J. Adhesion, Vol. 7 (1975), pp. 25-54.

17. A. K. Miller, "Micromechanical Aspects of the Environmental Behavior of Composite Materials," Ph. D. Thesis, Wyoming University, Laramie, Wyoming (1977).

18. R. B. Pipes, J. R. Vinson, and T. W. Chou, "On the Hygrothermal Response of Laminated Composite Systems," Journal of Composite Materials, Vol. 10 (April 1976), pp. 129-148.

19. F. W. Crossman and A. S. D. Wang, "Stress Field Induced by Transient Moisture Sorption in Finite-Width Composite Laminates," Journal of Composite Materials, Vol. 12, (Jan. 1978), pp. 2-18.

20. I. G. Hedrick and J. B. Whitesdies, "Effects of Environment on Advanced Composites Structures," American Institute of Aeronautics and Astronautics, Conference on Aircraft Composites: The Emerging Methodology for Structural Assurance, San Diego, CA (Mar. 1977), pp. 1-18.

21. C. D. Shirrill, "Moisture Sorption and Desorption in Epoxy Resin Matrix Composites," Proceedings of the Twenty-Third National Symposium and Exhibition on Selective Application of Materials for Products and Energy, Society for the Advancement of Material and Process Engineering (1978), pp. 175-191.

22. J. Unnam and D. R. Tenney, "Analytical Prediction of Moisture Absorption/Desorption in Resin Matrix Composites Exposed to Aircraft Environments," AIAA Paper 77-400, presented at AIAA Conference on Aircraft Composites, San Diego, CA (March 1977).

23. J. Whiteside, "Environmental Sensitivity of Advanced Composites," AFFDL Contract F35615-76-C-5324, presented at AF Mechanics of Composites Review, Dayton, Ohio (October 1977).

24. G. S. Springer, "Moisture Content of Composites Under Transient Conditions," Journal of Composite Materials, Vol. 11 (Jan. 1977), pp. 107-122.

25. G. E. Husman, "Characterization of Wet Composite Materials," AF Mechanics of Composites Review, Dayton, Ohio (Jan. 1976).

26. R. M. Verett, "Temperature-Humidity Effects on the Strength of Graphite-Epoxy Laminates," AIAA Paper No. 75-1011, 1975 AIAA Aircraft Systems and Technology Meeting, Los Angeles, CA, August 1975.

27. F. W. Crossman and R. E. Mauri, "Effect of Moisture and Thermal Cycling on Graphite-Epoxy Composites," Lockheed Research Report LMSC-D460822 (August 1975).

28. B. S. Marks, "New Graphite Fiber Surface Treatments and Effects on Composite Properties," Proceedings of the 12th Biennial Conference on Carbon, Pittsburgh, PA (July 1975).

29. J. M. Augl and A. E. Berger, "Moisture Effect on Carbon Fiber Epoxy Composites," SAMPE Technical Conference, Vol. 8 (1976) pp. 383-427.

30. P. W. R. Beaumont, and D. Harris, "The Energy of Crack Propagation in Carbon Fibre-Reinforced Resin Systems," Journal of Materials Science, Vol. 7 (Nov. 1972), pp. 1265-1279.

31. D. H. Kaelble, J. Adhesion, Vol. 5 (1973), pp. 245-264.

32. R. E. Bohlmann and E. A. Derby, "Moisture Diffusion in Graphite/Epoxy Laminates - Experimental and Predicted," Proceedings of Structures, Structural Dynamics and Materials Conference, March 1977, and Aircraft Composites: The Emerging Methodology for Structural Assurance, March 1977, San Diego, CA, pp. 219-226.

33. J. H. Powell and D. J. Zigrang, "Moisture Absorption and Desorption Characteristics of Three Epoxy-Graphite Systems," SAMPE Journal (Jul-Aug 1977), Vol. 13, pp. 4-13.

34. H. W. Bermann and C. W. Dill, "Effect of Absorbed Moisture on Strength and Stiffness Properties of Graphite-Epoxy Composites - For Shuttle Orbiter," Proceedings of the Eighth National Technical Conference on Bicentennial of Materials, Seattle, Wash. (Oct. 1976) pp. 244-256.

35. A. Ary; C. Axtell; L. Fogg; A. Jackson; A. M. James; B. Mosesian; J. Vanderwier; and J. Vanhamersveld, "Flight Service Evaluation of An Advanced Composite Empennage Component on Commercial Transport Aircraft, Phase 1: Engineering Development," Final Report--Lockheed-California, Burbank, CA (1975).

36. C. E. Browning, "The Mechanisms of Elevated Temperature Property Losses in High Performance Structural Epoxy Resin Matrix Materials After Exposures to High Humidity Environments," Diversity - Technology Explosion; Proceedings of the Twenty-second National Symposium and Exhibition, San Diego, CA, SAMPE (1977), pp. 365-394.

37. H. T. Hahn and R. Y. Kim, "Swelling of Composite Laminates," in Advanced Composite Materials - Environmental Effects; Proceedings of the ASTM Symposium, Dayton, Ohio, (1978) pp. 98-120.

38. J. A. DeRuntz, Jr., and F. W. Crossman, "Time and Temperature Effects in Laminated Composites," Nucl. Metall., V. 20, Pts. 1-2, 1976, Proceedings of the Int. Conference on Computer Simulation for Materials Applications, Gaithersburg, MD (Apr. 1976), Pt. 2, pp. 1085-1096.

39. H. T. Hahn and N. J. Pagano, "Curing Stresses in Composite Laminates," J. Composite Materials, Vol. 9 (January 1975), p. 91-106.

40. G. F. Sykes; H. D. Burks; and J. B. Nelson, "The Effect of Moisture on the Dynamic Thermomechanical Properties of A Graphite/Epoxy Composite," in Diversity - Technology Explosion; Proceedings of the Twenty-Second SAMPE National Symposium and Exhibition, San Diego, CA (1977), pp. 350-364.

41. Private communication from W. J. Warren, Lockheed Palo Alto Research Laboratory, to F. W. Crossman, 5 June 1978.

42. J. M. Whitney and G. E. Husman, "Use of the Flexure Test for Determining Environmental Behavior of Fibrous Composites," SESA Spring Meeting, 1977, and Experimental Mechanics, Vol. 18, May 1978, pp. 185-190.

43. A. S. D. Wang and Frank W. Crossman, "Some New Results on Edge Effect in Symmetric Composite Laminates," J. Composite Materials, Vol. 11 (Jan. 1977), p. 92-106.

44. A. S. D. Wang and Frank W. Crossman, "Edge Effects on Thermally Induced Stresses in Composite Laminates," J. Composite Materials, Vol. 11 (July 1977), p. 300-312

45. F. W. Crossman and A. S. D. Wang, "Analysis of Free Edge Stress Induced Fracture of Fiber Composite Laminates," Proceedings of Symposium on Applications of Computer Methods in Engineering, Univ. of Southern California, 23-26 August 1977, p. 213-220.

46. H. T. Sumsion and Y. D. S. Rajapakse, "Simple Torsion Test for Shear Moduli Determination of Orthotropic Composites," Proceedings of Second International Conference on Composite Materials, Toronto, Canada, 16-20 April 1978.

47. N. J. Pagano and R. Byron, "Some Observations on the Interlaminar Strength of Composite Laminates," Int. J. MEchanical Sciences, Vol. 15 (1973), pp. 679-692.

48. D. F. Adams and A. K. Miller, "Hydrothermal Microstresses in a Unidirectional Composite Exhibiting Inelastic Material Behavior," J. Composite Materials, Vol. 11 (July 1977), pp. 285-299.

49. C. C. Chiao, R. J. Sherry, and J. A. Rinde, "Transverse Tensile Characteristics of Fiber Composites with Flexible Resins: Theory and Test Results," Lawrence Livermore Laboratory Research Report UCRL-79983 (1977) to be published in Polymer Eng. Sci.

50. M. F. Kanninen, E. F. Rybicki, and H. F. Brinson, "A Critical Look At Current Applications of Fracture Mechanics to the Failure of Fibre-Reinforced Composites," Composites, V. 8 (Jan. 1977), pp. 17-22.

51. E. F. Rybicki, D. W. Schmueser, and J. Fox, "An Energy Release Rate Approach for Stable Crack Growth in the Free-Edge Delamination Problem," J. Composite Materials, Vol. 11 (Oct 1977), p. 470-487.

52. K. W. Garret and J. E. Bailey, "Multiple Transverse Fracture in 90 Degree Cross-ply Laminates of a Glass Fibre-Reinforced Polyester," Journal of Materials Science, Vol. 12 (Jan. 1977), pp. 157-168.

53. K. W. Garrett and J. E. Bailey, "Effect of Resin Failure Strain on the Tensile Properties of Glass Fibre-Reinforced Polyester Cross-ply Laminates," J. Materials Science, V. 12 (Nov. 1977) pp. 2189-2194.

54. A. Parvizi, K. W. Garrett, and J. E. Bailey, "Constrained Cracking in Glass Fibre-Reinforced Epoxy Cross-Ply Laminates," Journal of Materials Science, Vol. 13 (Jan. 1978), pp. 195-201.

55. M. G. Bader, P. T. Curtis, and R. S. Chhatwal, "The Micromechanics of Fracture in Fibre-Reinforced Thermoplastics," in International Conference on Composite Materials, Geneva Switzerland, April 7-11, 1975 and Boston, Mass., April 14-18, 1975, Proceedings, Vol. 2, Metallurgical Society of AIME, 1976, pp. 191-221.

APPENDIX A

MATERIAL PROCESSING INFORMATION

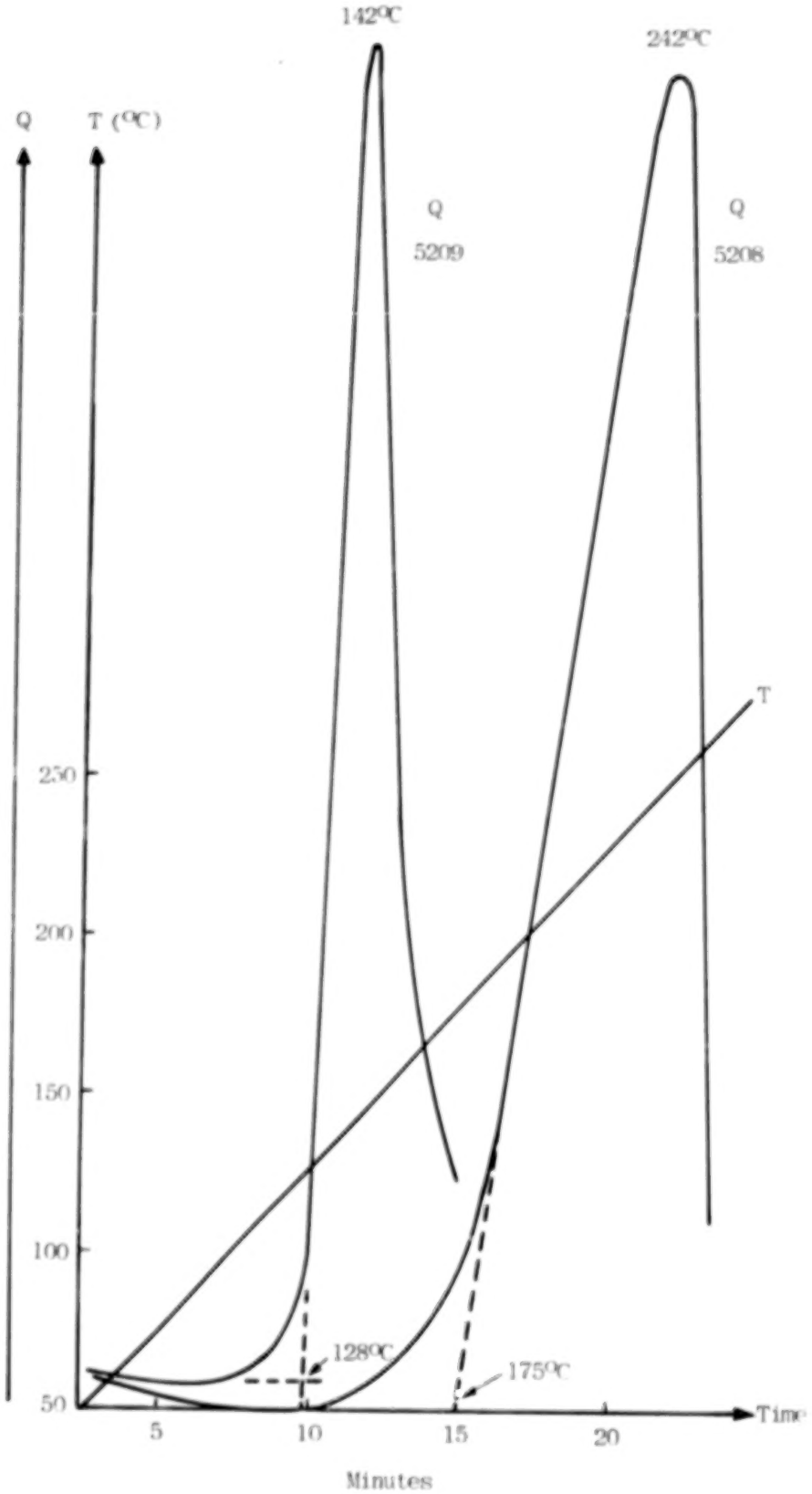

Figure A1. Differential Scanning Calorimetry of Narmco T300/5208 and T300/5209 Prepreg

BLANK

PAGE

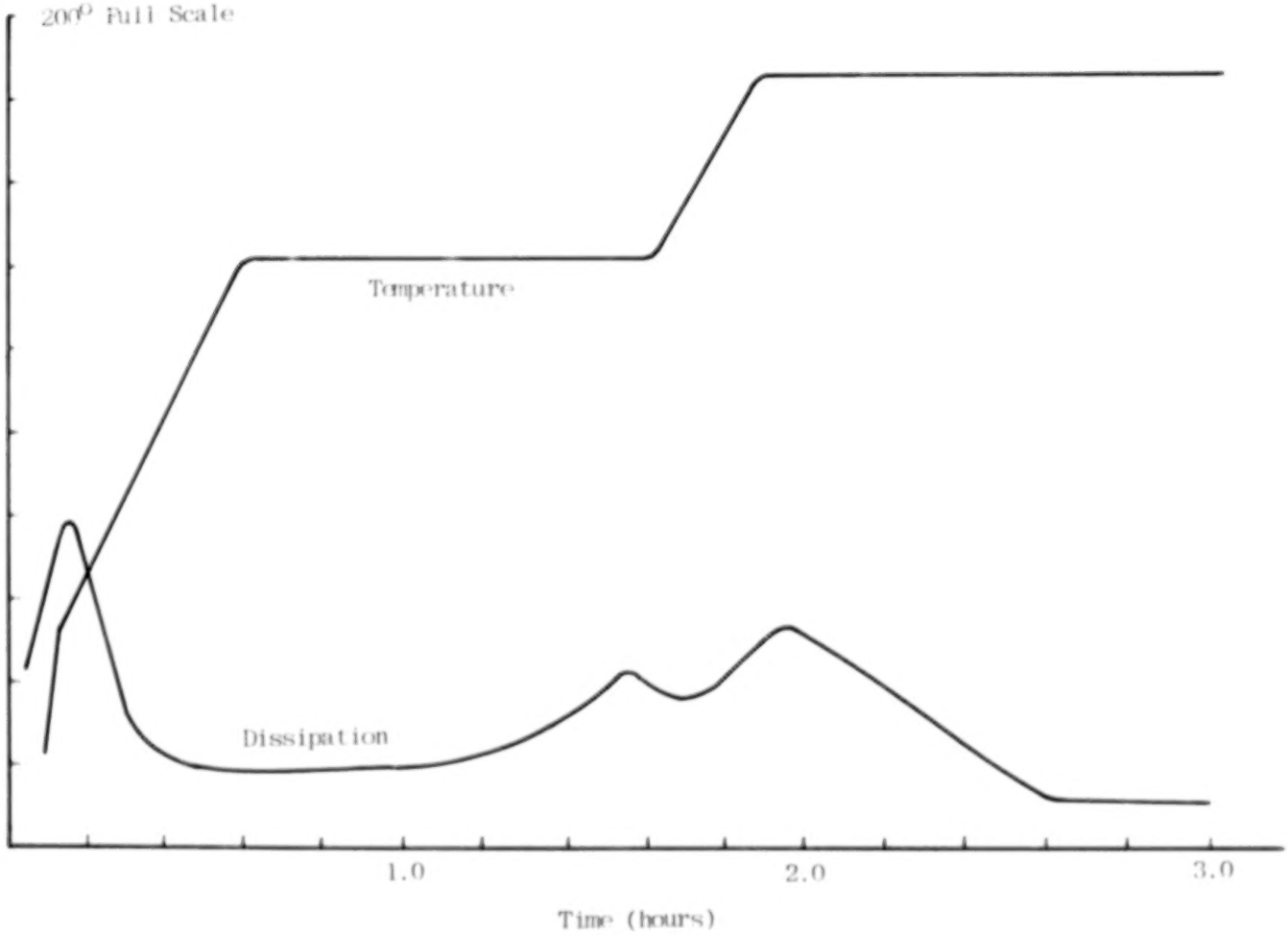

Figure A2. Dynamic Dielectric Analysis of T300/5208 Prepreg

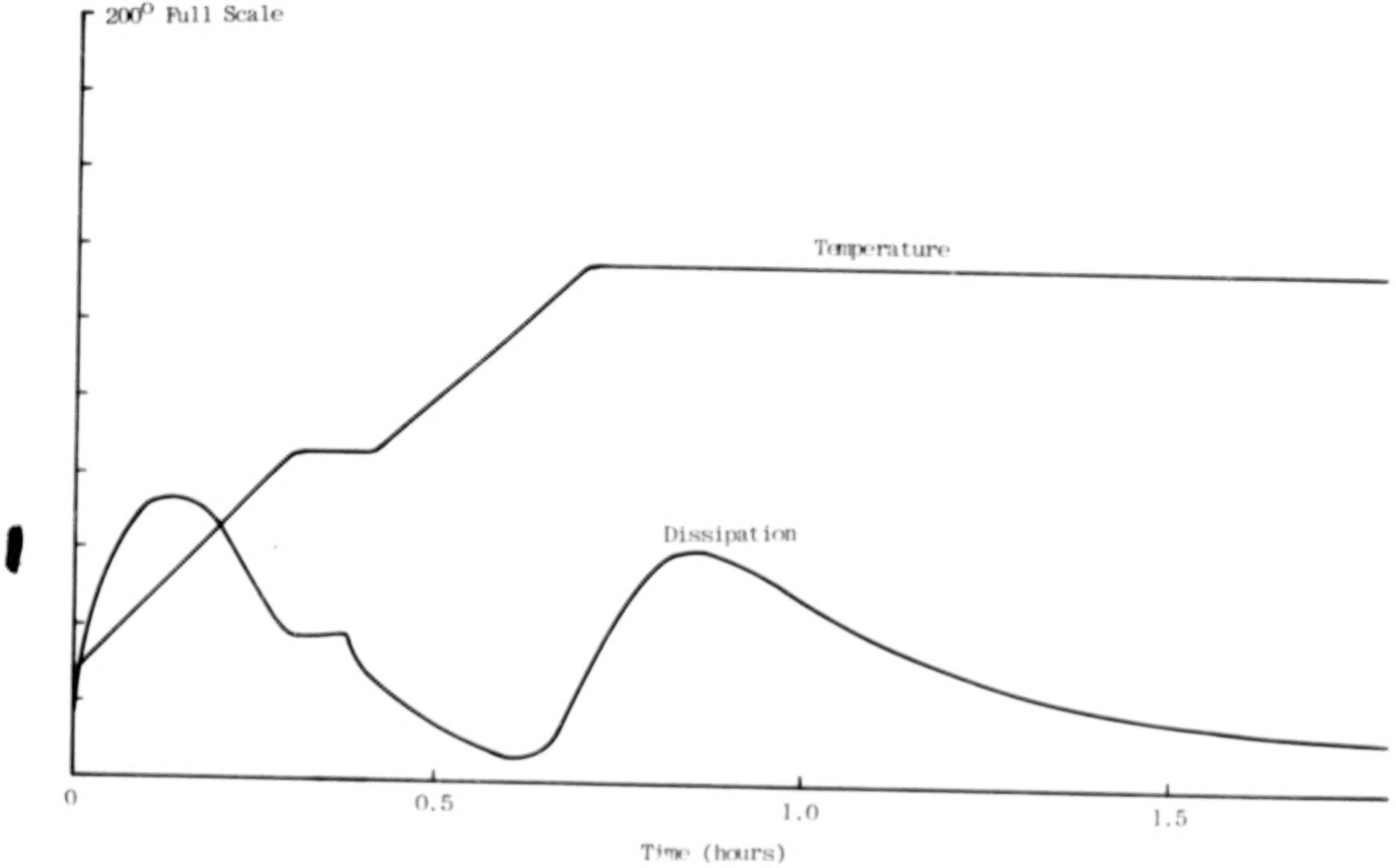

Figure A3. Dynamic Dielectric Analysis of T300/5209 Prepreg

T300/5208 Panel #17 75X

(a)

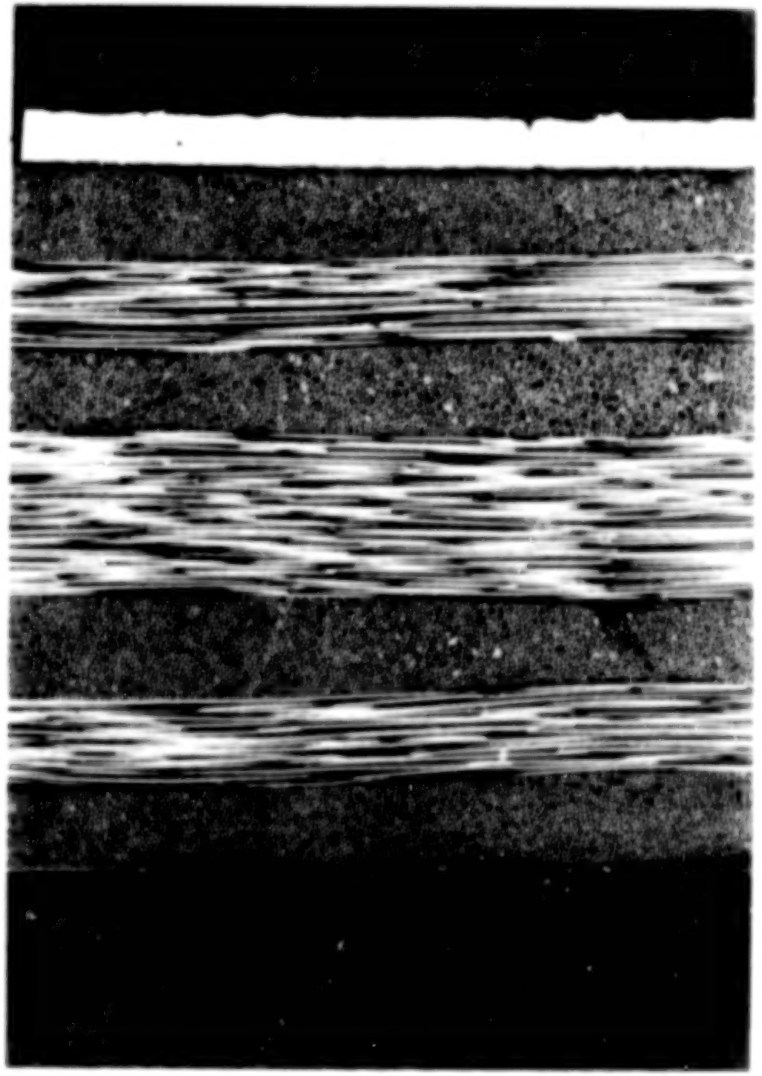

T300/5208 Panel #21

(b)

Figure A1. (a) T300/5208, Panel 17, As Fabricated.
(b) T300/5208, Panel 21, As Fabricated.

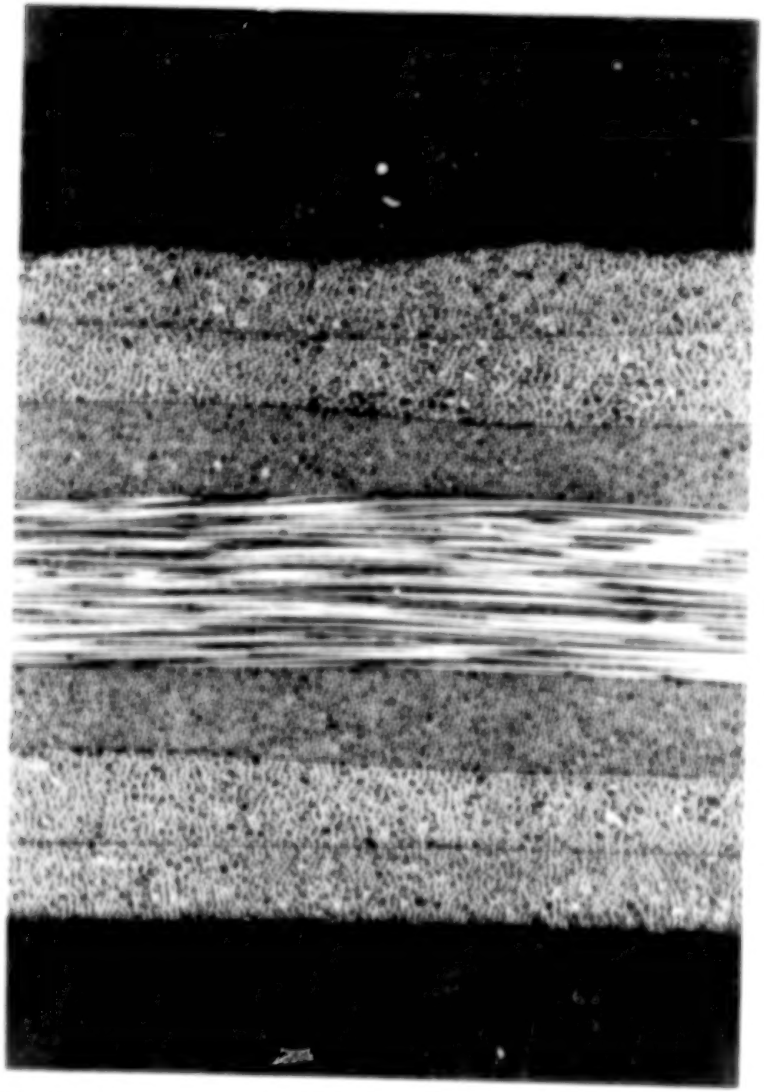

T300/5208 Panel #27 100X

(a)

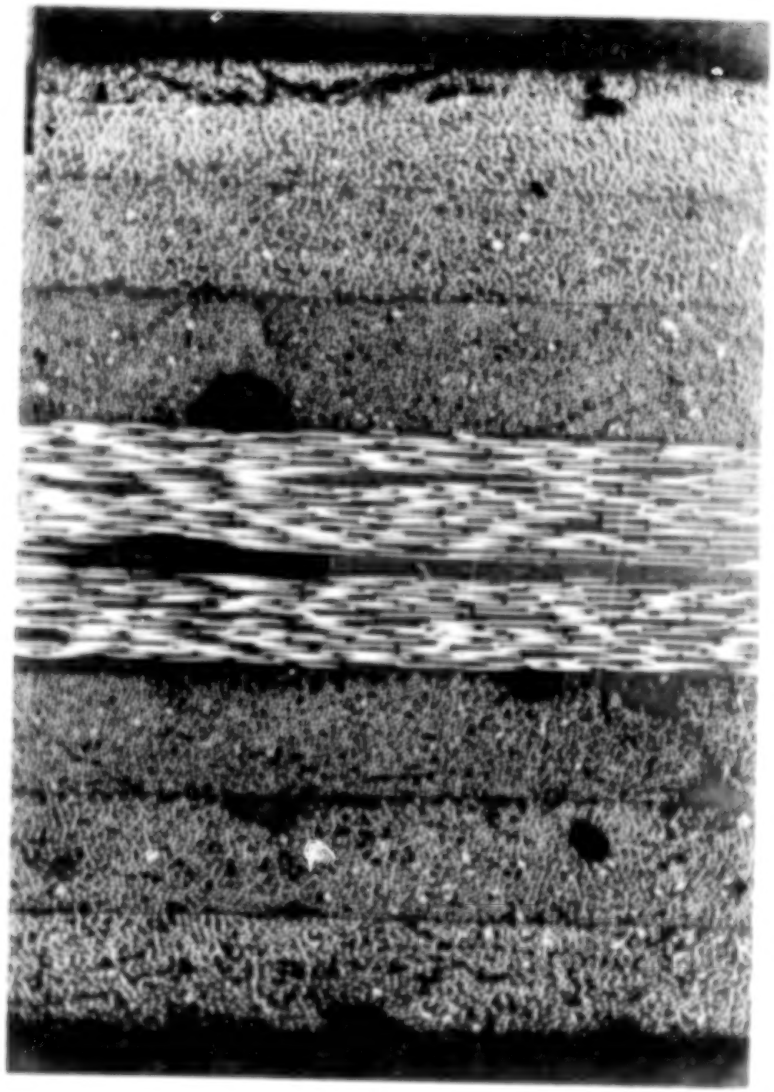

T300/5208 Panel #28 100X

(b)

Figure A5. (a) T300/5208, Panel 27, As Fabricated,
(b) T300/5208, Panel 28, As Fabricated.

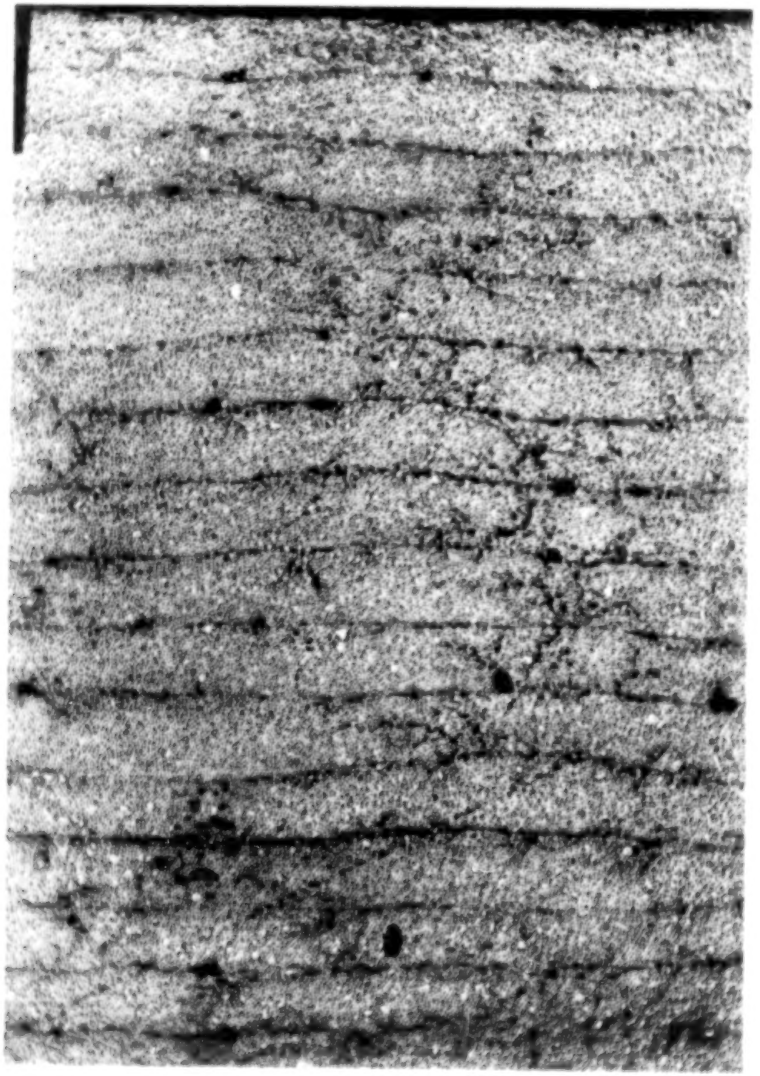

T300/5209 Panel #2 75X
(a)

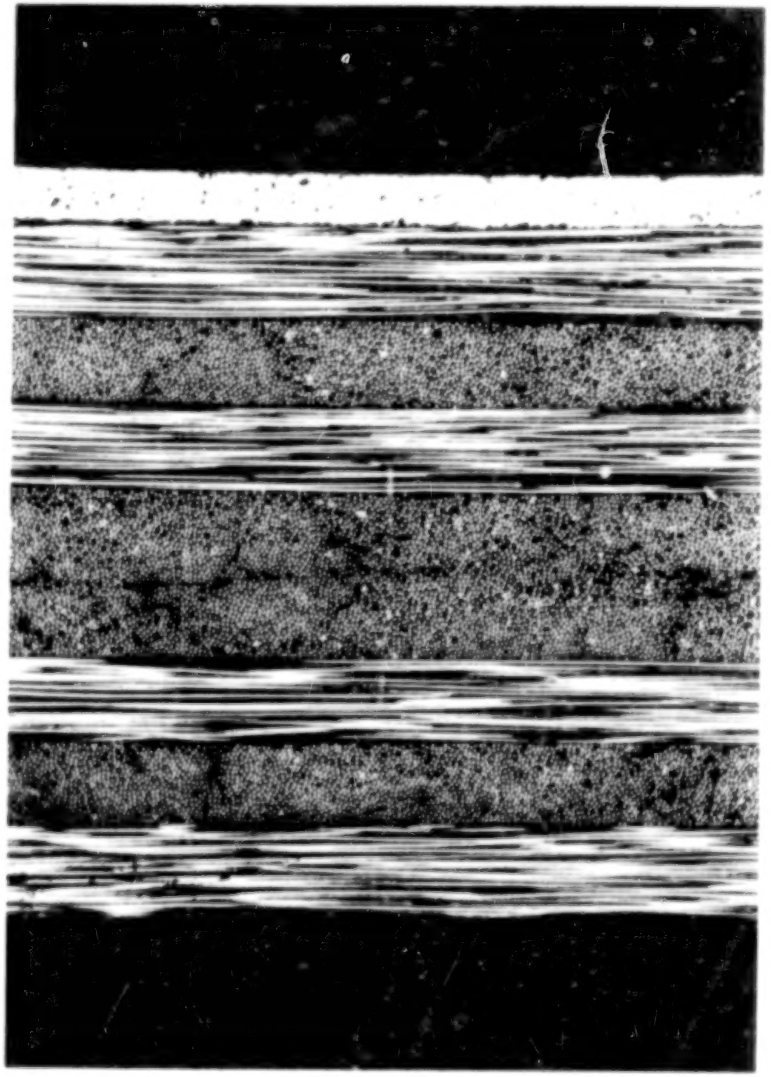

T300/5209 Panel #3 100X
(b)

Figure A6. (a) T300/5209, Panel 2, As Fabricated.
(b) T300/5209, Panel 6, As Fabricated.

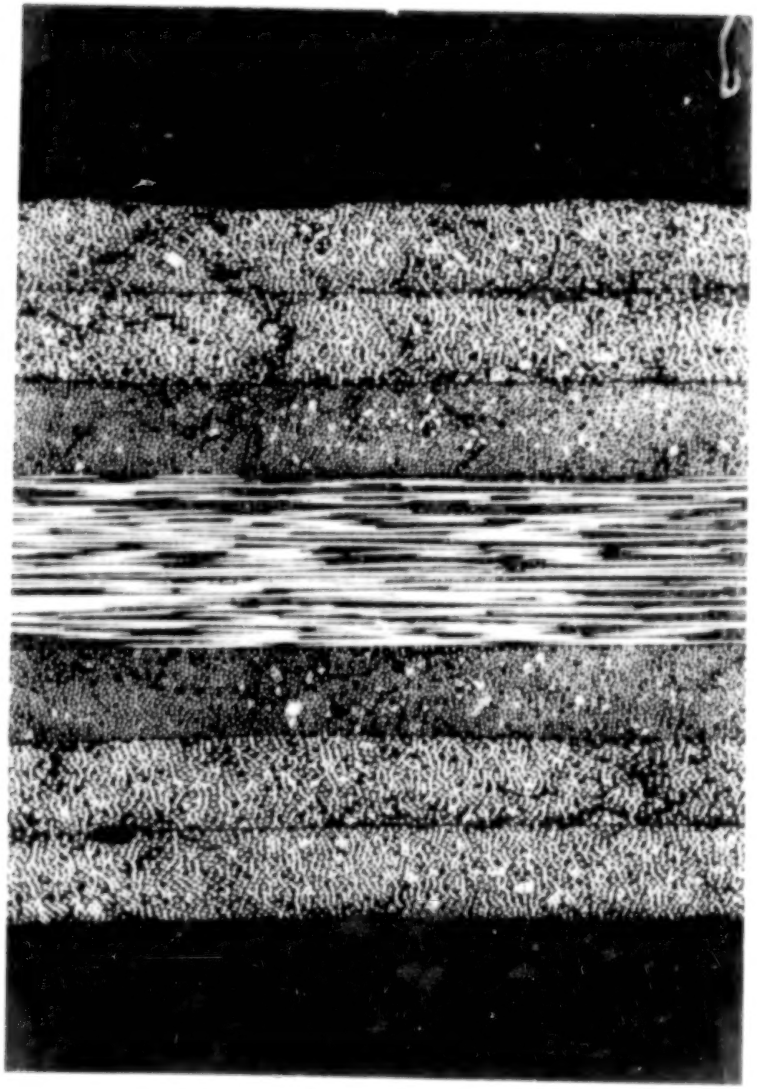

T300/5209 Panel #12 100X
(a)

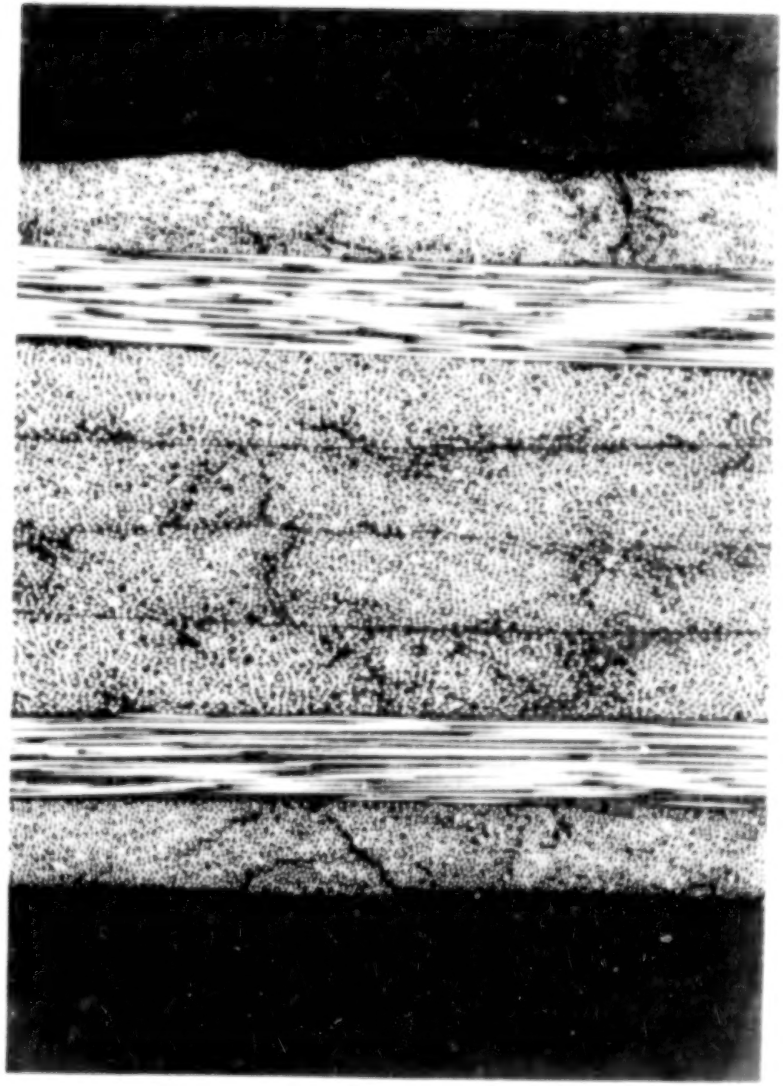

T300/5209 Panel #13 100X
(b)

Figure A7. (a) T300/5209, Panel 12, As Fabricated.
(b) T300/5209, Panel 13, As Fabricated.

Table A1

LAMINATE PROCESSING PROCEDURE

CURE PROCESS FOR T300/5208 LAMINATES	1. Heat to 275 $^{+5}_{-10}$ °F at 4-6°F/min under 20-25 in. vacuum 2. Hold one hour (start time when 265°F is reached). 3. Apply 100 psi (vent vacuum when pressure reaches 20 psi). 4. Heat to 355 $^{+10}_{-5}$ °F at 4-6°F/min. 5. Hold two hours at 355 $^{+10}_{-5}$ °F. 6. Cool under pressure to below 140°F. 7. Post cure by heating to 400 $\pm$ 10°F at 4-5°F/min and hold for 4 hours.
CURE PROCESS FOR T300/5209 LAMINATES	1. Heat to 175°F at 4-6°F/min under 20-25 in. vacuum. 2. At 165°F cut power for five minutes. 3. Apply 85 psi 4. Raise temperature to 260°F at 4-6°F/min. 5. Hold at 260°F for two hours. 6. Cool under pressure to below 140°F.

Table A2

VOLUME FRACTION ANALYSIS OF LAMINATE PANELS

(2 samples per panel)

Panel No.	Material	Layup	Fiber Volume %	Void Volume %
1	T300/5209	$[0]_{8T}$	64.9, 64.9	-.7, -.7
2	"	$[0]_{16T}$	62.9, 64.2	-.6, -.6
3	"	$[0]_{8T}$ Clad†	64.8, 64.8	-.8, -.8
4	"	$[0_4, 90_4]_T$	62.3, 63.8	-1.0, -.8
5	"	$[0_4, 90_4]_T$	67.0, 67.4	-.6, -.6
6	"	$[0, 90]_{2S}$ Clad	65.6, 65.4	-.6, -.6
7	"	$[\pm 45]_{2S}$	64.4, 64.9	-.3, -.6
8	"	$[\pm 45]_{2S}$	64.0, 64.1	-.7, -.6
9	"	$[\pm 45]_{2S}$	62.9, 64.2	-.8, -.4
10	"	$[\pm 45]_{2S}$	63.7, 63.1	-.6, -.4
11	"	$[\pm 45]_{2S}$	65.8, 65.6	-.4, -.6
12	"	$[\pm 45,0,90]_S$	64.0, 63.9	-.5, -.55
13	"	$[\pm 45,0,90]_S$ *	64.5, 64.6	-.6, -.7
14	"	$[\pm 45,0,90]_S$ Clad*	64.0, 64.3	-.5, -.7
15	"	$[90,0,\pm 45]_S$	63.8, 63.6	-.7, -.7
16	T300/5208	$[0]_{8T}$	68.8, 68.9	-.5, -.4
17	"	$[0]_{6T}$	67.5, 67.4	-.5, -.5
18	"	$[0]_{8T}$ Clad	68.6, 68.5	-.6, -.4
19	"	$[0_4, 90_4]_T$	69.4, 70.1	.6, -.3
20	"	$[0_4, 90_4]_T$	69.7, 69.8	-.5, -.4
21	"	$[0, 90]_{2S}$ Clad	68.0, 67.7	-.3, -.3
22	"	$[\pm 45]_{2S}$	67.7, 68.1	-.3, .2
23	"	$[\pm 45]_{2S}$	67.5, 67.7	-.2, -.1
24	"	$[\pm 45]_{2S}$	67.9, 68.9	-.2, .1
25	"	$[\pm 45]_{2S}$	67.7, 67.8	.3, -.2
26	"	$[\pm 45]_{2S}$	68.3, 68.1	0.3, 0.0
27	"	$[\pm 45,0,90]_S$	68.4, 68.5	0.0, 0.1
28	"	$[\pm 45,0,90]_S$*	58.1, 57.8	1.4, 1.6
29	"	$[\pm 45,0,90]_S$ Clad*	57.9, 58.4	.6, .7
30	"	$[90,0,\pm 45]_S$	68.4, 68.0	-.3, -.1

*"voidy" laminates

† Clad with 3 mil Al foil on one side

APPENDIX B

MECHANICAL TESTING TABUL/TION

Table B1

HYGROTHERMOELASTIC CONSTANTS AT 25°C

Property	Material	
	T300/5208	T300/5209
E_1 GPa (MSI)	148.14 (21.5)	135.73 (19.7)
E_2 GPa (MSI)	9.99 (1.45)	8.89 (1.29)
G_{12} GPa (MSI)	5.86 (0.85)	5.17 (0.75)
ν_{12}	0.31	0.31
α_1^* 10^{-6} °C^{-1}(°F^{-1})	-0.36 (-0.2)	-0.36 (-0.2)
α_2^* 10^{-6} °C^{-1}(°F^{-1})	28.8 (16.0)	28.8 (16.0)
β_1^{**} 10^{-6} per % H_2O	60.0	60.0
β_2^{***} 10^{-6} per % H_2O	0.55	0.55

* Handbook values assumed

** Based on in-house measurements on HMS/3501

*** Assumes no swelling below 0.4% H_2O (see Fig. 1)

Table B2

FOUR POINT FLEXURE TESTING

Material	Layup	Flex Orientation*	Al on Tensile (T) or Compressive (C) Side	Ultimate Strength (MPa)	Radius of Curvature at 50% of Ultimate (cm)
T300/5209	UD	L	T	1797	6.09
		L	C	1663	6.09
		T	T	109	9.61
		T	C	95	9.61
T300/5208	UD	L	T	1919	4.17
		L	C	1635	6.48
		T	T	121	5.75
		T	C	84	9.61
T300/5209	$(0,90)_{2s}$	L	T	1297	6.09
		L	C	1241	6.09
		T	T	874	4.33
		T	C	622	7.44
T300/5208	$(0,90)_{2s}$	L	T	1435	5.44
		L	C	1151	6.92
		T	T	737	6.09
		T	C	580	7.44

*L = 0° fibers parallel to specimen length

T = 90° fibers parallel to specimen length

BLANK

PAGE

B-4

Table B3

TENSILE TEST RESULTS - T300/5208 AND T300/5209 $(+45_2)_s$

Material	Exposure (T°C/RH%)	Specimen Number	% H_2O	Cycling Max. Temp. (100 Cyc. -54°C to T_{MAX} °C)	Tensile Test Temp. (°C)	E		ν_{xy}	G_{12}		τ^{ULT}_{12}	
						GPa	($\times 10^6$ psi)		GPa	($\times 10^6$ psi)	MPa	(ksi)
T300/5209	Dry	7-1	0	None	22	21.93	(3.18)	0.694	6.48	(0.939)	79.4	(11.5)
		2	0	None		20.41	2.96	0.714	5.97	0.865	79.9	11.6
		3	0	71		21.86	3.17	0.735	6.31	0.915	80.4	11.7
		4	0	71		22.90	3.32	0.781	6.42	0.931	82.0	11.9
		5	0	93		22.41	3.25	0.741	6.43	0.933	78.0	11.3
		6	0	93		22.34	3.24	0.769	6.32	0.916	79.8	11.6
	71/55	7	0.79	None		20.34	2.95	0.781	5.71	0.828	72.0	10.4 †
		8	0.84	None		19.66	2.85	0.809	5.43	0.787	72.6	10.5 †
		9	0.81	71		23.45	3.40	0.813	6.47	0.938	72.1	10.4 †
		10	0.81	71		21.52	3.12	0.769	6.08	0.882	72.6	10.5 †
		11	0.81	93		20.34	2.95	0.931	5.26	0.763	70.2	10.2 †
		12	0.80	93		21.31	3.09	0.752	6.09	0.883	72.3	10.5 †
	71/95	13	2.19	None		18.00	2.61	0.758	5.15	0.747	47.7	6.9 †
		14	2.09	None		19.17	2.78	0.833	5.23	0.759	50.2	7.27†
		15	2.18	71		17.31	2.51	0.752	4.94	0.717	45.9	6.65†
		16	2.16	71		18.83	2.73	0.862	5.06	0.733	49.7	7.12†
		17	2.12	93		16.97	2.46	--	--	--	49.3	7.15†
		18	2.18	93		18.07	2.62	0.813	4.99	0.723	49.9	7.24†
	71/95+Dry	8-19	2.16+0	None		20.97	3.04	0.772	5.92	0.858	73.8	10.7
T300/5209	"	20	2.14	None	22	21.38	3.10	0.719	6.23	0.903	73.3	10.6

(continued)

Table B3 (continued)

TENSILE TEST RESULTS - T300/5208 AND T300/5209 $(\pm 45_2)_s$

Material	Exposure (T°C/RH%)	Specimen Number	% H_2O	Cycling Max. Temp. (100 Cyc. -54°C to T_{MAX} °C)	Tensile Test Temp. (°C)	E		ν_{xy}	G_{12}		τ_{12}^{ULT}	
						GPa	($\times 10^6$ psi)		GPa	($\times 10^6$ psi)	MPa	(ksi)
T300/5209	71.95+Dry	8-21	2.08	71	22	21.24	(3.08)	0.769	6.01	(0.872)	72.6	(10.5)+
		22	2.09	71		20.90	3.03	0.671	6.25	0.906	73.7	10.7
		23	2.16	93		20.97	3.04	0.690	6.19	0.898	78.0	11.3 +
		24	2.10	93		20.90	3.03	0.694	6.17	0.894	75.5	10.9
	Dry	25	0	None	71	15.79	2.29	0.877	4.21	0.611	51.2	7.42+
		26	0	None		17.03	2.47	0.874	4.55	0.660	Tab	Tab
		27	0	71		17.03	2.47	0.754	4.86	(.705	53.5	7.75+
		28	0	71		15.52	2.25	0.813	4.28	0.620	53.7	7.78+
		29	0	93		16.41	2.38	0.807	4.54	0.658	48.2	6.98+
		30	0	93		14.76	2.14	0.699	4.34	0.629	47.2	6.85+
	71/55	31	0.84	None		7.45	1.08	0.769	2.11	0.306	22.9	3.32+
		32	0.87	None		5.86	0.85	0.676	1.74	0.252	20.3	2.95+
		33	0.82	71		12.97	1.88	0.926	3.37	0.489	30.3	4.39+
		34	0.81	71		11.66	1.69	0.909	3.05	0.442	32.9	4.76+
		35	0.84	93		8.83	1.28	0.901	2.32	0.336	29.5	4.28+
		36	2.05	93		12.97	0.58	0.909	3.40	0.493	Tab	Tab
	71/95	9-37	2.00	None		4.00	0.74	0.877	1.07	0.155	Tab	Tab
		38	2.01	None		5.10	0.40	0.986	1.29	0.187	21.5	3.14+
		39	2.03	71		2.76	0.23	0.873	0.745	0.108	16.9	2.45+
		40	2.07	71		1.59	0.40	1.06	0.380	0.0551	12.6	1.83+

(continued)

Table B3 (continued)

TENSILE TEST RESULTS - T300/5208 AND T300/5209 $(+45_2)_s$

Material	Exposure (T°C/RH%)	Specimen Number	% H_2O	Cycling Max. Temp. (100 Cyc. -54°C to T_{MAX} °C)	Tensile Test Temp. (°C)	E		ν_{xy}	G_{12}		$^{ULT}\tau_{12}$	
						GPa	($\times 10^6$ psi)		GPa	($\times 10^6$ psi)	MPa	(ksi)
T300/5209	71/95	9-41	2.07	93	71	2.76	(0.40)	0.938	0.717	(0.104)	15.6	(2.26)+
		42	2.01	93		3.52	0.51	0.956	0.890	0.129	19.0	2.75+
	71/95+Dry	43	2.05+0	None		14.34	2.08	0.781	3.91	0.567	Tab	Tab
		44	2.08	None		16.55	2.40	0.809	4.57	0.662	Tab	Tab
		45	2.03	71		17.79	2.58	0.775	5.01	0.726	47.6	6.90+
		46	2.02	71		16.34	2.37	0.859	4.41	0.639	48.4	7.02+
		47	2.07	93		16.34	2.37	0.794	4.56	0.661	Tab	Tab
		48	2.05	93		13.59	1.97	0.772	3.84	0.557	45.7	6.62+
	Dry	49	0	None	93	14.14	2.05	0.909	3.70	0.537	Tab	Tab
		50	0	None		--	--	--	--	--	--	--
		51	0	71		16.48	2.39	0.800	4.58	0.664	53.2	7.71+
		52	0	71		17.66	2.56	0.800	4.91	0.712	51.1	7.41+
		53	0	93		14.62	2.12	0.806	4.89	0.709	49.9	7.24+
		54	0	93		18.07	2.62	0.870	4.83	0.700	53.5	7.76+
	71/55	10-55	0.82*	None		9.52	1.38	0.952	2.43	0.352	31.7	4.59+
		56	0.82*	None		--	--	--	--	--	--	--
		57	0.82*	71		9.86	1.43	0.833	2.70	0.391	27.6	4.00
		58	0.82*	71		--	--	--	--	--	--	--
		59	0.82*	93		9.45	1.37	0.952	2.42	0.351	Tab	Tab
		60	0.82*	93		9.24	1.34	--	--	--	29.8	4.32+

(continued)

Table B3 (continued)

TENSILE TEST RESULTS - T300/5208 AND T300/5209 $(\pm 45_2)_s$

Material	Exposure (T°C/RH%)	Specimen Number	% H_2O	Cycling Max. Temp. (100 Cyc. -54°C to T_{MAX} °C)	Tensile Test Temp. (°C)	E		ν_{xy}	G_{12}		ULT τ_{12}	
						GPa	($\times 10^6$ psi)		GPa	($\times 10^6$ psi)	MPa	(ksi)
T300/5209	71/95	10-61	2.09*	None	93	1.12	(0.163)	0.961	0.287	(0.0416)	10.0	(1.45)+
		62	2.09*	None		--	--	--	--	--	--	--
		63	2.09*	71		1.02	0.148	1.09	0.245	0.0355	10.7	1.50+
		64	2.09*	71		1.11	0.16	0.961	0.283	0.0411	10.6	1.53+
		65	2.09*	93		1.56	0.226	1.08	0.376	0.0545	12.4	1.79+
		66	2.09*	93		1.47	0.213	1.04	0.360	0.0522	11.0	1.60+
	71/95+Dry	67	1.74+0	None		13.93	2.02	0.885	3.69	0.535	36.4	5.28+
		68	1.76	None		13.17	1.91	0.847	3.57	0.518	40.1	5.81+
		69	1.79	71		14.90	2.16	0.806	4.13	0.599	40.6	5.89+
		70	1.82	71		14.83	2.15	0.822	4.08	0.591	43.3	6.28+
		71	1.82	93		15.52	2.25	0.833	4.23	0.614	45.8	6.63+
		72	1.79	93		13.79	2.00	0.787	3.87	0.561	45.3	6.56+

(continued)

Table B3 (continued)

TENSILE TEST RESULTS - T300/5208 AND T300/5209 $(\pm 45_2)_s$

Material	Exposure (T°C/RH%)	Specimen Number	% H_2O	Cycling Max. Temp. (100 Cyc. -54°C to T_{MAX} °C)	Tensile Test Temp. (°C)	E		ν_{xy}	G_{12}		τ_{12}^{ULT}	
						GPa	($\times 10^6$ psi)		GPa	($\times 10^6$ psi)	MPa	(ksi)
T300/5208	Dry	22-1	0	None	22	21.93	(3.18)	0.746	6.28	(0.911)	76.8	(11.1)
		2	0	None		22.00	3.19	0.763	6.23	0.904	80.1	11.6
		3	0	71		23.10	3.35	0.746	6.61	0.958	81.6	11.8
		4	0	71		24.07	3.49	0.730	6.97	1.01	80.7	11.7
		5	0	93		21.45	3.11	0.719	6.23	0.903	77.8	11.8
		6	0	93		23.24	3.37	0.787	6.50	0.942	80.0	11.6
	71/55	7	0.83	None		21.03	3.05	0.730	6.07	0.880	77.7	11.3
		8	0.83	None		21.93	3.18	0.769	6.19	0.898	77.6	11.2
		9	0.81	71		21.52	3.12	0.741	6.18	0.896	77.4	11.2
		10	0.83	71		21.52	3.12	0.794	6.00	0.870	77.7	11.3
		11	0.80	93		24.00	3.48	0.826	6.58	0.954	80.7	11.7
		12	0.80	93		24.21	3.51	0.816	6.68	0.968	78.0	11.3
	71/95	13	1.41	None		20.48	2.97	0.730	5.92	0.859	77.8	11.3
		14	1.42	None		22.97	3.33	0.794	6.40	0.928	77.3	11.2
		15	1.41	71		22.41	3.25	0.870	5.99	0.869	77.3	11.2
		16	1.39	71		22.41	3.25	0.769	6.34	0.919	75.6	11.0
		17	1.39	93		20.97	3.04	0.806	5.81	0.842	74.8	.8+
		18	1.40	93		21.45	3.11	0.725	6.23	0.903	77.1	11.2+
	71/95+Dry	23-19	1.41+0	None		24.97	3.62	0.714	7.24	.05	78.0	11.3
		20	1.39	None		21.93	3.18	0.699	6.46	0.937	80.1	11.6

(continued)

Table B3 (continued)

TENSILE TEST RESULTS - T300/5208 AND T300/5209 $(\pm 45_2)_s$

Material	Exposure (T°C/RH%)	Specimen Number	% H_2O	Cycling Max. Temp. (100 Cyc. -54°C to T_{MAX} °C)	Tensile Test Temp. (°C)	E		ν_{xy}	G_{12}		τ_{12}^{ULT}	
						GPa	(x10^6 psi)		GPa	(x10^6 psi)	MPa	(ksi)
T300/5208	71/95→Dry	23-21	1.42	71	22	23.10	(3.35)	0.699	6.80	(0.986)	78.7	(11.4)
		22	1.40	71		24.07	3.49	0.800	6.69	0.970	79.9	11.6
		23	1.43	93		25.24	3.66	0.758	7.17	1.04	80.0	11.6
		24	1.43	93		25.31	3.67	0.784	7.10	1.03	74.6	10.8
	Dry	25	0	None	71	19.52	2.83	0.775	5.49	0.796	68.5	9.93
		26	0	None		18.55	2.69	0.714	5.41	0.784	69.8	10.1
		27	0	71		19.79	2.87	0.769	5.59	0.810	71.5	10.4
		28	0	71		25.24	3.66	--	--	--	66.7	9.67
		29	0	93		18.14	2.63	0.702	5.34	0.774	71.0	10.3
		30	0	93		19.59	2.84	0.733	5.65	0.819	69.2	10.0
	71/55	31	0.82	None		16.28	2.36	0.797	4.52	0.656	Tab	Tab
		32	0.83	None		18.69	2.71	0.816	5.14	0.745	Tab	Tab
		33	0.82	71		19.72	2.86	0.760	5.61	0.813	66.6	9.66+
		34	0.81	71		18.62	2.70	0.804	5.17	0.749	63.8	9.25+
		35	0.83	93		17.17	2.49	0.819	4.73	0.686	65.2	9.45+
		36	0.83	93		18.97	2.75	0.809	5.25	0.761	67.0	9.71+
	71/95	24-37	1.41	None		18.83	2.73	0.820	5.18	0.751	62.3	9.03+
		38	1.41	None		15.45	2.24	0.862	4.14	0.600	Tab	Tab
		39	1.39	71		20.21	2.93	0.797	5.62	0.815	Tab	Tab
		40	1.42	71		17.79	2.58	0.833	4.86	0.704	Tab	Tab

(continued)

Table B3 (continued)

TENSILE TEST RESULTS - T300/5208 AND T300/5209 $(\pm 45_2)_s$

Material	Exposure (T°C/RH%)	Specimen Number	% H_2O	Cycling Max. Temp. (100 Cyc. -54°C to T_{MAX} °C)	Tensile Test Temp. (°C)	E		ν_{xy}	G_{12}		τ_{12}^{ULT}	
						GPa	($\times 10^6$ psi)		GPa	($\times 10^6$ psi)	MPa	(ksi)
T300/5208	71/95	23-41	1.44	93	71	21.31	(3.09)	0.909	5.58	(0.809)	Tab	Tab
	↓	42	1.43	93	↓	16.41	2.38	0.741	4.72	0.685	59.2	(8.58)†
	Dry	43	0	None		18.48	2.68	0.806	5.21	0.741	69.5	10.1
	↓	44	0	None		20.41	2.96	0.754	5.83	0.845	69.9	10.1
		45	0	71		19.38	2.81	0.817	5.32	0.772	69.7	10.1
		46	0	71		18.21	2.64	0.767	5.14	0.746	68.0	9.86
		47	0	93		18.90	2.74	0.809	5.23	0.758	72.5	10.5
		48	0	93		18.90	2.74	0.704	5.54	0.803	72.4	10.5
	71/95+Dry	49	1.29+0	None	93	16.76	2.43	0.794	4.67	0.677	66.0	9.57
	↓	50	1.25	None	↓	--	--	--	--	--	--	--
		51	1.34	71		20.41	2.96	0.813	5.62	0.815	67.0	9.72
		52	1.32	71		22.07	3.20	0.804	6.11	0.886	68.4	9.92
		53	1.31	93		19.52	2.83	0.820	5.37	0.779	65.3	9.47
		54	1.07	93		18.62	2.70	0.833	5.08	0.737	68.4	9.91
	71/55	25-55	0.82*	None		18.34	2.66	0.909	4.81	0.697	66.8	9.69†
	↓	56	0.82*	None		--	--	--	--	--	--	--
		57	0.82*	71		21.93	3.18	0.781	6.16	0.893	64.6	9.37†
		58	0.82*	71		19.24	2.79	0.800	5.34	0.775	64.8	9.39
		59	0.82*	93		20.07	2.91	0.726	5.21	0.756	59.2	8.59
		60	0.82*	93	↓	19.45	2.82	0.833	5.32	0.771	63.5	9.20†

(continued)

Table B3 (continued)

TENSILE TEST RESULTS - T300/5208 AND T300/5209 $(\pm 45_2)_s$

Material	Exposure (°C/%RH)	Specimen Number	% H_2O	Cycling Max. Temp. (100 Cyc. -54°C to T_{MAX} °C)	Tensile Test Temp. (°C)	E		ν_{xy}	G_{12}		τ_{12}^{ULT}	
						GPa	($\times 10^6$ psi)		GPa	($\times 10^6$ psi)	MPa	(ksi)
T300/5209	71/95	25-61	1.41*	None	93	15.93	(2.31)	0.800	4.42	(0.641)	Tab	Tab
		62	1.41*	None		--	--	--	--	--	--	--
		63	1.41*	71		16.55	2.40	0.833	4.52	0.655	56.0	(8.13)†
		64	1.41*	71		15.72	2.28	0.855	4.25	0.616	55.0	7.98†
		65	1.41*	93		15.59	2.26	0.885	4.14	0.600	Tab	Tab
		66	1.41*	93		15.52	2.25	0.804	4.30	0.623	54.1	7.85†
	71/95+Dry	67	1.41*	None		18.67	2.71	0.833	5.09	0.738	70.0	10.1
		68	1.41*	None		16.07	2.33	0.800	4.46	0.646	59.9	8.69
		69	1.34	71		19.79	2.87	0.833	5.39	0.782	67.4	9.77
		70	1.41*	71		18.90	2.74	0.817	5.21	0.755	67.2	9.74
		71	1.34	93		19.24	2.79	0.752	5.49	0.796	69.4	10.1
		72	1.33	93		19.38	2.81	0.816	5.34	0.775	69.6	10.1

NOTES:

1. 'Tab' denotes failure of adhesive between tensile specimen and aluminum end tabs during tensile test.
2. * Dry weights were inadvertently not recorded on these specimens. Listed moisture percentages were therefore obtained by averaging values obtained for other specimens experiencing identical exposure conditions.
3. † τ taken at $\epsilon_L = 3.5\%$.

Table 84

$(0_{16})_T$ T300/5208 AND T300/5209 INTERLAMINAR SHEAR STRENGTH RESULTS

Material	Exposure T°C/RH%	Specimen Number	% H_2O Before Drying	After Drying τ_{MAX} MPa	After Drying (KSI)
T300/5209	25/0	2-1	0	75.11	(10.89)
		2	0	76.97	(11.16)
		3	0	76.38	(11.07)
		4	0	75.95	(11.01)
		5	0	76.66	(11.12)
		6	0	76.82	(11.14)
		7	0	76.82	(11.14)
		8	0	77.71	(11.27)
		9	0	75.95	(11.01)
	93/95	10	3.17	55.39	(8.03)
		11	3.13	56.97	(8.26)
		12	3.1[illegible]	58.16	(8.43)
		13	3.11	58.61	(8.50)
		14	3.03	53.17	(7.71)
		15	3.11	59.74	(8.66)
		16	3.12	57.66	(8.36)
		17	3.06	57.26	(8.30)
		18	2.88	60.32	(8.75)
	93/55	19	1.27	73.08	(10.60)
		20	1.30	69.95	(10.14)
		21	1.26	76.23	(11.05)
		[illegible]	1.30	76.08	(11.03)
		23	1.27	74.08	(10.74)
		24	1.21	74.23	(10.76)
		25	1.30	73.57	(10.67)
		26	1.26	75.07	(10.89)
		27	1.24	70.19	(10.18)

(continued)

Table B4 (continued)

$(0_{16})_T$ T300/5208 AND T300/5209 INTERLAMINAR SHEAR STRENGTH RESULTS

Material	Exposure T°C/RH%	Specimen Number	% H_2O Before Drying	After Drying	
				τ_{MAX} MPa	(KSI)
T300/5208	25/0	17-1	0	91.27	(13.23)
		2	0	86.72	(12.57)
		3	0	90.58	(13.13)
		4	0	96.66	(14.02)
		5	0	93.55	(13.54)
		6	0	95.47	(13.84)
		7	0	89.77	(13.02)
		8	0	95.26	(13.81)
		9	0	93.90	(13.61)
	93/95	10	1.46	93.21	(13.52)
		11	1.51	89.90	(13.04)
		12	1.47	93.92	(13.62)
		13	1.47	87.71	(12.72)
		14	1.41	90.90	(13.18)
		15	1.49	90.58	(13.13)
		16	1.53	91.36	(13.25)
		17	1.44	90.26	(13.09)
		18	1.56	88.98	(12.90)
	93/55	19	0.85	88.69	(12.86)
		20	0.85	91.75	(13.30)
		21	0.85	95.83	(13.90)
		22	0.82	96.54	(14.00)
		23	0.84	98.43	(14.27)
		24	0.86	93.35	(13.54)
		25	0.81	96.32	(13.97)
		26	0.88	96.47	(13.99)
		27	0.84	95.38	(13.83)

TABLE OF CONTENTS

Chapter	Title	Page	
	FOREWORD	i	1/A5
	ABSTRACT	ii	1/A6
	LIST OF TABLES	v	1/A9
	LIST OF FIGURES	vi	1/A10
1	HYGROTHERMAL DEGRADATION OF GRAPHITE-EPOXY COMPOSITES	1-1	1/B1
	1.0 INTRODUCTION	1-1	1/B1
	1.1 ASSESSMENT OF HYGROTHERMAL DEGRADATION - LITERATURE REVIEW	1-6	1/B6
	1.1.1 Definition of Environment	1-6	1/B6
	1.1.2 Effect of Moisture on Mechanical Properties	1-7	1/B7
	1.1.3 Effect of Hygrothermal Cycling on Kinetics of Moisture Sorption	1-10	1/B10
	1.1.4 Effect of Hygrothermal Cycling on Mechanical Properties	1-12	1/B12
	1.1.5 Assessment of Hygrothermal Degradation Mechanisms	1-12	1/B12
	1.2 PROGRAM DESCRIPTION	1-14	1/B14
	1.3 MATERIAL PROCESSING	1-19	1/C5
2	THE COUPLING BETWEEN APPLIED AND RESIDUAL STRESS AND MOISTURE SORPTION	2-1	1/C8
	2.1 DIMENSIONAL CHANGES CAUSED BY MOISTURE ABSORPTION	2-1	1/C8
	2.2 MOISTURE ALTERED RESIDUAL STRESSES	2-5	1/C12
	2.3 DESORPTION UNDER STRESS	2-9	1/D4
	2.4 INFLUENCE OF APPLIED STRESS DURING DESORPTION ON RESIDUAL STRESSES	2-17	1/E2
	2.5 HYGROTHERMAL CYCLING EXPERIMENTS	2-20	1/E7
3	THE INFLUENCE OF HYGROTHERMAL HISTORY ON MATRIX AND INTERFACE DOMINATED LAMINATE PROPERTIES	3-1	1/E12
	3.1 INPLANE SHEAR TESTS	3-1	1/E12
	3.2 INTERLAMINAR SHEAR TESTS	3-10	1/F7
4	MICROSCOPIC EVIDENCE FOR DAMAGE DUE TO HYGROTHERMAL CYCLING	4-1	1/G8
	4.1 MICROSCOPIC EXAMINATION AFTER 10 HYGROTHERMAL CYCLES	4-1	1/G8
	4.2 MICROSCOPIC EXAMINATION AFTER 100 HYGROTHERMAL CYCLES	4-1	1/G8

TABLE OF CONTENTS (continued)

Chapter	Title	Page	
5	ANALYSIS OF HYGROTHERMALLY INDUCED STRESS IN GRAPHITE-EPOXY LAMINATES	5-1	2/A10
	5.1 ANALYSIS DESCRIPTION	5-1	2/A10
	5.2 ANALYSIS OF MOISTURE INDUCED STRESSES	5-3	2/A12
	5.3 HYGROTHERMAL STRESS ANALYSIS	5-7	2/B2
6	DISCUSSION OF RESULTS	6-1	2/C14
	6.1 ASSESSING PERMANENT AND REVERSIBLE INTERFACIAL BOND DEGRADATION	6-1	2/C14
	6.2 ENERGY CONCEPTS FOR INITIATION AND GROWTH OF HYGROTHERMAL DAMAGE	6-5	2/D4
	6.3 CONCLUSIONS	6-11	2/D10
	REFERENCES	7-1	2/D13
Appendices			
A	MATERIAL PROCESSING INFORMATION	A-1	2/E4
B	MECHANICAL TESTING TABULATION	B-1	2/F7

1 Report No. NASA CR-3154	2 Government Accession No.	3 Recipient's Catalog No.
4 Title and Subtitle HYGROTHERMAL DAMAGE MECHANISMS IN GRAPHITE-EPOXY COMPOSITES		5 Report Date December 1979 6 Performing Organization Code
7 Author(s) FRANK W. CROSSMAN, R. ERNEST MAURI, AND W. JOHN WARREN		8 Performing Organization Report No. LMSC-D626480 10 Work Unit No.
9 Performing Organization Name and Address LOCKHEED PALO ALTO RESEARCH LABORATORY LOCKHEED MISSILES AND SPACE CO., INC. PALO ALTO, CALIFORNIA 94304		11 Contract or Grant No. NAS2-9563 13 Type of Report and Period Covered CONTRACTOR REPORT
12 Sponsoring Agency Name and Address NATIONAL AERONAUTICS AND SPACE ADMINISTRATION WASHINGTON, D.C. 20546		14 Sponsoring Agency Code

15 Supplementary Notes

AMES RESEARCH CENTER, NASA, TECHNICAL MONITOR - HOWARD NELSON

16 Abstract

An experimental and analytical study of T300/5209 and T300/5208 graphite-epoxy laminates was conducted: (1) to determine the coupling between applied stress, internal residual stress, and moisture sorption kinetics, (2) to examine the microscopic damage mechanisms due to hygrothermal cycling, (3) to evaluate the effect of absorbed moisture and hygrothermal cycling on inplane shear response, (4) to determine the permanent loss of interfacial bond strength after moisture absorption and drying, and (5) to evaluate the three-dimensional stress state in laminates under a combination of hygroscopic, thermal and mechanical loads. Specimens were conditioned to equilibrium moisture content under steady exposure to 55 or 95% RH at 70 or 93°C. Some specimens were tested subsequent to moisture conditioning and 100 cycles between -54°C and either 70°C or 93°C.

The transverse and through thickness expansion of unidirectional composites due to absorption of equilibrium moisture concentrations were determined. Desorption of moisture at 70°C was found to be insensitive to initial moisture content, applied stress and internal residual stress. Dimensional changes on $(0_4, 90_4)_s$ laminates were measured during hygrothermal cycling to assess alteration of laminate residual stress. Elastic laminated plate theory was successfully used to predict the moisture altered residual stress state of T300/5208 laminates. In T300/5209 the strong dependence of residual stress on hygrothermal history was indicative of viscoelastic behavior.

The inplane shear response was determined as a function of moisture content, temperature, and hygrothermal cycling history. Permanent alteration in room temperature interlaminar shear strength after hygrothermal cycling was also assessed. Cycling was found to have no measurable effect on inplane shear and interlaminar shear response and caused no significant microstructural damage after 100 cycles.

Finite element analysis showed that the most severe stresses near laminate free edges were introduced during moisture desorption and combined mechanical loading. Arguments based on fracture mechanics concepts indicate that edge cracking due to hygrothermal loading alone will be more pronounced in thick laminates and suppressed in the thin 8-ply laminates examined in this study.

17 Key Words (Suggested by Author(s))	18 Distribution Statement
Graphite-epoxy Hygrothermal damage Moisture sorption Residual stress Matrix strength Bond strength	Unlimited STAR Category - 24

19 Security Classif. (of this report)	20 Security Classif. (of this page)	21 No. of Pages	22 Price*
Unclassified	Unclassifed	155	$8.00

*For sale by the National Technical Information Service, Springfield, Virginia 22161

NASA-Langley, 1979

B-14

90%

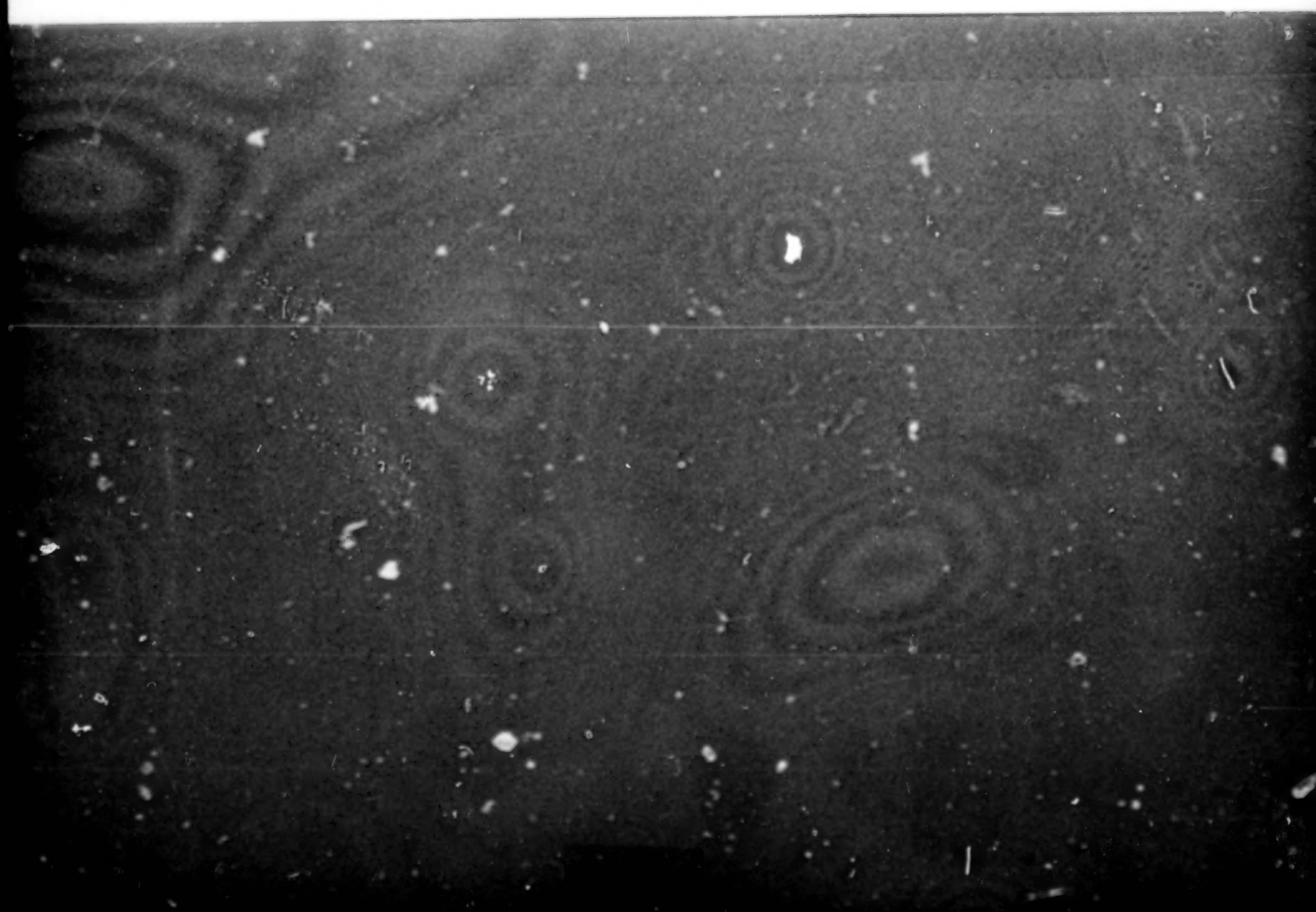

END